Friction Stir Spot Welding of Aluminium Alloy AA5052 With and Without Carbon Fiber-reinforced Polymer Composite Interlayer

Omer Kalaf

Submitted to the
Institute of Graduate Studies and Research
in partial fulfillment of the requirements for the degree of

Doctor of Philosophy
in
Mechanical Engineering

Eastern Mediterranean University
August 2021
Gazimağusa, North Cyprus

Approval of the Institute of Graduate Studies and Research

Prof. Dr. Ali Hakan Ulusoy
Director

I certify that this thesis satisfies all the requirements as a thesis for the degree of Doctor of Philosophy in Mechanical Engineering.

Prof. Dr. Hasan Hacişevki
Chair, Department of Mechanical Engineering

We certify that we have read this thesis and that in our opinion it is fully adequate in scope and quality as a thesis for the degree of Doctor of Philosophy in Mechanical Engineering.

Asst. Prof. Dr. Mohammed Asmael
Co-Supervisor

Asst. Prof. Dr. Babak Safaei
Supervisor

Examining Committee

1. Prof. Dr. Tien-Chien Jen
2. Prof. Dr. Alireza Setoodeh
3. Assoc. Prof. Dr. Shaban Ismael Albrka
4. Assoc. Prof. Dr. Qasim Zeeshan
5. Asst. Prof. Dr. Mohammed Asmael
6. Asst. Prof. Dr. Babak Safaei
7. Asst. Prof. Dr. Davut Solyali

ABSTRACT

In this dissertation, similar aluminum alloys AA5052 with additional carbon fiber-reinforced polymer composite (CFRP) interlayer were selected to investigate the effect of welding parameters (rotational speed and dwell time) on the mechanical properties, joint efficiency, and microstructure of friction stir spot weld joint. The maximum tensile shear load was 1779.6 N with joint efficiency of 14.6% obtained at rotational speed of 2,000 rpm and 2 s dwell time, which is 39.5% higher than the value at low rotational speed 850 rpm and 2 s dwell time whereas the joints without interlayer the maximum tensile shear load was 2439 N with joint efficiency of 19.4% obtained at 1300 rpm and 2 s dwell time, which is 48% higher than the value at low rotational speed 850 rpm and 5 s dwell time. Meanwhile, the maximum microhardness 58 HV was attained in the keyhole region at rotational speed of 2,000 rpm and dwell time of 5 s, which is 22.4% higher compared to low rotational speed. On the other hand the specimens without carbon fiber interlayer, the maximum microhardness was 37.2 HV was obtained at 850 rpm and 2 second dwell time in thermal mechanical affect zone, which is about 51% higher compared to low rotational speed. The SEM-EDS results reveal the presence of intermetallic compounds (Al–Mg–C), which enhance the intermetallic bonding between elements. The microstructure without interlayer images showed that welding parameters such as rotational speed and dwell time have high effect on hook deformation and penetration around the pin area. It was proposed a novel prediction model to predict tensile shear load of samples with and with CFRP interlayer by applying various machine learning models i.e. artificial neural network (ANN), Adopted neuro fuzzy-inference system (ANFIS), support vector machine (SVM) and multi linear regression (MLR). According to test results, it has an incentive

effect for future studies to know that MLR model produce better results to estimate tensile shear load in both cases of with and without additional interlayer rather than the other model and the average error was just 0.333% and 3.64 % respectively.

Keywords: friction stir spot welding; interlayer; carbon fiber-reinforced polymer composite; aluminum alloys; mechanical properties; microstructure; machine learning.

ÖZ

Bu savunma tezinde, kaynak parametrelerinin (dönme hızı ve bekleme süresi) mekanik özellikler, bağlantı verimliliği ve sürtünme karıştırma noktasının mikro yapısı üzerindeki etkisini araştırmak için ek karbon fiber takviyeli polimer kompozit (CFRP) ara tabakalı benzer alüminyum alaşımları AA5052 seçilmiştir. kaynak bağlantısı. Maksimum çekme kesme yükü 1779,6 N olup, 2.000 rpm dönme hızı ve 2 sn bekleme süresinde elde edilen % 14,6 eklem verimliliği ile, düşük dönme hızı 850 rpm ve 2 sn bekleme süresindeki değerden% 39,5 daha yüksektir, oysa eklemsiz eklemler ara tabaka maksimum gerilme kesme yükü 2439 N idi ve 1300 rpm'de ve 2 sn bekleme süresinde elde edilen% 19,4'lük eklem verimliliği, 850 rpm düşük dönme hızı ve 5 sn bekleme süresindeki değerden% 48 daha yüksektir. Bununla birlikte, anahtar deliği bölgesinde 2.000 rpm dönme hızında ve 5 saniyelik bekleme süresinde maksimum mikro sertlik 58 HV elde edildi, bu da düşük dönme hızına göre% 22.4 daha yüksek. Öte yandan karbon fiber ara tabakası olmayan numunelerde maksimum mikro sertlik 850 rpm'de 37,2 HV ve düşük dönme hızına göre yaklaşık% 51 daha yüksek olan termal mekanik etki bölgesinde 2 saniye bekleme süresinde elde edilmiştir. SEM-EDS sonuçları, elementler arasındaki intermetalik bağı güçlendiren intermetalik bileşiklerin (Al – Mg – C) varlığını ortaya koymaktadır. Katmanlar arası görüntülerin olmadığı mikro yapı, dönme hızı ve bekleme süresi gibi kaynak parametrelerinin kanca deformasyonu ve pim alanı etrafındaki penetrasyon üzerinde yüksek etkiye sahip olduğunu göstermiştir. Yapay sinir ağı (YSA), Kabul edilen nöro bulanık çıkarım sistemi (ANFIS), destek vektör makinesi (SVM) ve çoklu doğrusal regresyon (MLR). Test sonuçlarına göre, MLR modelinin her iki durumda da diğer modelden ziyade ilave ara katmanı olan ve olmayan çekme kesme yükünü tahmin etmede daha iyi sonuçlar

ürettiğini ve ortalama hata sadece sırasıyla % 0,333 ve 3,64 olduğunu bilmek gelecekteki çalışmalar için teşvik edici bir etkiye sahiptir.

Anahtar Kelimeler: sürtünme karıştırma noktası kaynağı; ara katman; karbon fiber takviyeli polimer kompozit; alüminyum alaşımları; Mekanik özellikler; mikroyapı; makine öğrenme

DEDICATION

To My Family

ACKNOWLEDGMENT

My greatest and most sincere gratitude is to Asst. Prof. Dr. Babak Safaei, my supervisor, and Asst. Prof. Dr. Mohammed Asmael Co-Supervisor. I have very much appreciated his excellent guidance, valuable suggestions, and continuous support while writing scientific papers and PhD thesis times. They have provided me with outstanding and helpful advice on the research idea and its method and presentation.

Besides that, I would like to thank Assoc. Prof. Dr. Qasim Zeeshan, for his insightful comments and also for the hard questions which incented me to widen my research from various perspectives. Also, I would like to thank Prof. Dr. Hasan Hacişevki head of department. Finally, great thank to all jury member.

I would also like to thank my wife for everything you has done for me during the hardest time of my PhD, my mother with special thanks to my father, for their support and efforts.

Furthermore, I am grateful for my friends for their support and encouragement in every stage of my studies. Without their support, it would not be possible to overcome the most difficult times during my studies.

TABLE OF CONTENTS

LIST OF TABLES

LIST OF FIGURES

LIST OF ABBREVIATIONS

AA	Aluminum Alloy
ANFIS	Adaptive Neuro-Fuzzy Inference System
ANN	Artificial Neural Network
AZ	Adhesion Zone
CFRPs	Carbon Fiber-Reinforced Composites
EDS	Energy-dispersive X-ray Spectroscopy
FSSW	Friction Stir Spot Welding
FSW	Friction Stir Welding
HAZ	Heat Affected Zone
JT	Joining Time
MLR	Multi Linear Regression
NZ	Nugget Zone
PD	Plunge Depth
PPS	Polyphenylene Sulfide
PP-SCF	Short Carbon Fiber Polypropylene
RSW	Resistance Spot Welding
RFSSW	Refill Friction Stir Spot Welding
RPM	Rotational Speed
SEM	Scanning Electron Microscope
SVM	Support Vector Machine
SVR	Support Vector Regression
SZ	Stir Zone
η	Efficiency

Chapter 1

INTRODUCTION

1.1 Overview

The application of lightweight materials such as aluminum, magnesium and metal foams, as typical porous materials have been increased in automotive and aerospace industries. Also, it is a critical challenge to reduce the weight in these industries to improve the performance of vehicle and airplane [1]. Aluminum alloys are one of the most promising lightweight material [2]. This is due to high strength to weight ratio, high corrosion resistance, high fatigue, light weight, impact resistance, high mechanical performance, and good efficient in weldability [3-6].The aluminum alloys AA 5052 is widely used in many application such as automotive, aerospace, marine, and pacing industries [7]. The AA 5052 generally non-heat treatable alloy that strengthened by cold deformation and activation of the strain hardening mechanism [8,9]. To take the advantage of carbon fiber interlayer, the carbon fiber was placed between two plates of AA 5052 during friction stir spot welding. By contrast with the case without interlayer two interesting aspects were addressed.

In recent years, composite materials have triggered world-wide investigations to manufacture improved structures with superior mechanical characteristics [10]. Carbon fiber-reinforced composites (CFRPs) have excellent thermal and mechanical properties and commonly applied in the fabrication of polymer–matrix composites [11]. CFRP industry is developing by constant growth of demand from defense and

aerospace to automotive sectors [12]. The machining of CFRP composites types are carried out mainly on plain-woven carbon fiber and epoxy resin matrix, including directional, unidirectional, and multidirectional CFRP laminates [13]. However, interlayer considerably increases the protection of weld against corrosive environments [14].

Friction stir spot welding FSSW is a solid state joining technique and has been applied to aluminum alloys such as 2000 and 5000 series [15]. These alloys are apt to solidification and liquation cracking, which can be avoided by friction stir spot welding [16]. FSSW is an advanced form of friction welding which is mostly used to weld the similar and dissimilar alloys [17]. FSSW provides reduction in energy consumption up to 90 % and 40 % in capital cost compared to resistance spot welding (RSW) [18]. Despite the benefits of using different lightweight materials in a structure, the joining of dissimilar materials such as metal alloys and composites presents a great challenge due to their distinct physicochemical properties [19]. In addition, bonding of thermoplastic composites requires special pretreatments to increase the intrinsic adhesion between the composite and the adhesive to improve the wettability and surface tension of the thermoplastics [20].

Friction stir spot welding is an alternative joining technology for producing metal-composite joints, patented by and developed at Helmholtz-Zentrum Geesthacht, Germany [21]. The heat generated by FSSW in nugget zone (NZ) is the cause of dissolving large fraction of the phase and dislocation loss [22].

1.2 Thesis Objectives

i. To achieve full FSSW joint of similar AA 5052 with and without carbon fiber interlayer.

ii. To investigate the effect of welding parameters on mechanical and microstructure properties of FSSW joint.

iii. To correlate the results obtained with the earlier microstructural characterization and thermal analysis.

iv. To evaluate the effect of carbon fiber interlayer on welding parameters of intermetallic compounds in the Keyhole, SZ, and TMAZ of FSSW joint.

v. Recently, interlayers are getting more advantageous in welding applications.

1.3 Problem Statement

By vast application of wrought aluminum in industries and utilization of variety of alloys, joining of similar materials seems to be necessary. Moreover, during welding process of heat treated wrought aluminum alloys heat generation has to be controlled and kept adequately. Aluminum alloys of 5000 series are known and applied in industries due to their elevated mechanical property compared with other series. Among aluminum alloys of 5000, 5052 is famous and available in the market around the globe. The primary reason behind this is that the formation of discontinuity results from the irregular plasticized material flow. Evidence suggests that as the tool rotates and moves, the plasticized material around the tool probe flows into a cavity formed at the trailing edge of the probe. Under proper welding conditions, the plasticized material flow is highly periodic with respect to the frequency of the tool rotation. In these works, the main characteristics of the process, its bonding mechanisms, joint microstructure, and the mechanical properties.

In addition, as reported FSSW condition has significant effect on properties of FSSW joint. However, effects of similar FSSW of AA5052 with and without carbon fiber interlayer in terms of heat generation, heat distribution and heat disposal pattern is still

unclear. Many researchers have investigated both in process monitoring of defect formation and prediction of welding quality. However, no detailed investigation into the metal-polymer bonding mechanisms and interface, process-related physicochemical changes on the polymer or composite, or any failure and fracture analysis were carried out.

The reaction between aluminum and carbon fiber during welding processes caused to form aluminum carbide (Al_4C_3) at temperatures above 500 ºC which negatively affected the performance of interfacial layer in composites.

1.4 Structure of This Thesis

- Chapter 2 is the literature review of this thesis which analyze the existing research, with a view to understanding the currently say about this topic.
- Chapter 3 is methodology which is include material selection, tool design, experimental and thermocouple setup, as well as micro hardness and tensile test also SEM-EDS analysis.
- Chapter 4 is simply a presentation and description of the results of the temperature evolution, mechanical tests and microstructure analysis.
- Chapter 5 is metamodeling.
- Chapter 6 is conclusions of the dissertation.

Chapter 2

LITERATURE REVIEW

2.1 Introduction

Friction welding (FW) is a joining approach for solid materials, which creates material coalescence under compressive force when workpieces are moved or rotated relative to each other producing heat and plastically displacing material from faying interface [23]. In the last few decades, (FW) has been considered as a major development in joining materials and has been applied in shipbuilding, high speed rail, aerospace and automotive industries [24,25].

FW is an appropriate approach for joining solid materials [26]. Work pieces rotate or move relative to each other resulting in the coalescence of materials under pressure [27]. During the welding process, melting effects due to the generated heat should not be visible in the final welded product. In this process, filling and protective gas are not always required and the work piece is generally kept constant while tool moving.

In many industrial applications, such as wind power towers [28,29], bridge construction and transportation [30], lightweight structures are becoming highly popular [31,32]. To decrease the weight of the structures even more, carbon fiber-reinforced thermoplastic are being used in aerospace [33,34]. Although application of various materials is advantageous in different structures, making joints between dissimilar materials such as composites and metal alloys is a difficult task because they

have different physicochemical properties [35-37]. Due to large different chemical and physical properties between plastic and metal, the bonding between metal and plastic are more difficult [38]. Several researchers have studied different splicing techniques of metal and plastic such as ultrasonic spot welding, friction welding [39]. The physical and chemical characteristics of plastics and metals are very different and therefore, they cannot be joined easily.

Generally, friction welding, adhesive bonding method and mechanical fastening technique [40-42] are the most commonly applied approaches to join metals and plastic materials [43,44]. In terms of manufacturing standard, joining of metal stack-ups and composites imposes huge costs because structural completion requires many labor-intensive steps. Also, as stress is increased, the cross-sectional areas of structures are reduced because of the existence of bolt holes [45,46].

Commonly used approaches for joining metals and carbon fiber-reinforced polymers (CFRPs) to such as adhesive bonding, riveting, bolting, etc. are non-thermal processes while welding a thermal process [47,48]. Friction heating has been applied in thermoplastic matrix localized melting [49-51]. All abovementioned thermal approaches rely on matrix material partial melting within (CFRPs), resulting in the interlocking and bonding of adhesive to the surface of metal [52,53]. FW is traditionally performed by displacing the components relative to each other at the interface along with application of compressive force across the joint. The main point in FW is the lack of molting in materials and formation of solid-state weld. This procedure is environmentally friendly since no spatter or fume is created and no reflected laser beams or arc glare are formed [54].

Because of their excellent electrical, thermal and mechanical properties, carbon fibers are commonly applied in the fabrication of polymer–matrix composites [55,56]. Therefore, extensive research has been performed on the application of conventional pitch-based carbon fibers in improving and optimizing the characteristics of a wide variety of structures [57]. Although its high cost has generally been considered as a great challenge in the application of carbon fibers in CFRP, these structures are extensively being applied in automotive sector [58].

Despite the fact that the extraordinary mechanical characteristics of carbon fibers make them an attractive option for designers, they have to outperform existing lightweight structural automotive materials: magnesium and aluminum. Aluminum has a long and successful history of application in the designing, assembling, fabricating and recycling different structures which has constantly grown, as showed in Figure 1. Currently, numerous well-known automotive companies use this material. Among them are Goodyear Eagle tires, the inner structure of rear deck lid of Ford GT, roof of BMW M6, the floor and front fenders of Corvette Z06. Also, other industries such as trim and cosmetic pieces which are available in the aftermarket as well as underbody structures, A-pillars, spoilers, drive shafts, various body panels and other low-volume, high-performance cars use this material [59,60].

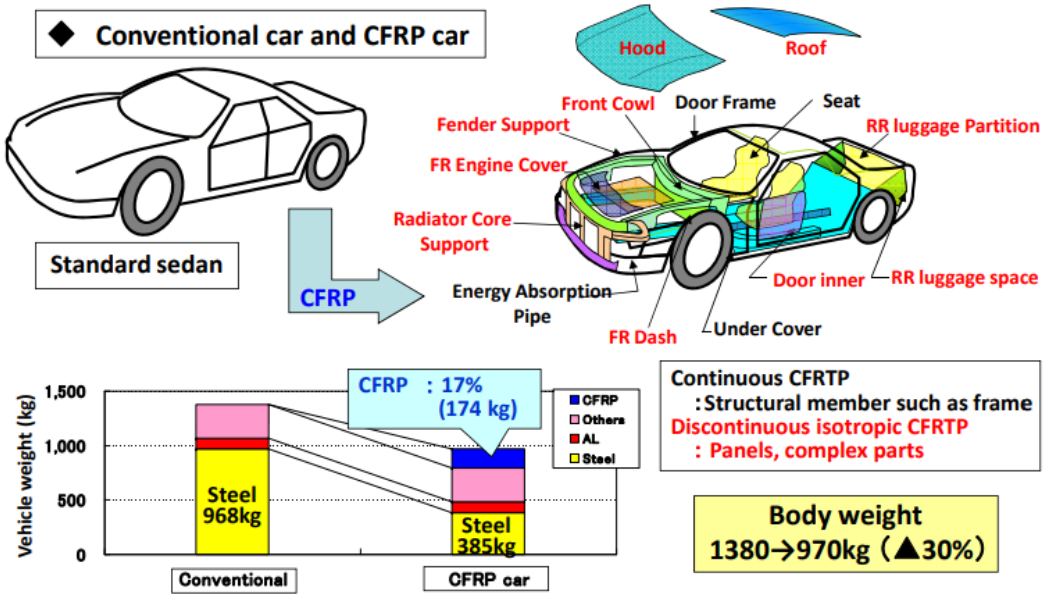

Figure 1: Application of CFRTP can reduce body weight by 30% [61].

Application of composite materials in commercial aircrafts has become attractive since they reduce the weight of airframe decreasing fuel consumption and therefore, operation cost [62]. Airbus was the first company to apply composite materials in a commercial aircraft reducing 2000 metal fin parts (excluding fasteners) to fewer than 100 in composite fin which resulted in lower weights and manufacturing costs. Composite materials account for about 50 % of the material used in the production of Boeing 787 which reduce its average weight by 20 %. Composite materials are applied in key structural components of several modern helicopters, including V22 tilt-rotor aircraft, in which composites comprise about 50 % of the total weight. The formability property of composite materials has been employed in helicopter manufacturing to decrease the number of components and consequently cost [63,64].

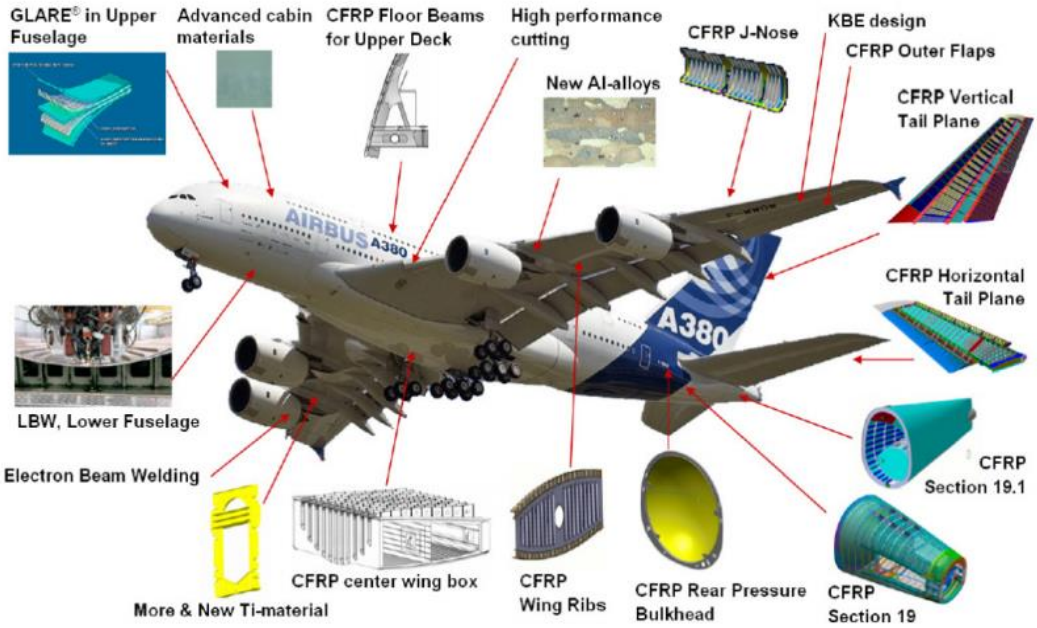

Figure 2: The AIRBUS A380 aircraft composite applications [65].

Few research works have been performed on joining matrix composites and metal. However, in some studies, FSSW has been employed to form an in-situ metal matrix composite during welding [66,67]. Normally, polymer materials are joined by adhesives or fasteners. The thermoplastic plastic polymer or composite could be succeed joints with metals by friction welding and achieved best results [68-70]. However, conventional FSSW provides a convenient and fast alternative for these approaches and has been applied to join polypropylene, dissimilar polymethyl, high density polyethylene [71,72].

In recent years, refill friction stir spot welding (RFSSW) has also been employed to join polymethyl-methacrylate plates and the strengths similar to ultrasonic welding or adhesively bonded area were achieved [73]. The aim of this research, focus on friction welding techniques such as FSSW, RFSSW and FSW. Also, present joints of carbon fiber with metal and non-metal in different welding processes.

2.1.1 Aluminum and Aluminum Alloys

Aluminum constitutes 7.3% of the mass in the earth's crust, thus it comes in third place. In nature, it is a very stable combinations with other materials and was not established until 1808. Aside from steel and cast iron, aluminum is one of the most widely used metals due to their properties compared to the other metal. In industrial applications, pure aluminum cannot be used due to its low strength. Therefore, some elements are added to pure aluminum to increase its strength and hardness in the form of alloys, and thus the properties are refined and ready for manufacturing Generally, aluminum alloys can be classified into two main categories: cast alloys and wrought alloys [74]. Aluminum is widely used in various industries and is considered one of the few minerals that are not mined and do not exist naturally, such as gold, silver or iron. Aluminum has unusual properties and different welding requirements. Rather it is a product of bauxite which it can be found in almost every shovel full of earth throw-out the world. Through an electrolytic process (bauxite refined into alumina), and which is further refined into pure aluminum [75]. Although aluminum has a number of valuable properties, it is known for its light weight and high strength and is therefore widely used in airframes. The tensile strength of aluminum is also changeable, and therefore through the cold rolling of the metal, that is, the tensile strength can be increased from 89.63 MPa to 179.26 MPa during cold rolling. Tensile strength can be increased even further 689.48 MPa by alloying, heat-treating, cold-working and aging. Metals commonly alloyed with aluminum are silicon, zinc, magnesium, copper and manganese.

Aluminum is well resistant to corrosion in most conditions compared to parts manufactured from iron. Strong oxide is formed very quickly on the surface of the

aluminum that works to prevent air leakage and be self-protection as a restoration shield.[76].

Both wrought and cast aluminum alloys are divided into alloys which can be heat treated in order to increase the mechanical properties and alloys which cannot be heat treated [74].

2.1.2 Casting Alloys

These alloys suffer from higher shrinkage (up to 7%) which occurs during cooling or solidification. To increase the mechanical properties in these alloys can be achieved by controlling the level of impurities, solidification parameters and grain size, like cooling rate. A system of four-digit numerical designation is used to identify aluminum and aluminum alloys in the form of castings and foundry ingots. The second and third digits identify the aluminum alloy or indicate the minimum aluminum percentage. The last digit, which is to the right of the decimal point, indicates the product form: XXX.0 indicates castings, and XXX.1 and XXX.2 indicate ingots [81].

2.1.3 Classifications of Aluminum Alloys

Aluminum is often alloyed with various metals to produce different properties especially suited for particular application, theses alloys use the aluminum association numbering system for identifying the various alloying elements and metals properties. The numbering system has been standardized, i.e., 4XXX, so that the first digit indicates the major alloying element, the second digit modifications to the original alloy such as heat treating or cold working and the last two digits identify the specific alloy content or degree of aluminum purity. There are eight major series of aluminum alloys as listed in Table 1and they are given in a numerical designation according to the most important alloying metal in the mixture [77]. Since the aluminum can be

manufactured in a variety of strengths, a standardized system of suffixes (O-F-H-T) are added to the end of the four digit classification to represent strength of the material.

Table 1: Aluminum series with its major alloys elements [78]

Alloy	Series No.	Example
Al	1XXX	1060
Co	2XXX	2219
Mn	3XXX	3004
Si	4XXX	4043
Mg	5XXX	5005
Mg/Si	6XXX	6061
Zn	7XXX	7005
Other	8XXX	8011

Where, O indicates an alloy in the annealed state, F as fabricated, but has not received any additional strengthening, Has strain hardened are non-heat treatable alloys and are strengthened by strain hardening or cold working and T suffix alloys are heat treatable in order to increase harness, .i.e., quenching process [79].

2.1.4 Applications of Aluminum Alloys

Aluminum is a good conductor of heat and electricity, and is three times faster than steel and second only to copper. This property is useful for the manufacture of heat exchangers and many home cookware. The melting point of pure aluminum is relatively low at 659 ° C and must be cast for use in high temperature applications. There are two special properties that make aluminum of great value for electrical applications. Aluminum is less expensive because only one pound of aluminum would be twice the level of copper when producing a conductor. In some designs, aluminum is preferred instead of other metals, which require the least possible weight, such as airplanes and electric cars. As a result of these characteristics, aluminum has become at the forefront of the most used material in many mechanical and electrical applications that require more care in design [80].

Table 2: Aluminum series and its relative application [81]

Series No.	Application
1000	Electrical conductors
2000	Aircrafts
3000	Automobiles
4000	Welding filler metals
5000	railroad gondola
6000	Highway railing
7000	Armor plating

2.2 Friction Stir Spot Welding (FSSW)

Classification FSSWs are form by the retraction of a rotating tool and plunging into and out of the materials to be joined. At the end of welding areas formed by this approach, a keyhole region is remained [82]. FSSW generally takes 2 s to 5 s and during this short time, heat formation in sheathing case and flipping region creation links the contacting plates. The energy density created by tool rotation is very high during spot welding [83]. FSSW uses non consumable tool and generates heat by friction.

In FSSW, heat is needed and is also generated between workpieces and parts. The rotation between sleeve and pin independent and the parts being joined are held with the ring [84]. Increase temperature due to the friction between sleeve and work piece to locally plasticize and plasticize of work piece. Then, molten layer consolidates under pressure inducing adhesion and snarl between materials and composites [85].

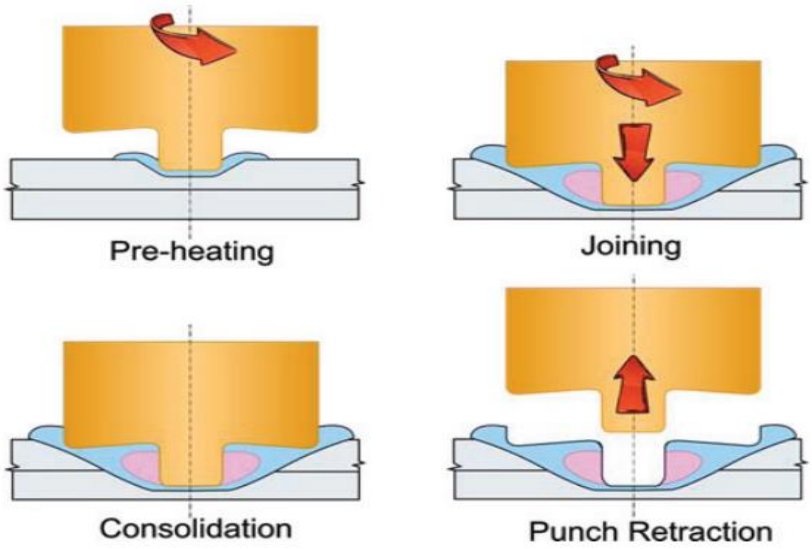

Figure 3: Schematic diagram of FSSW process [86].

The key factor in the generation of heat is tool rotation, [87] because tool torque is responsible for almost the total energy generated in FSSW [88,89], which also controls material stirring around the tool. The torque of the tool is also responsible for heat generation and thermal cycle [90], and increase of rotation rate increases temperature resulting in higher mixing intensity of materials. This additional energy input directly relates to weld strength and bonded area [91].

Sheet thickness and pin length determine tool penetration depth into contacting sheets, which are the most effective factors in weld strength and bond dimensions. The macrostructure of weld is highly related to the depth of shoulder plunge. By the increase of the depth of shoulder plunge, stirring zone is expanded and material flows upward from the lower sheet [92]. The shoulder penetration has to be deep enough to guarantee horizontal alignment of interface tip to avoid fracture by the interfacial fracture [93]. However, tensile shear load is bilaterally affected by the depth of shoulder penetration; a great amount of material is extruded from the top sheet when exposed to excessive shoulder penetration, resulting in excessive top sheet thinning,

creating upward bending and gap formation between the sheets [94,95]. Therefore, 0.2 mm shoulder penetration is generally applied in conventional FSSW [96,97].

In conventional FSSW, heat generation by the shoulder of tool is somehow low except if a dwell time were applied. During dwell period, shoulder effect in the generation of heat and flow of material is significantly enhanced in case of the highest fraction of energy generation takes place during this period [98]. Moreover, addition of dwell periods extend spot welding cycle which could be an important issue when the completion time of target weld has to be less than or equal to that of resistance spot welding (RSW). In pinless FW, much greater direct contact area is made between the material and shoulder enhancing the flow of material and significantly increasing temperature when applying a short dwell time [99]. Such fast welding cycles (<1s) cause less HAZ softening in heat treatable Al alloys [100-102]. The mechanism of heat generation during FSSW differs from that in linear FSW because FSSW is a very cross joining process [103]. In pinless FSSW, generally a shoulder with the diameter of 10 mm is applied [104-106].

The results obtained from numerical simulations reveal that sleeves with greater outer diameters greatly increase flow velocity, heat input, and welding spot area where a sleeve 9.0 mm in diameter was most commonly applied in (RFSSW) [107-112]. The comparison between adhesion bonding joints and friction stir spot welding, the results show that there is no significant of use adhesions instead of FSSW, also the mechanical performance by FSSW were higher than adhesive [113,114]. Goushegir et al. [115] studied the performance of mechanical parameters of aluminum carbon fiber reinforced poly (CF-PPS) and aluminum alloy AA 2024-T3 with rotating speed of 1900 rpm to 2900 rpm. Plunge depth was in the range of 0.5 mm to 0.8 mm and the

obtained results revealed that tool plunge depth significantly affected lab shear force. Also, plunge depth influences of metallic nub and therefore the macro mechanical interlocking between aluminum and carbon fiber. Joining time is also an important parameter; when time is short the molten PPS the viscosity is low to maintain while it became less for long. Lap shear force varies in the range of 1698 N-2310 N. During friction welding, temperature varies in the range of 370 ºC -474 ºC. The rare of cooling and heating in this study were 17 ºC /s and 97 ºC /s, respectively, which is very fast. Andre et al. [116] investigated the effects of rotating speed and joining pressure on the mechanical strength and microstructure of friction spot welding of carbon fiber and aluminum alloy AA2024-T3 with 100 μm PPS film interlayer. Joining pressure and rotational speed vary in the ranges of 0.2 MPa -0.3 MPa and 1900 rpm-2900 rpm, respectively. They reported that lap shear force increased from 2700 N to 3070 N which was higher than those for joints without interlayer because of their improved micro-mechanical interlocking, better load distribution and larger bonding area. The temperature were measured on surface which ranged from 325ºC to 417ºC. In the microstructure of interfaces two bonding, the PPS into the crevices of aluminum and carbon fiber entrapment by aluminum deformed as shown in Figure 4. However, joint without interlayer a transition zone with high air bubbles between adhesion zone and plastically deformed zone.

Goushegir et al. [117] applied aluminum alloy A2024-T3 and carbon fiber poly (phenylene sulfide) CF-PPS as test specimen and presented fiction spot welding of single lap joints and evaluated their microstructure and mechanical performance. In this case, plunge depth and joining time were fixed at 0.5 mm and 4.8 s, respectively. Rotational speed varied from 1900 rpm to 2900 rpm. The higher rotation speed

obtained optimum value of shear force around 1254 N. Joining time and rotating speed increase heat generation and changes microstructure and lap shear strength while intermediate rotational speeds and longer joining times lead to greater consolidated polymeric layers at metal-composite interface. Esteves et al. [118] studied the parameters effective on the mechanical strength and microstructure of carbon fiber CF-PPS and aluminum alloy AA6181-T4 joined by friction spot welding. In this study, rotating speed varied from 1200 rpm to 1600 rpm. Maximum shear force was 3523 N with rotating speed 1200 rpm and plunge depth and joining time were 1.15 mm and 6 s, respectively. Increase of joining time and rotating speed directly increased heat generation and changed lap shear strength and microstructure. Heat input is responsible for PPS molten layer in the joint interface increasing bonding area, as shown in Figure 5.

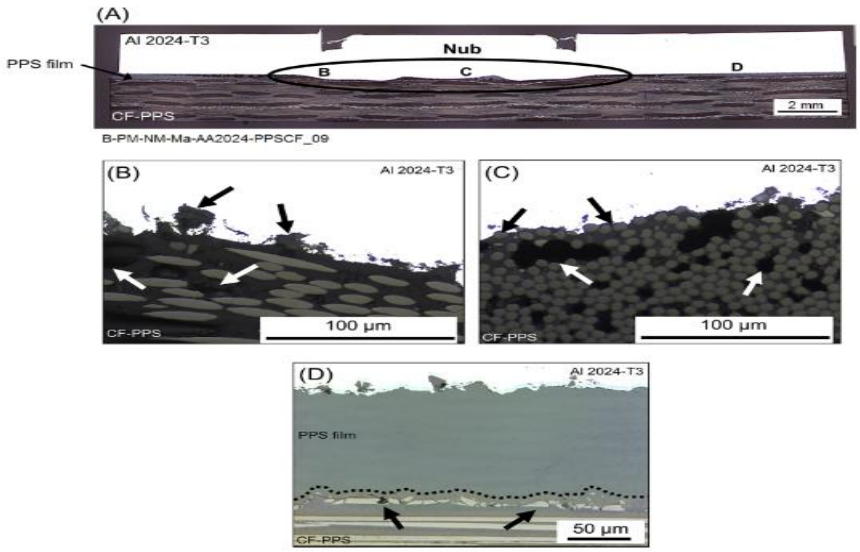

Figure 4: Microstructural details of joint (a) cross section with interlayer (b) molten polymer of Al surface (c) deformed aluminuim (d) interface of Al/ interlayer [116].

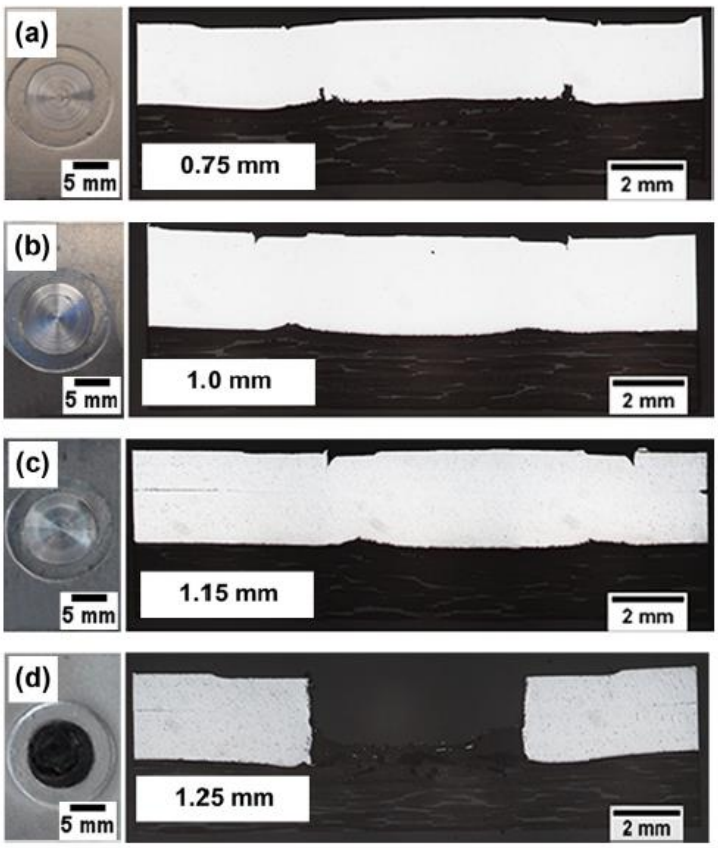

Figure 5: Cross section micrographs from top and mid views in differnt plunge depth (a) 0.75 mm , (b) 1.0mm, (c) 1.15 mm (d) 1.25 mm [118].

Andre et al. [119] evaluated the mechanical performance of aluminum alloyAA7075-T6 and carbon fiber CFRP by FSSW. In this study, rotating speed, joining time and plunge depth were 1900 rpm, were 4 s and 0.8 mm, respectively, and joining force was varying from 4 kN to 8 kN. The obtained result showed lap shear force was 4068 N and joining force significantly affected nub geometry at 6 kN. Maximum temperature on aluminum surface was 331ºC. Bonding area was divided into various zones of adhesion zone (AZ), transition zone (TZ) and plastically deformed zone (PDZ), as shown in Figure 6. These zones were formed during welding process and air bubbles were formed when molten matrix moved from the center to the edge of the joint.

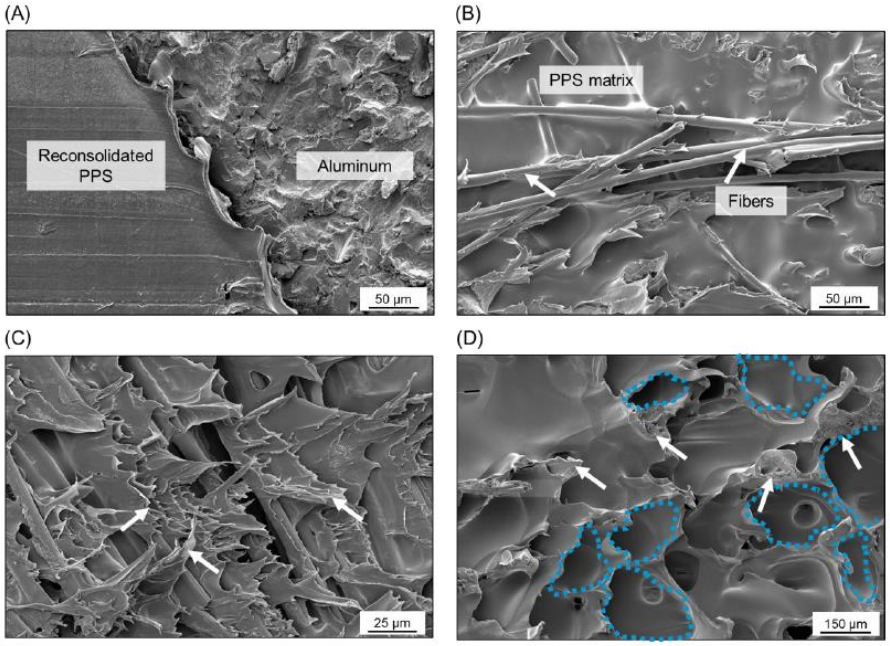

Figure 6: SEM image (a) transmission between AZ and TZ (b) PDZ of AL surface (c)PDZ (d) TZ on top composite [119].

Andre et al. [120] studied the mechanical performance and microstructure of carbon fibers and aluminum alloy AA2024-T3 joints formed by FSSW with additional PPS film interlayer. Rotating speed was varying from 1300 rpm to 2500 rpm. Optimal tensile shear force of about 2000 N was obtained at 1900 rpm rotating speed, 0.8 mm plunge depth and 6 s joining time and showed linear elasticity before final catastrophic failure. The area around the nub cohesive failure dominates, and obvious from the polymer matrix and remain of carbon fiber attached the aluminum. On the influence parameters of this study show that the important of plunge depth on lap shear force. Andre et al. [121] improved the adhesion mechanisms and mechanical performance of aluminum alloy AA 2024-T3 and carbon fiber with 100μm PPS film additional interlayer fiction spot welding. In this study, rotating speed, plunge depth and joining time were 1900 rpm, 0.8 mm and 4 s, respectively. The optimal tensile shear force was 3068 N in strong, high roughness effect on contact surface area. Also, sandblasting

was found to be the most effective treatment which maximized joint mechanical performance.

Andre et al. [122] studied the influence of PPS film interlayer with different thicknesses on the mechanical performance and microstructure of aluminum alloy AA2024-T3 and carbon fiber CF-PPS by friction spot welding. In this work, rotating speed, plunge depth and joining time were 1900 rpm, 0.8mm, 4 s, respectively, and two different interlayer thicknesses of 100 μm and 500 μm were investigated. The results showed that maximum temperature was 360 ºC in both cases. The volume of metal deformation was embedded slightly in carbon fiber during welding with 100 μm interlayer. On the other hand, with 500 μm interlayer, metallic nub formation arose through embedding of the deformed without reaching the carbon fiber. Also, bubbles were trapped in polymer and resulted in the creation of cavities after welding joint was solidified. Maximum shear forces were 2093 N and 708 N in the case of 100 μm and 500 μm interlayer, respectively. Ogawa et al. [123] studied the effects of welding properties of FSSW of aluminum alloy AA5182 and carbon fiber. Tool rotating speed was 3000 rpm and welding time was set to 1 s, 2 s and 5 s. The results showed that the temperature on aluminum surface varied from 200 ºC to 250 ºC. Also, average static strength for 1 s, 2 s and 5 s welding times were 4.1 kN, 5.5 kN and 7.1 kN, respectively. Static strength was significantly improved with increasing welding time. Microstructural results showed that pores were formed on CFRP side which mainly concentrated under tool center. Resin-based CFRP was melted just under tool periphery and a layer of resin was preserved between the two materials. Goushegir [124] studied friction spot welding of carbon fiber CF-PPS and aluminum alloy AA2024-T3. Rotating speed, plunge depth and joining time were 2900 rpm, 0.8 mm 4

s, respectively. The obtained results showed that temperature varied between 345 ºC and 474 ºC. Microstructural zones were divided into different areas: polymer heat affected zone (PHAZ), heat affect zone (HAZ), thermo-mechanical affect zone (TMAZ) and stir zone (SZ), as shown in Figure 7. Different microhardness values were observed in different zones; in base material (zone 1) the average hardness was 135 HV, in string zone high microhardness of 151 HV was observed, the average hardness of thermo-mechanical affect zone was 139 HV and the lowest microhardness of 123 HV was witnessed in heat affect zone. Also, the average ultimate lap shear force was 8264 N while reference bonded show 5459 N.

Ogawa et al. [125] studied FSSW of carbon fiber and aluminum alloy AA5182. Rotating speed was 3000 rpm. It was confirmed that pores were present inside CFRP, irrespective of the treatment of surface in the microstructure of welding joint. They were assumed to be developed either by the air entrapped by molten resin flow or during CFRP molding which was then expanded because of frictional heat. The average static strengths of untreated, porous layer and organic coating series were obtained 5.7 kN, 6.6 kN and 7.4 kN, respectively. Hence, surface treatment was found to enhance FSSW joint static strength. The shoulder diameter was 10 mm, probe length of 0.35 mm. Amancio-Filho et al. [126] studied the FSW of magnesium AZ31 and carbon fiber reinforced (PPS-CF), glass fiber reinforced (PPS-GF). Rotating speed from 900 rpm-3000 rpm, plunge depth from 0.25 mm to 1.75 mm, and joining time from 3 s-8 s. The results showed that on PPS-CF/AZ31 surface, temperature was varied in the range of 400 ºC -440 ºC (1500 rpm, 0.25 mm, 8 s). Stir zone was characterized by fine dynamic recrystallized grains. When fully examining the microstructure of stir zone, finder $Mg_{17}Al_{12}$ dispersed particles could be observed. A

thin transition zone between heat affect zone and stir zone is called thermo mechanical affected zone, as illustrated in Figure 8. Tensile shear force was 2000 N in AZ31/PPS-GF but 1500 N in AZ31/PPS-CF.

Goncalves et al. [127] studied FSSW of polyamide 66 laminate reinforced with carbon fiber. During the welding, plunge was depth 2 mm and rotation speed was 3000 rpm. According to theses parameters, the average strength of lap shear was 26.8 MPa from a nominal area of 63.6 mm^2 in the external diameter of sleeve. Mechanical and thermal effects were evident in the material around the sleeve. This region was called stir zone, as showed in Figure 9, which was mixed between polymer and broken carbon fiber.

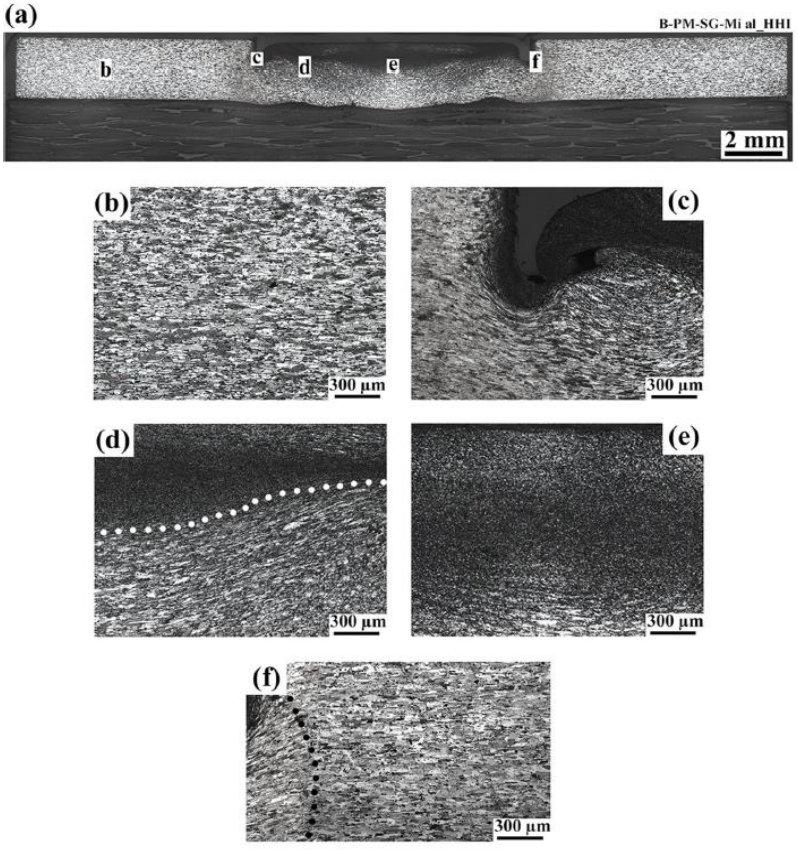

Figure 7: Microstructural zones of AL(a) General zone (b) BM (c) MTMAZ (d) MTMAZ and MSZ (e) MSZ (f) MTMAZ and MHAZ [124].

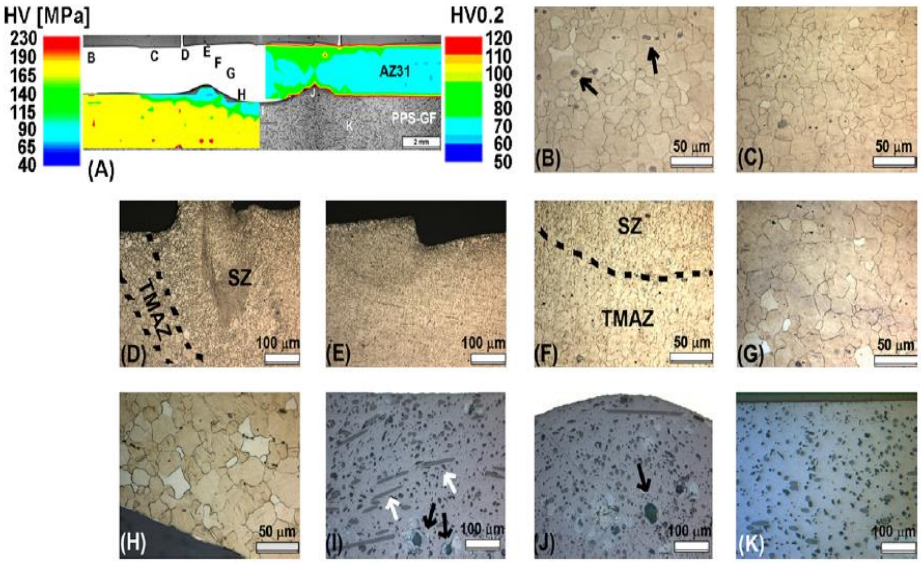

Figure 8: Hardness and microstructure of AZ31 joint: (a) cross section microhardness and macrograph maps; (b) AZ31 base material upper region; (c) AZ31 volume below clamping ring; (d) transition details between SZ and TMAZ; (e) SZ center; (f) transition region of TMAZ and SZ ; (g) heat affact zone central region; (h) polymer-metal interface within metallic nub; (i) consolidated polymer layer underneath metallic nub; (j) consolidated polymer layer close to metal polymer interface and (k) the upper portion of base material polymeric plate [126].

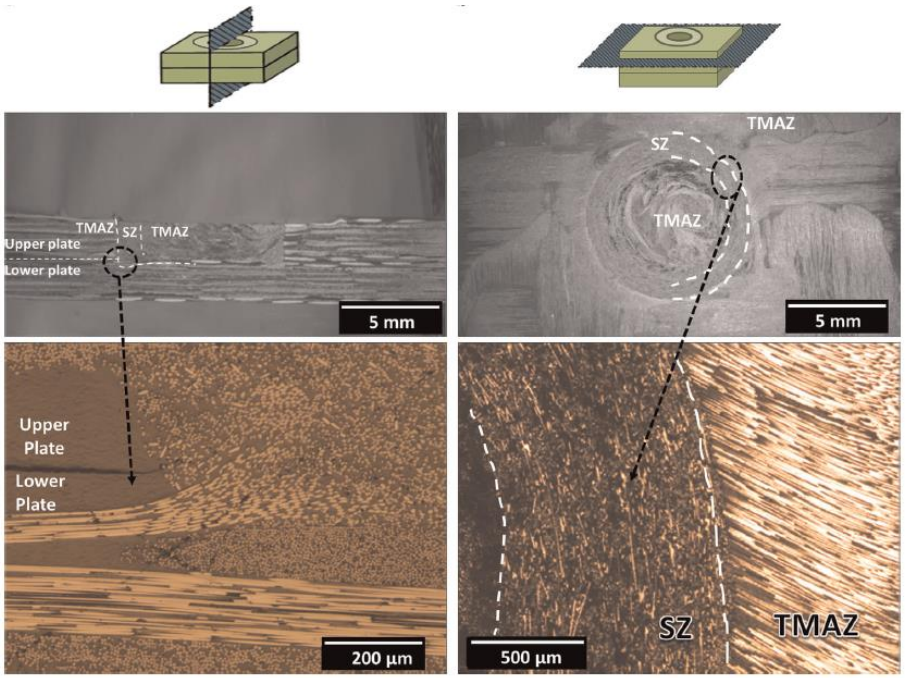

Figure 9: CF-PA66 weld microstructure produced by FSSW [127].

Huang et al. [128] studied carbon fiber polyetherimide laminate friction spot welding.

In this study, plunge depth was 2.2 mm, dwell time was 2 second, and rotating speed

varied from 800 rpm to 1200 rpm. Welding tool was from titanium alloy to reduce the heat loss, which consists of a clamping ring, sleeve and pin. At low rotating speeds, thermoplastic materials cannot be softened completely. With the increase of rotating speed, defects are reduced and only appeared at the border of sleeve. Thickness reduction or unfilling defect appeared at pin refilling zone (PRZ) on joint surface. The microstructure in this joint divided in sleeve stirring zone (SSZ), thermos-mechanically affected zone. Carbon fiber and polyetherimide laminate showed long circular fibers because of stacking sequence. Also, the maximum and minimum tensile shear force were about 1600 N and 1250 N at rotating speeds of 1200 rpm and 800 rpm, respectively.

Goncalves et al. [129] studied the improvement of friction welding joining polyamide 6 and polyamide 66/ carbon fiber laminate. There were two conditions in this work. Rotation speed and depth of penetration were fixed at 1500 rpm and 3.8 mm, respectively. Diameter of clamping was 14.5mm in condition A and 22 mm in condition B. The results showed that maximum temperatures were 280 ºC and 352ºC, respectively. Microstructure cross section in condition A had depth 3.08 mm, while in condition B it was only 0.74 mm. The corresponding tensile shear forces were 1323 N and 2196 N in condition B. Bolouri, et al. [130] studied new design of joining aluminum alloy Al 1050 and carbon fiber with 50% fiber with FSSW. Rotating speed was varied in the range of 2500 rpm-3000 rpm and joining time and dwell time were 4 s and 2 s second, respectively. Plunge depths were in the range of 0.8 mm - 1.0 mm and average temperature was increased from 310 ºC to 400 ºC by increasing rotating speed from 2500 rpm to 3000 rpm. Changes of the feed rate and plunge depth of pin affect joining temperature. The joint between aluminum and carbon fiber was

unsuccessful at plunge depth of 0.75 mm. Increase of plunge depth to 1.25 mm resulted in successful joint. Also, increase of plunge depth from 1.25 mm to 1.30 mm enhanced lap shear strength from 230 N to 241 N. Interlocking between aluminum and carbon fiber increased the performance of joint and shear force showed brittle fracture in the joint. Rafiei et al. [131] investigated the mechanical properties of dissimilar friction welding of aluminum (AA5052)-magnesium and aluminium (AA2024)- copper. The processes parameters were rotational speed 1,250 rpm and feed rate 160 mm/min. The hardness was low in heat-affected zone and thermal-mechanical affected zone (TMAZ) due to welding defects such as hook defect. Khosa et al. [132] evaluated the effect of thermomechanical during FSSW of AA6082-T6. The result showed that the effect of temperature on the microstructure and mechanical properties was severe due to the deformation and material flow of welded sample. Kubit et al. [133] studied additional sealant interlayer in AA7075-T6 alloy. The obtained results show that the joint properties of weld joint could be improved by optimal thickness of interlayer. Sadoun et al. [134] evaluated the effect of interlayer in dissimilar aluminum AA2024 and AA7075 alloys. The obtained result showed 18% improvement in joint strength due to grain refinement compared to without interlayer joint. Abed et al. [135] proposed the effect of FSSW of aluminium alloys of AA6061-T6 with copper interlayer and found that the increase of dwell time and plunge depth was beneficial to the formation of joint and directly increased tensile shear load. Joint formation was improved with cupper interlayer addition and this improvement could be related to the increase of bonding area and intermetallic compound from the reaction of metal and interlayer. High load fracture occurred in cupper interlayer rather than those without interlayer. Dedeoğlu and Güler Özgül [136] studied the joint properties of similar aluminium alloys AA5754 by FSSW and evaluate their microstructure and mechanical

performance. The plunge depth and dwell time were fixed at 1.6 mm and 6 s, respectively. Rotational speed varied from 1350 to 2530 rpm. The maximum tensile shear load and micro hardness were 1.35 kN and 92.2 HV, respectively at 1850 rpm. Suresh et al. [137] investigated the influence of the different rotation speed on the mechanical properties of the AA7075-T6 and Al_2O_3 . The dwell time was fixed at 10 second, whereas the rotational speed were varying from 900-1700 rpm. The results show that high lap shear load was obtained at 1300 rpm and low value was at 900 rpm. On the other hand, high rotational speed more than 1500 rpm, the results in excessive heat generation in stir zone. Also, microhardness value was low for the joints more than 1300 rpm, due to increased heat generation. The high heat lead for the grain growth. Nasir et al. [138] evaluated the effect of rotational speed and dwell time on the microstructure and mechanical performance of dissimilar AA 5754 and AA7075-T651 by friction stir spot welding. Rotational speed and dwell time vary in the ranges of 1000 rpm-1400 rpm, and 2 second-5second respectively. The maximum tensile shear force were 806.3 N at 1000 rpm and 2 s dwell time. The material become soft at 1400 rpm compared to lower speed of 1000 rpm. Suryanarayanan and Sridhar [139] investigated the effect of processes parameters in pinless FSSW of AA5754 and AA6061. The results show that shoulder diameter was the most significant parameters followed by rotational speed, and dwell time. In the microhardness profile the highest value was obtained at nugget zone and created by the formation due to dynamic recrystallization. The microstructural showed the formation of fatter fragmented hooks at the bonding region in nugget region and typical hook at the heat affected zone as shown in Figure 10.

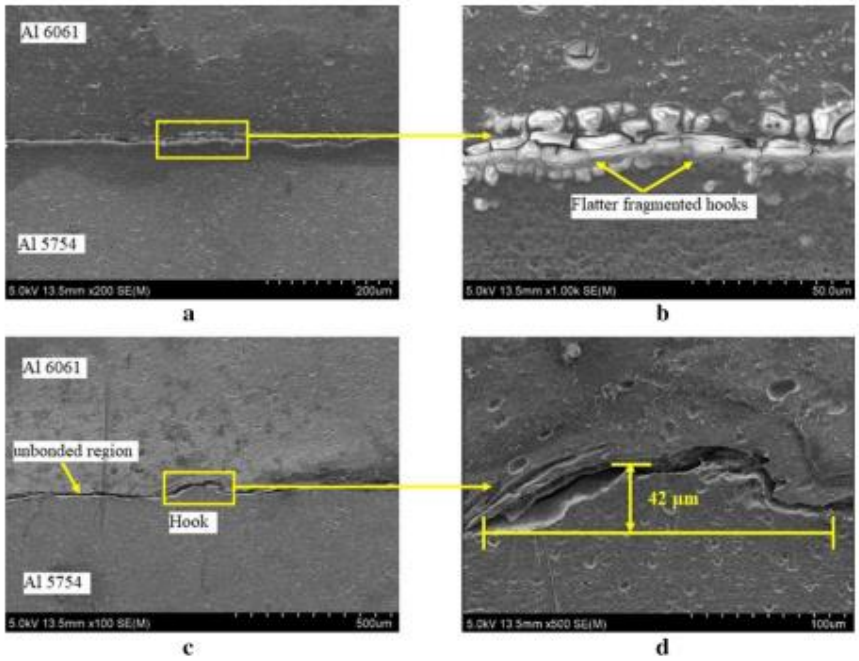

Figure 10: Formation of hooks at the weld interface [139].

Li, Chu et al. [140] evaluated the microstructure of A2198-T8 were lap-welded with probeless friction stir spot welding. Dwell time and rotational speed vary in the ranges of 3 second -15 second and 600 rpm-1500 rpm, respectively. The results show that tensile shear strength had maximum value when the dwell time extension from 3 second to 6 second about 92%, whereas dwell time over 9 second the hook defects extends and decrease the tensile. The dwell time and rotational speed significant effect on tensile shear strength but the plunge depth has minimum effect. Pathak et al. [141] studied the of mechanical and microstructure performance of welded AA 5754 sheets by friction stir spot welding. In this study were considering different welding parameters such as tool rotational speed, plunge depth and dwell time with two different pin design tools (circular and tapered). In FSSW-C weld, peak temperature was around 380 ºC at a tool rotation of at 2000 rpm. Similarly, in FSSW-T weld, maximum temperature was 350 ºC at a tool rotation of 2000 rpm. They reported that lap shear load 4.3 kN with tool rotational speed 2000 rpm with circular tool and

decreased with low tool rotational speed. The highest microhardness was achieved in stir zone SZ. The circular pin made large area of dynamic recrystallized SZ compared to those made by tapered pin.

Researchers at Helmholtz-Zentrum Geesthacht (Germany) introduced and patented refill friction stir spot welding (RFSSW) in 1999 for joining two or more sheets made of lightweight materials like Al and Mg alloys in lap configurations [142]. Joint was prepared by plasticization and material displacement in a process to be welded. The most important advantage of (RFSSW) is the lack of keyhole structure in the weld where the welding flow on the surfaces of original sample. According to Figure 6, the tool applied in RFSSW comprised an inner pin, a sleeve and an outer stationary clamp ring. Clamping ring firmly held workpieces in contact throughout welding and prevented the sheets from separating and lifting when plasticized material was displaced by sleeve and pin [143-145].

Using one single motor, pin and sleeve rotated at the same speed and along the same direction and were independently moved on the top and down by different actuators. RFSSW process is more complicated than conventional FSSW, and, depending on the plunging component, could be classified into sleeve plunge and pin plunge variants. Schematic diagram of sleeve plunge variant is shown in Figure 10. Firstly, sleeve was plunged into workpiece to a previously calculated depth for material plasticization while pin moved upward to form an accurate cylindrical cavity for the accommodation of the plasticized metals squeezing out by sleeve. Once a fixed dwell time is passed, pin and rotating sleeve returned to their original locations and extruded the softened materials inside joint creating a spot weld with zero or minimum surface indentation. The sleeve plunge variation over pin plunge variant was its highly strong weld because

of greater nugget size. However, this variant demanded higher plunge forces [144,146-149].

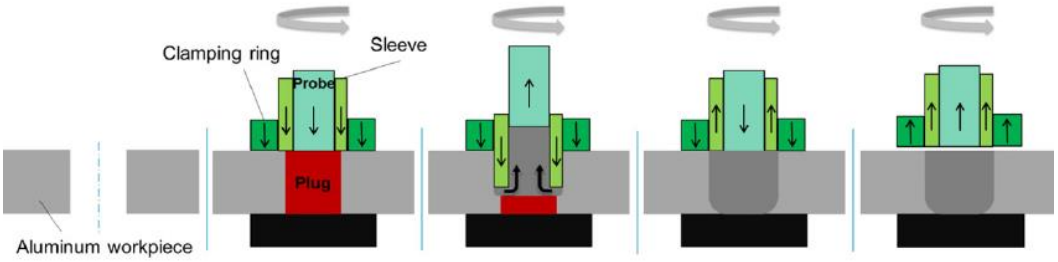

Figure 11: Schematic diagram of RFSSW [150].

RFSSW process showed high tensile shear load compared to resistance spot welding and normal friction stir spot welding, with joining times of almost similar to the latter [151]. Also, RFSSW has some advantages such as the ability to join lightweight materials including polymers and Mg and Al alloys [152], and dissimilar pairs such as polymers to metals and ferrous metals [153-155] to non-ferrous metals [156,157]. RFSSW has been successfully applied including fabrication of skin stiffened panels [158], filling of keyholes resulting from FSW, rivet or fastener replacement, RSW replacement, repairing fatigue cracks, and as a tacking welding method for FSW [159].

When tool pin is penetrated into bottom sheet, it contributes to bond formation providing mechanical strength. At the rotational speed of 2000 rpm, the numerically obtained velocity field of the material just under tool pin is about 50% of that beneath the shoulder. It is noteworthy that the bottom of pin has a certain distance from the bottom of shoulder and therefore its contribution remarkably enhanced. With the increase of pin length, its role in total velocity field is increased. At a critical length, pin increases weld zone size and improves weld joint strength [160]. At pin lengths beyond material flow zone formed by the shoulder, strength could be decreased

because of excessive plunging resulting in the extrusion of a portion of bottom sheet significantly decreasing the thickness of bottom sheet under the pin [161-163].

Threads in RFSSW are generally machined on pin and sleeve to decrease the contamination of interfaces among three tool components [164]. Ji et al. [165] applied a 3D finite element model to study grooved sleeve effects on the flow of materials and concluded that grooved sleeves increased the velocity of material flow and grooves on the inner walls of sleeves outperformed grooves with lower widths on the outer walls of sleeves. Scrolled grooves were more favorable than concentric circular grooves at the bottom of sleeves in decreasing the thickness of bonding ligament and increasing the area of bonding. Pabandi et al. [166] studied RFSSW of aluminum alloy AA5252 with short carbon fiber polypropylene (PP-SCF) and applied 500 rpm -2000 rpm rotating speed, 5 s dwell time. A cylindrical tool from heat treated H13 steel composed of a shoulder with a diameter of 20 mm was employed as the welding tool. They found that optimal shear tensile was 350 N at 2000 rpm and the high hardness were 68 HV in 500 rpm, as shown in Figure 11. Temperature evaluation was measured at various distances from the center of joint and the maximum value was found to be 340 ºC 10mm from joint center. SEM images showed 15μm at the interface reaction layer and it seemed that the layer was formed by erosion mechanism. Also, a reaction layer was created between aluminum and molten polymer and was re-solidified inside the hole, as illustrated in Figure 12.

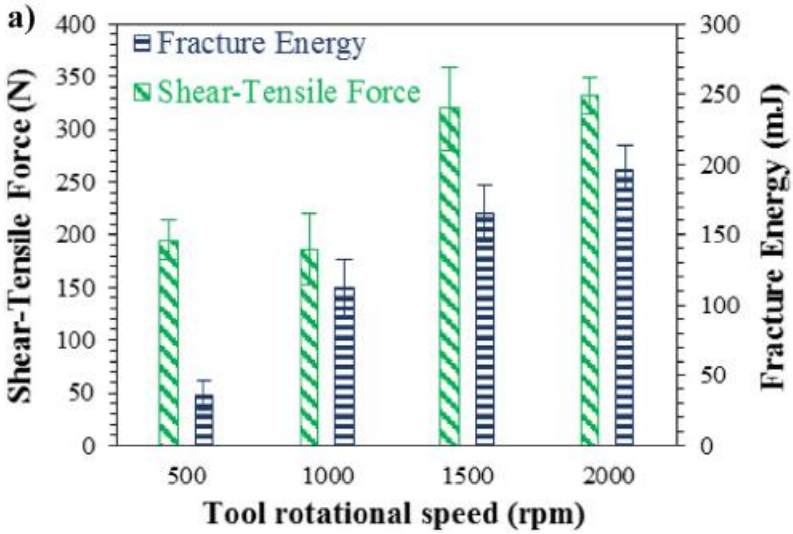

Figure 12: Hardness and crystallinity percentage at differnt rotating speeds [166].

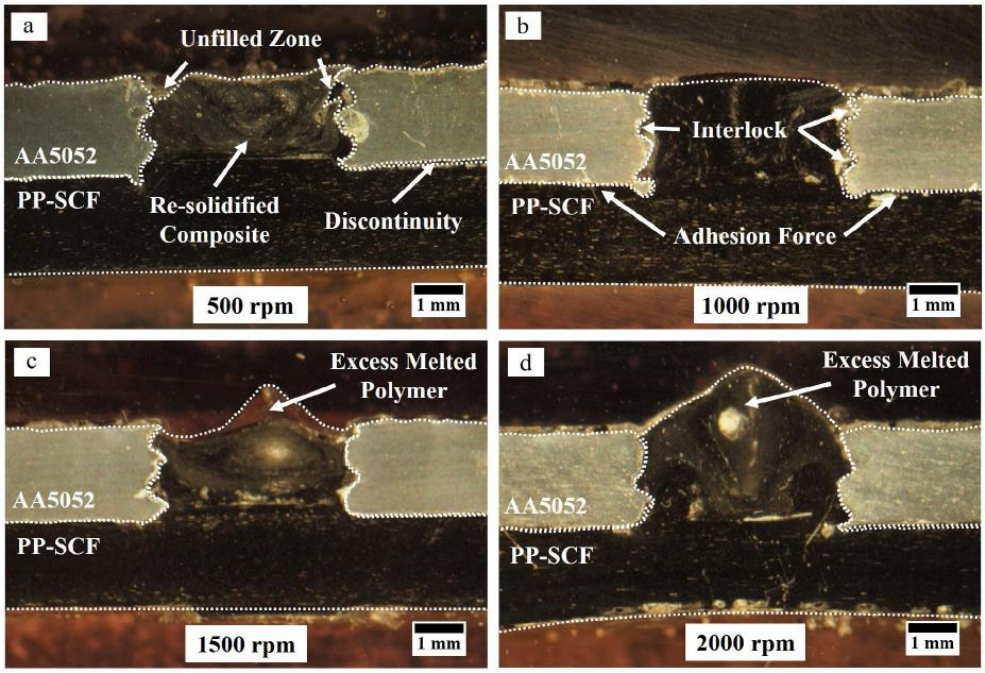

Figure 13: Cross section at different rotating speeds (a) 500 rpm , (b) 1000 rpm , (c) 1500 rpm , (d) 2000 rpm [166].

Ashong et al. [167] studied the RFSSW of dissimilar carbon fiber and AA6014 alloy. Join was created at 1000 rpm rotating speed, 1.5 s joining time and 1.9 mm plunge depth. The results showed that average tensile shear force was 1.63 kN and joint efficiency was 10%. Microscopy of carbon fibers and aluminum showed tight bonding on the interface of joint with no visible defects. The current work has compared the

obtained results with those of other joints after surface treatment and found that refill friction spot welding suitable method for manufacturing metal polymer hybrid production. Micro mechanical and chemical interlocking were main in tensile shear force.

Table 3: Summary of research works performed on FSSW and RFSSW of carbon fiber with materials

No.	Type of material And thickness in (mm)		Type of welding	Parameters					Temperature process °C	Tensile Shear Load (N)	Type of sample	Ref.
				Rotational speed (RPM)	Joining time JT(s)	Plunge depth PD(mm)	Joining pressure JP(MPs)	Dwell time (s)				
1	CFRP /8	AZ-31 /12	FSSW	900-3000	3 - 8	0.25 - 1.75	2-3	-	400 - 440	1500	Single Lab Joint	[126]
	CFRP /2.1			900-3000	4 - 8	0.25 - 0.35	2.4-3			2000		
2	CFRP /2.17	AA2024-T3 /2	FSSW	1900	4.8	0.5	-	-	350	950.6	Single Lab Joint	[117]
				2900	4.8	0.5	-		400	1254		
3	CFRP /2.17	AA6181-T4 /1,1.5	FSSW	1200	1	0.75	1.15	-	-	2107-3523	Single Lab Joint	[118]
				1400	4	1	6	-	-	3241-3254		
				1600	7.5	1.15	8.3	-	-	3153-3248		
4	CFRP 2.17	AA7075-T6 /2	FSSW	1900	4	0.8	-	-	331	2500	Single lab Joint	[119]
5	CFRP /2	polyamide 66 &2	FSSW	3000	7.5	2	12 KN	-	266	-	Single lab Joint	[127]
6	CFRP /2	polyamide 66 laminate &4	FSSW	1500	-	-	-	2	280	1323	Single lab Joint	[129]
				1500	-	-	-	8	352	2196		
7	CFRP /2	AA6014 /2	RFSSW	1000	1.5	1.9	-	-	-	1630	Single lab Joint	[167]
8	CFRP /2	AA1050 /2	FSSW	2500 - 3000	4	0.8	-	2	310 - 400	230-241	Single lab Joint	[130]

9	CFRP /2	PEI laminate	FSSW	800-1000 - 1200	-	2.2	-	2	-	Max 1600	Single lab Joint	[128]
10	CFRP /2.17	AA2024-T3 /2	FSSW	2900	4	0.8	0.3	-	345 - 474	5459-8264	Single lab Joint	[124]
11	CFRP /2.17	AA2024-T3 /2	FSSW	1900	4	0.8	0.3	-	360	2093-708	Interlayer (100 -500) μm	[122]
12	CFRP /3	AA5182 /1.2	FSSW	3000	1, 2, 5	1	-	-	200 - 250	4100,5500,7100	Single lab Joint	[123]

2.3 Friction Stir Welding (FSW)

The section described friction stir welding (FSW) technique in more detail, since the main goal of this work was to investigate this technique. The Welding Institute (TWI) first introduced FSW in 1991 in UK [168-172]. As discussed in introduction section, FSW was first developed for welding similar materials, such as AAs and other light alloys [173], but it can also be applied for joining dissimilar materials [174,175]. This method has been applied in a wide variety of industries such as automotive, aerospace and maritime industries [176,177]. In aerospace industry, this method could be employed in producing thin alloy skins, fuel tanks and airframes [178] and contains all major European manufacturers of airframe and some research Institutes address FSW problems [179,180]. Therefore, material is softened and mixed. With the progress of tool, joint is cooled and consolidated [181,182]. It should be noted that tool material has to be more resistanted compered to samples to be welded [183]. A schematic diagram of the technique is depicted in Figure 13.

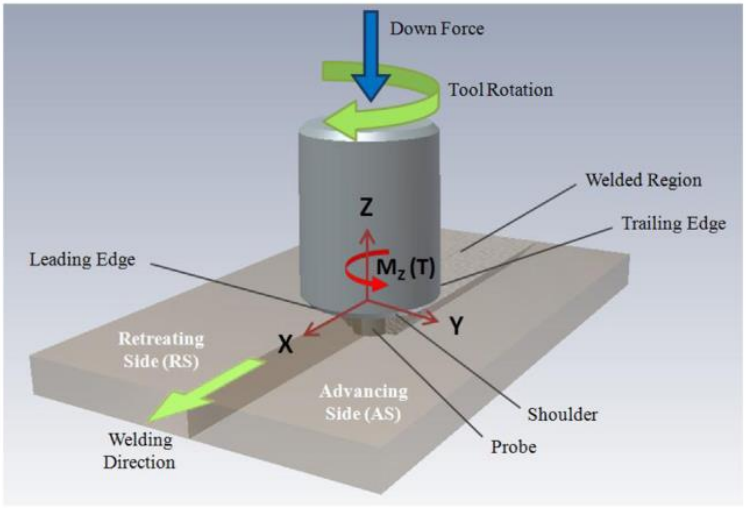

Figure 14: Schematic diagram of the FSW processes [177].

Key technique parameters included feed rate, shoulder penetration, applied force, rotational speed and tool geometry [184-186]. Tool geometry refers to pin shape (tapered or simply cylindrical) and the diameter of pin and tool [187]. The key advantage of FSW is that it does not need to reach component melting points. Therefore, the developed residual distortions and stresses are significantly lower than other common welding methods [188-191]. It also has other advantages including non-consumable tool nature, joint resistance to corrosion and no need for filler materials. The most important drawback of FSW is that to date, no special equipment has been developed for FSW [192]. The reason for this was that FSW is a novel method and has not been fully investigated yet [193]. The existing methods were not effective in welding some aluminum alloys AAs and therefore, other methods, such as FSW were investigated [194,195]. Krasnowski et al. [196] studied the effect of the geometry of tool on FSW welding of Al 6082. Among the three tool types which were applied, the best results were achieved for conventional and Triflute tools. Figure 14 presents the 3 different models of tools employed in this work.

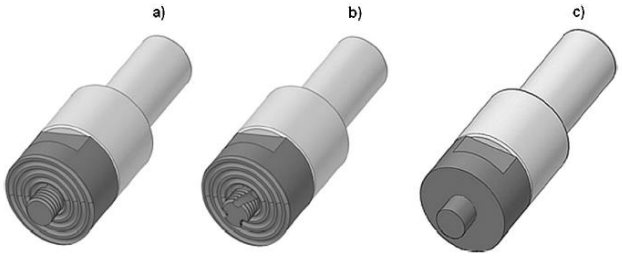

Figure 15: Tool geometries: a) conventional; b) triflute; c) simple [196].

In Honda Accord model 2013, stamped steel engine cradle and cast aluminum were joined using this method [197]. In this particular example, a remarkable innovation was the application of a C-frame linear FSSW exerting total axial load on the tool to avoid the necessity of using extremely high load capacity and stiff fixtures and robots for applying axial force on the tool. Another critical point in the method devised by Honda was the application of a sealant to prevent crevice corrosion during field operations. However, limited details are available on the mechanical characteristics of the joints created using this method [198,199]. Haghshenas et al. [200] showed that in which an H13 steel tool heat treated and has good resistance to thermal fatigue, erosion and wear, and is widely used for making molds and dies . It is noteworthy that other works involving adhesive and diffusion bonding have shown decrease of the thickness of intermetallic compound regions or reaction layer increased joint strength [201,202]. Welding parameters also significantly affected weld temperature [203], heating rate, weld integrity [204] and hook geometry.

Meanwhile, a great fraction of energy was dissipated into adjoining heat sinks and percentage limited amount of the energy generated was needed for the formation of SZ decreasing energy efficiency. Hence, the rotation speed of the tool had to be increased to enhance heat input and decrease welding time to make it comparable to RSW and make the axial force of tool compatible with the available welding robot

capabilities [205-207]. Another key parameter is dwell time which supplies the energy needed for the formation of lower and upper stir zones in sheets [208-210]. In metals which have higher melting points, longer dwell times are required for significant increase of heat input to obtain the temperature needed for plastic flow. In addition, contributions of power input and dwell time are remarkably decreased when a quasi-static state is reached, because torque and axial force are remarkably decreased in dwell period [211,212].

An axial force is applied by the shoulder onto the top surface of workpiece to create the forging action required for welding consolidation, constrain plasticized metals around the tool pin [213-215]. It was found that the generation of heat under the large area of the shoulder of the tool was a dominant characteristic in FSW [216-218]. Huang et al. [219] studied friction stir welding of aluminum alloy AA 2060-T8 and carbon fiber reinforced poly-ether-ether-ketone (SCF/PEEK). The tool contained a stationary shoulder, a rotational shoulder and a tapered thread pin with the triple facets. Rotating speed varied from 1400 rpm to 2000 rpm and dwell time was in the range of 10 s to 15 s. The results showed that maximum shear force was 1550 N for 1600 rpm, as illustrated in Figure 15. Also, hardness was decreased with the increasing of rotating speed, as showed in Figure16.

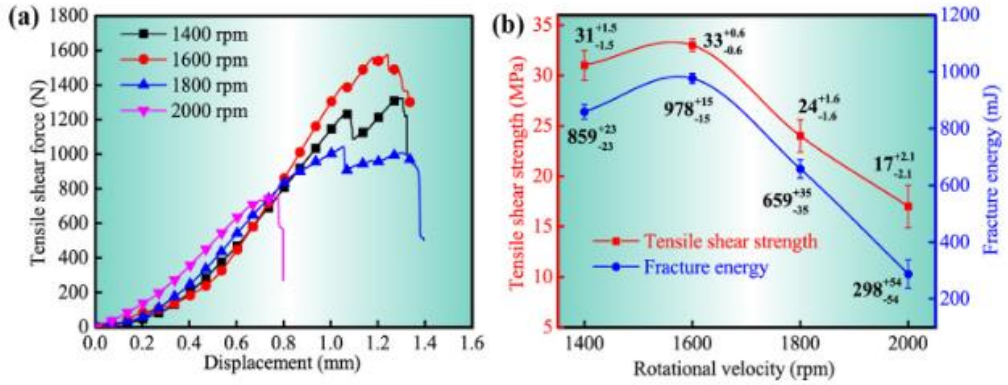

Figure 16: (a) Tensile shear force in differnt distance (b) Tensile shear strengh of hybrid joints at differnt rotating speed [219].

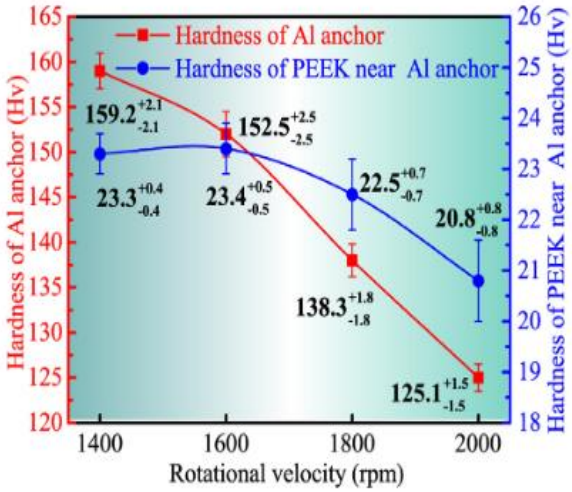

Figure 17: Hardness of typical locations for Al anchor [219].

At the rotating speed of 1600 rpm, increase of frictional heat improved plasticized material transfer and eliminated cavity defect. Surface pre-treatments needed to be evaluated for further increasing of the strength of interfacial joining between thermoplastic and material. Also it is difficult to transfer the heat input by tool rotating speed from the top to the bottom plate due to low thermal conductivity of the SCF/PEEK (0.92 $K/m^{-1}k^{-1}$), Therefore, the partial spin pin only comes into contact with the AA2060-T8 and then produces low friction heat, as a result of large aluminium anchor. Das and Bang [220] performed numerical and experimental tests on the joining of aluminum alloy AA5052 and carbon fiber with polyamide 66 CFRP.

In this study, rotating speed and plunge depth were fixed to be 400 rpm 0.2 mm, respectively. For temperature evaluation at different joining speeds, the experimentally obtained peak temperatures were 474.2 K and 486 K with 0.8 mm/s and 1 mm/s, respectively, but corresponding numerically obtained values were 474.2K and 463.5 K at the same joining speeds which was due to decrease in peak temperature attributed to the reduction of heat generation in length joint according to increase joining speed. Bang et al. [221] studied friction stir welding of aluminum alloy AA 5052 and carbon fiber-reinforced plastic CFRP. In this study, pinless tool at 400 rpm rotating speed and 0.2 mm plunge was used. The results showed that maximum shear force was 2000 N and strength was 8 MPa. Aluminum surface as locking material to interlock molten carbon fiber into aluminum to improve the strength joint. Nagatsuka et al. [222] investigated the joining of carbon fiber-reinforced plastic CFRP with aluminum alloy AA5052 by friction stir welding. In the first case used AA5052 as received (unground) whereas the second case use wet grinding with 800 emery paper (ground) .The results showed that the tensile shear force of unground aluminum /carbon fiber was 1 KN while that of ground aluminum and carbon fiber was increasing significantly and reached 2.9 KN. The maximum temperatures for ground AA 5052 and CFRP were 760K and 725 K at joining speeds of 100 mm/min and 1600 mm/min, respectively, and fixed plunge depth of 0.9 mm. With the decrease of join speed, the concave downward deformation of aluminum which was pressed against underlying carbon fiber increased tool passed zone. Hunag et al. [223] improved the mechanical properties of joins of aluminum alloy AA2060-T8 with short carbon fiber-reinforced PEEK (SCF/PEEK) by friction stir welding. The bonding mechanisms can be divided in to: electrostatic force for chemical bonding, mechanical interlocking and physical interaction .In this study, they applied different rotating speeds from 1400 rpm up to

2000 rpm and used taper screwed pin at plunge depth of 0.2 mm. The results showed that maximum micro hardness was 22.6 HV at 1400 rpm, but tensile shear strength was 18 MPa at 1600 rpm. Microstructures at different rotating speeds are illustrated in Figure 17. Also, this type of tool has huge advantage to improve.

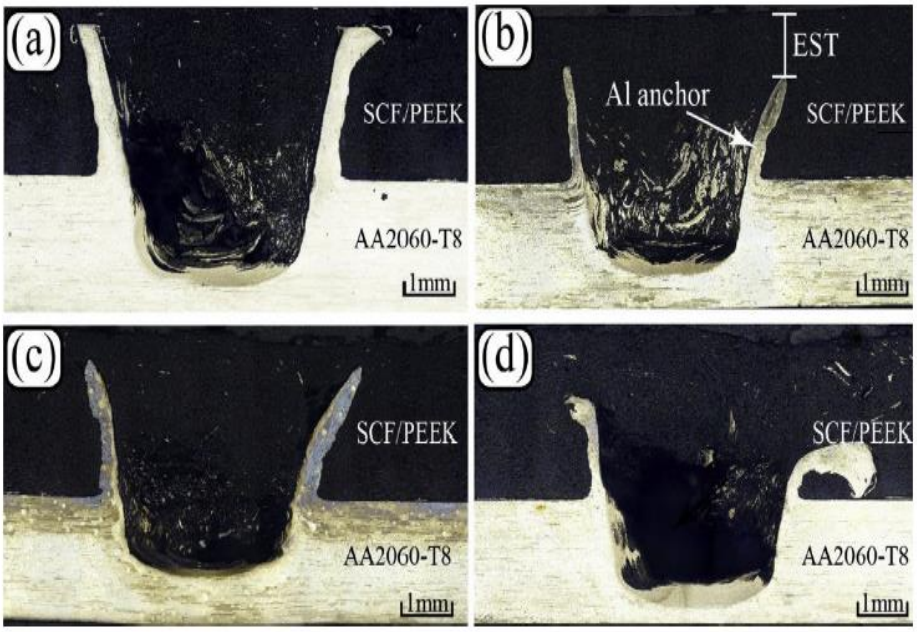

Figure 18: Microstructures at : (a) 1400 rpm (b), 1600 rpm (c) ,1800 rpm ,(d) 2000 rpm [223].

Franke et al. [224] investigated solid state of aluminum alloy AA 6061-T6 and carbon fiber via friction stir welding. Rotating speed was varied in the range of 1200 rpm - 2500 rpm and plunge depth was in the range of 0.2 mm-0.6 mm. The tool made from H13 steel. Infiltration distances of aluminum into carbon fiber bed were measured using the cross-sectional images of samples which showed that the plasticized aluminum was modeled as a highly viscous fluid. FSW can melt and displace polymer matrix, plasticize metal constituent, and force it to flow around the fibers. Wu et al. [225] investigated the mechanical properties of oxygen-free copper and carbon fiber CRFTP. The rotating speed was varying from 600 rpm to 2000 rpm and plunge depth

was 0.9 mm. Temperature was measured at the center of sample, 7.5 mm from retreating side (RS) and advancing side (AS) and 15 mm from retreating side (RS). The results showed that temperature was 550 ºC, 430 ºC, 450 ºC, and 360 ºC respectively at 1500 rpm. Maximum tensile shear force was achieved at 1500 rpm. Joint parameters were enhanced from 0.89 kN -2.25 kN to 1.71 kN -3.54 kN by tool offsetting. During the process, increase of rotating speed, increased peak temperature. Higher thickness of re-solidified zone with more bubbles could be due to higher rotation speeds and temperatures. Bubble generation could be described by the fact that when tool was plunged into cupper, carbon fiber in the some specific regions was melted under tool downforce. For high quality of copper /carbon fiber welding joint with high tensile shear force and low number of bubbles, tool offsetting is a good choice, as illustrated in Figure 18.

Wu et al. [226] investigated the direct joint of and oxygen-free copper by FSW. Rotating speed was fixed at 1500 rpm and plunge depth was 0.9 mm. Maximum temperature was 350 ºC and tensile shear force was 2.3 kN which was mainly affected by joining area. The large number of bubbles was created due to melted zone, thermal decomposition of plastic, or air and water vapor. Large joining areas with small degradations generate small number of bubbles. Wang et al. [227] investigated FSW of AZ31 magnesium sheet and thermoplastic carbon fiber-reinforced polymer. The tool was made of steel H13 with thread pins. Tool (A) pin length was 2.1 mm with shoulder of 18 mm and tool (B) was 2 mm long with 12.7 mm shoulder. Rotating speed was varied from 800 rpm to 1200 rpm. More heat generation at high rotational speeds improved material flow around tool pin. The results showed that average load was 1.87 KN. Maximum micro hardness value was 69.9 HV on base AZ31, stir zone 57.5 HV

and unmodified interlock 59.3 HV. Choi et al. [228] investigated the feasibility of FSW on pure titanium and carbon fiber. Rotating speed was varied from 50 rpm to 300 rpm at 0.9 mm plunge depth. Argon was applied to avoid oxidation during FSW. Maximum temperature was about 600 °C and tensile shear strength out of stir zone was 7 kN. Titanium and carbon fiber could be completed welded due to sufficiently high friction heat input during FSW, as shown in Figure 19.

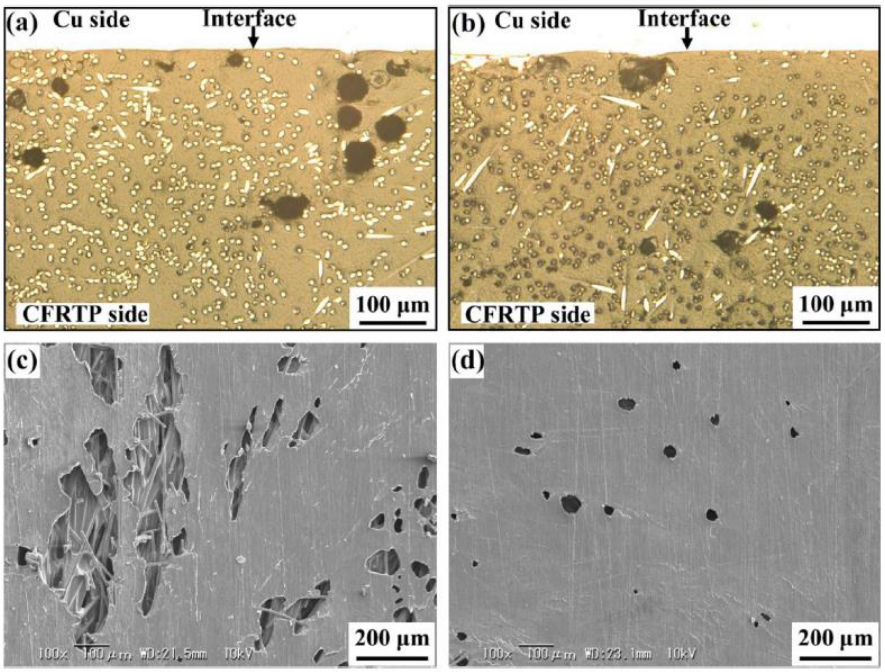

Figure 19: Bubble comparison normal at differnt rotating speeds and cross sections (a) normal friction lap joint at 1500 rpm, (b) offset joins at 1500 rpm, (c) normal joint at 2000 rpm (d)offset joint at 2000 rpm [225].

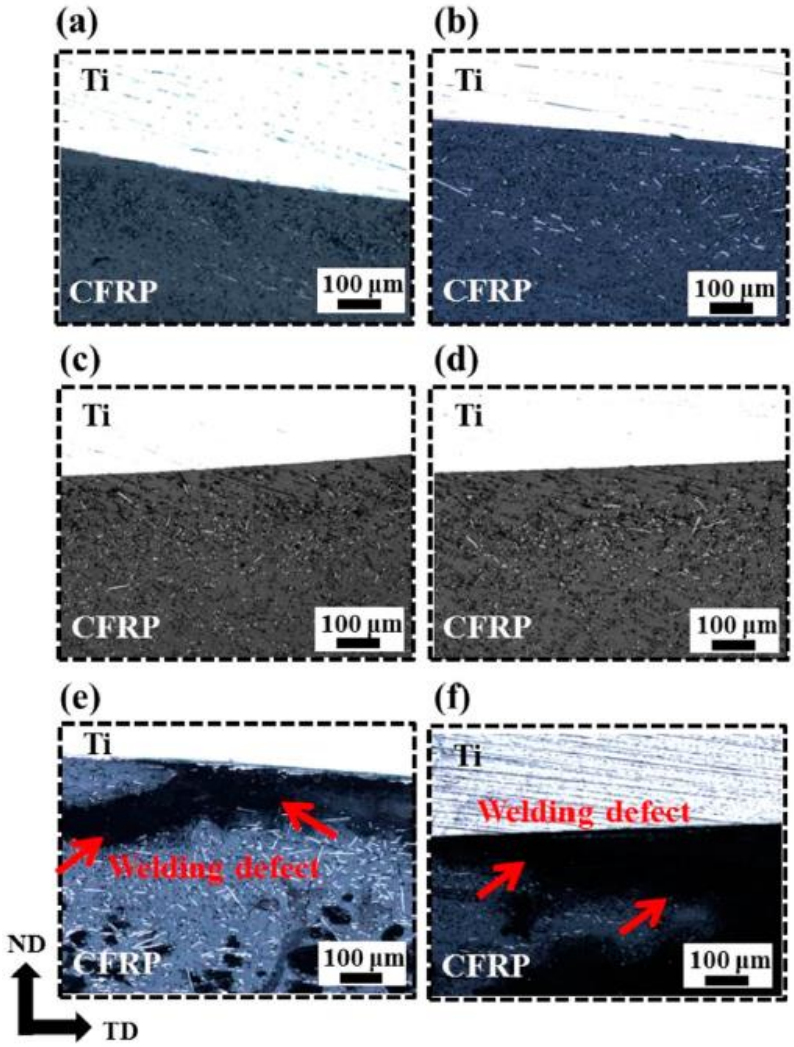

Figure 20: Cross sections of titanuim and carbon fiber at rotational speeds of (a) 100 rpm ,(b)125 rpm, (c)150rpm, (d) 175 rpm,(e) 200 rpm, (f) 300 rpm [228].

Lambiase et al. [229] studied FSW of carbon fiber and polycarbonate at 0.25 mm plunge depth and 6000 rpm rotating speed. The results showed high mechanical strength of up to 12 MPa and average temperature of about 300 ºC. The joints showed delamination failure between the first and second plies of carbon fiber. Joints with low plunge depths showed high strength but low absorbed energy. Lambiase et al. [230] investigated the joints of carbon fiber and amorphous polymers formed by FSW. Rotating and joining speeds were varied in the ranges of 2000 rpm-6000 rpm and 10 mm/min-40 mm/min, respectively. Only one joint was succeeded at 4000 rpm and

20mm/ min and the others failed between stirred region and polycarbonate base and maximum strength was 17 MPa under optimal conditions.

Table 4: Summary of research on FSW CFRP with material

No.	Type of material And thickness in (mm)		Parameters			Temperature process °C	Shear force (N)	Type of joint	Ref.
			Rotational speed (RPM)	Dwell time (s)	Travel speed				
1	CFRP /3	AA2060-T8 /2	1400	10 - 15	30 mm/min	-	1250	Single Lab Joint	[219]
			1600			-	1550		
			1800			-	700		
			2000			-	1000		
2	CFRP /1.5	AA5052 /1	400	-	0.8-1 mm/s	213-210	-	Single Lab Joint	[220]
3	CFRP /3	Oxygen-free Cu/2	1500	-	600 mm/min	≃ 450	2300 - 3600	Single lab Joint	[225]
4	CFRP - PA66/1.5	AA5052 /2.5	400	-	0.6-1 mm/s	-	2000	Single lab Joint	[221]
	CFRP /1.5	AA5052 /1							
5	CFRP /3	AA5052 /2	2000	-	100-1600 mm/min	452 - 487	600 - 4300	Single lab Joint	[222]
6	CFRP /3	Oxygen-free Cu/2	1500	-	200-1600 mm/min	350	2300	Single lab Joint	[226]
7	CFRP /3	AA2060-T8 /2	1400	15	30 mm/min	-	-	Single lab Joint	[223]
			1600						
			1800						
			2000						
8	CFRP /2	AZ31/2.3	800, 1200	12	250 mm/min	-	1870	Single lab Joint	[227]
9	CFRP /2	Pure Ti/2	50-300	-	100 mm/min	600	7000	Single lab Joint	[228]
10	CFRP /1.5	Polycarbonate /3	2000 - 6000	-	10-100 mm/min	180-260	-	Single lab Joint	[230]

2.4 Comparison of Friction Stir Spot Welding and Resistance Spot Welding for Aluminium

Resistance spot welding RSW is able to join multilayer aluminium stacks comprising individual sheets from 0.9 mm to 4 mm in a wide range of alloys and the external surfaces are relatively smooth and flat on both sides of the joint. The weld button

revealed after a joint stack has been peeled apart .The majority of spot welding guns presently employed in the automotive sector use pneumatic actuators to apply the electrode force. However, many new installations have installed electric servomotor actuators eliminating the need for pneumatics on the assembly line. These servo guns offer faster cycle times by improved control of the aperture and closing speed. The joint of dissimilar aluminuim and steel were development of Medium Frequency Direct Current welding power supplies, which offer significant process control improvements over 50/60Hz Alternating Current . On the other hand Friction Stir Spot Welding (FSSW) is a relatively new discrete process derived from the continuous friction stir welding method. The process promises significant cost advantages in terms of simple equipment, minimal consumables and low power consumption. Most of the research published so far has focussed on two-layer joints .The effect of different tool designs and process parameters is being investigated by a number of research centers. Dissimilar material joints such as aluminium to steel and aluminium to magnesium have also recently been reported.

An RSW gun designed for welding steel is unlikely to provide enough current or electrode force for welding aluminium however, a RSW gun designed for welding aluminium can be fully capable of welding steel. This configuration offers the valuable flexibility of being able to spot weld both steel and aluminium components using the same equipment. To fully optimize the process for either material would simply require a changeover of electrode geometry and adoption of a slightly different electrode maintenance strategy. FSSW joints uses a low amount of energy per joint and is an attractive process for applications where many similar joints are required in thin materials e.g. closure panels. If the problems of long process time in thicker

materials, limited tool flexibility and joining multi-layer stacks can be addressed, then FSSW could become a widely used process in the future. The combination of a discrete joining process with a structural adhesive to form hybrid joints offers the potential to exploit the best features from each method whilst compensating for deficiencies in the other. The ability RSW to produce a wide range of joints, both with and without the presence of adhesive, makes them attractive to manufacturing engineers. Inevitably, in a complex structure such as a vehicle body in light weight, several different joining techniques will be required. Whilst it might seem appropriate to employ numerous joining methods highly optimized for specific applications, too many techniques in a single manufacturing operation will be prohibitively expensive to install and maintain. Getting the correct balance of joining methods will be interdependent on many factors including; vehicle design, performance requirements, intended production volumes, economics, environmental concerns, repair ability and others.

It conclude that, FSSW have advantage such as joining thin materials , low running costs but have long process times for thick materials and gun flexibility while, RSW have advantage like low cost of equipment and gun flexibility and automation but have consistency remains to be proven and electrode maintenance needed.

2.5 Macrostructure and Properties of FW of Similar Aluminium Alloys

Aluminium alloys mainly used for structural components in many application such as automotive and aerospace. Some elements such as magnesium, manganese, copper and zinc are added to the aluminum alloy. The added elements provide corrosion resistance, heat treatment ability and improve mechanical properties. To decrease the heat input, friction welding was the best method compared to other choice for

aluminium alloys joints. In the microstructure and mechanical performance, many researches have been presented that aluminium and aluminium alloys give good characteristics.

Kimura et al. [231] investigated the effect of friction welding parameters on mechanical performance of AA 5052 joints. The AA5052 heat treated have different tensile properties, for example H34 has 259 MPa tensile strength whereas H112 with 188 MPa on base metal. The results presented the joint efficiency and joining time on the welding joints of both cases of AA5052. The base material of AA 5052-H112 had been fractured and obtained 100 % of joint efficiency. On the other hand AA5052-H34, the joint efficiency was less than 100 % due to a slight softening in the peripheral region and the difference in the anisotropic properties of the base material between the longitudinal and radial directions. Kimura et al. [232] evaluated the effect of friction welding parameters on the microstructure and mechanical performance of AA7075-T6 joints, by applying LHI in which the heat input is lower than that in the conventional method. The roughness and the cleanliness of the contacting surfaces are important in aluminium samples. While, decrease the rotation speed and dwell time directly effect on welding joint quality. Increase joining time and rotational speed caused for high welding zone temperature which give rise to excessive flow of material from the welding zone to the joint sides. Finally, the micro hardness does not vary across the welding zone due to the narrow heat affected zone.

2.6 Summary in Literature Review

After revising the literature review, it can be noticed a few gaps within authors researches:

- No sufficient studies about the effects of different welding parameters of Friction stir spot welding on carbon fiber as interlayer in aluminium alloys.
- There are no adequate experimental studies on welding similar aluminium with carbon fiber interlayer by FSSW process.
- In addition, Microstructure and mechanical properties behavior due to FSSW of AA 5052 on carbon fiber interlayer plates is not yet reported.

Chapter 3

METHODOLOGY

3.1 Introduction

This chapter covers the research approach in terms of materials preparation, welding setup, and investigations of mechanical behavior (tensile shear load and microhardness) and microstructure (SEM-EDS and Optical) of similar AA 5052 with and without interlayer) by FSSW weld joint. The flow chart below summarizes the experiment steps clearly in Figure 21.

3.2 Material Preparation

Aluminum alloy AA5052 plates were chosen in this study. The thick 4 mm of sheets. CFRP with thickness 0.5 mm was applied as interlayer between similar aluminum sheets. The dimension of interlayer are 25x25 mm. In current research, the average tensile strength and modulus of CFRP tendons were 2070 MPa and 156 GPa, respectively, at room temperatures. Density was 1.6 g/cm^3 and fiber content 65%. The transition temperature (Tg) and the decomposition temperature (Td) were 126 ◦C and 405 ◦C, respectively. The surface of material was cleaned using alcohol to remove contaminants that could generate oxides. The tool was rotated at high speed, then forced into workpiece until the shoulder contacted top metal surface.

3.3 Experimental Setup

The experiment has been conducted on drilling machine as shown in Figure 22. The aluminum alloy of 4 mm thick plates of AA5052 used for FSSW and 0.5 mm CFRP interlayer. Material plates are clamping with a holder. Two aluminum plates were

placed as a lap joined. The dimensions of the plate were 100 mm × 25 mm × 4 mm, based on American Welding Society standard (AWS C1.1M/C1.1:2012) [135] as showed in Figure 23.

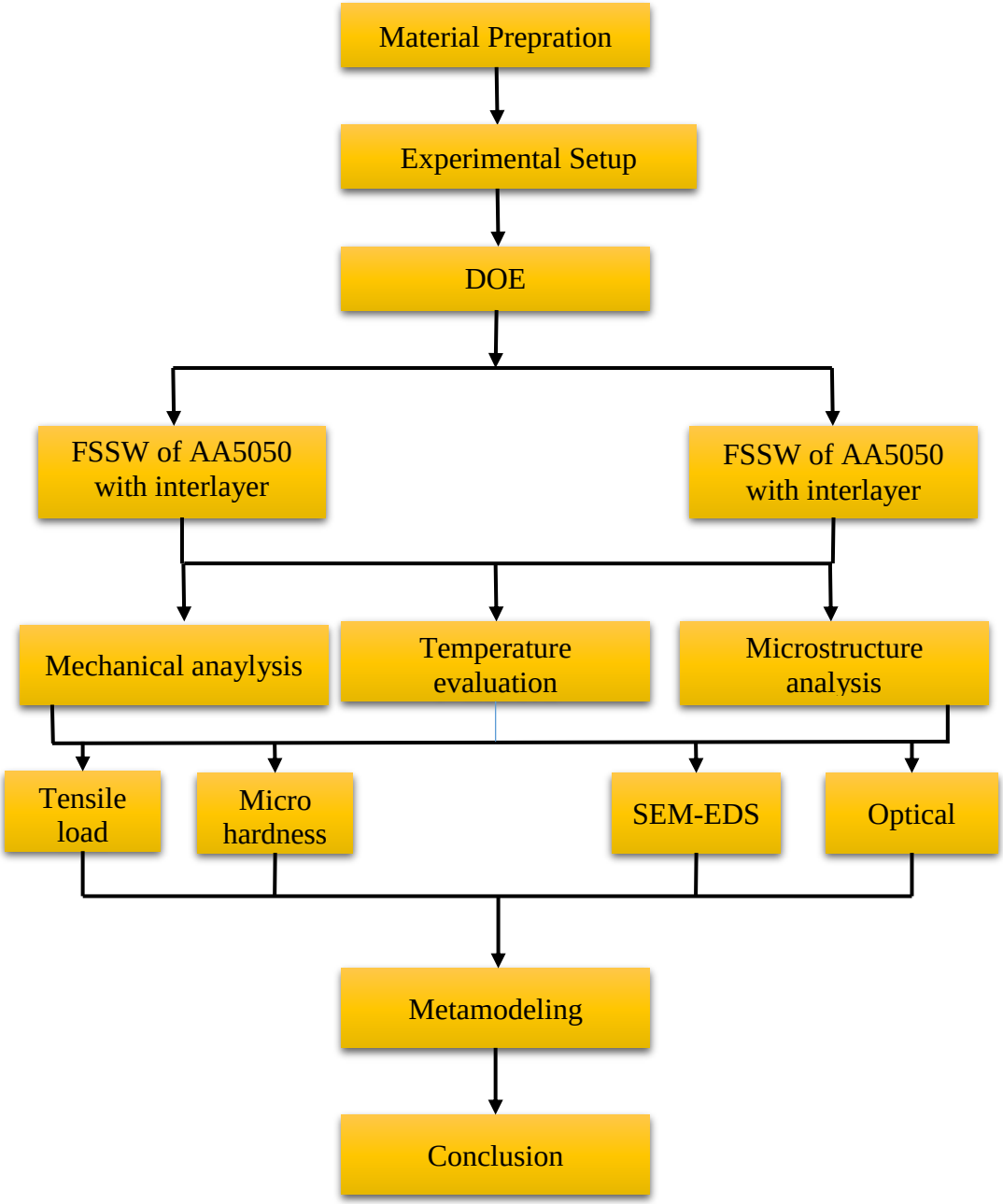

Figure 21: Research methodology process.

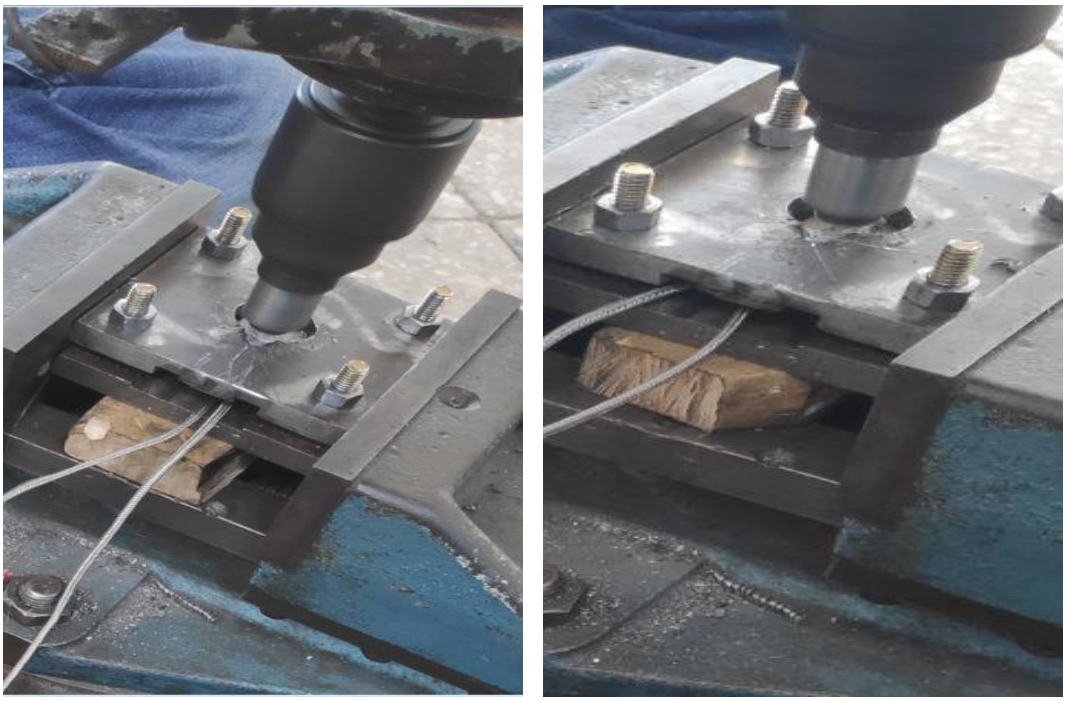

Figure 22: Drilling machine

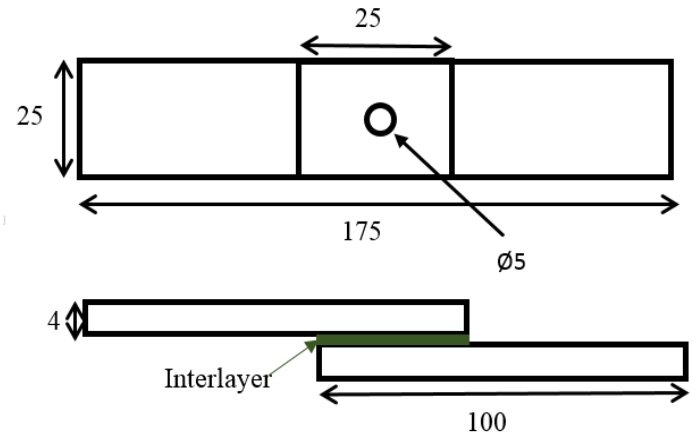

Figure 23: Schematic diagram of lab joint (mm).

In order to establish the FSSW tests, a correctly designed clamping fixture were established to fix the specimen's during the welding operation. The figure illustrates the fixture position of the specimen. Friction stir spot welding consists of three stages: plunging, stirring, and retracting, as showed in Figure 24.

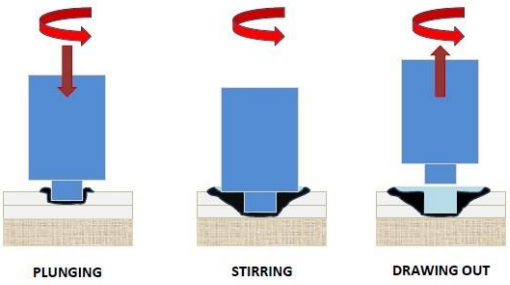

Figure 24: Friction stir spot welding processes.

The tool was made from steel alloy AISI 4340 (UNS G43400), as showed in Figure 25. The length of the pin was 6.2 mm for specimen and its diameter was 5 mm with cylindrical design. The pin length used to control plunge depth during FSSW process.

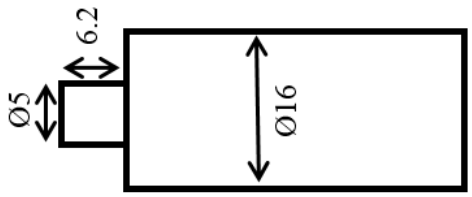

Figure 25: Tool dimension in (mm).

3.4 Full Factorial Design (DOE)

Full factorial design was selected to study the factors effect on the response (Shear load). Additionally, assuming that; factors are fixed, designs are completely randomized and usual normality assumption are satisfied. Two factors (A = rotation speed; B = Dwell time) with two levels "low" and "high" denoted by (-, +) were selected respectively.

3.5 Mechanical Test

Similar to other joining techniques, the characteristic of FSSW is steady by calculating the mechanical properties of the joint. The mechanical testing and material testing we

perform may be part of a quality assurance program, manufacturing engineering program, failure analysis or for materials research and development. In-house mechanical testing equipment is used for the following material tests such as tensile shear test and microhardness (Vickers).

Table 5: Design of experiment (DOE)

Serial Number	Rotational Speed	Dwell Time	Interlayer
1	2000	5	without layer
2	2000	5	without layer
3	1300	2	with layer
4	1300	5	without layer
5	850	5	with layer
6	1300	2	without layer
7	850	2	with layer
8	2000	5	with layer
9	850	2	without layer
10	2000	2	without layer
11	2000	2	with layer
12	1300	5	without layer
13	1300	2	without layer
14	850	2	with layer
15	1300	2	without layer
16	850	5	without layer
17	2000	2	with layer
18	850	5	without layer
19	1300	2	with layer
20	850	5	without layer
21	2000	2	without layer
22	850	2	without layer
23	850	5	with layer
24	2000	5	without layer
25	2000	5	with layer
26	850	5	with layer
27	1300	2	with layer
28	850	2	without layer
29	850	2	with layer
30	1300	5	with layer
31	1300	5	with layer
32	1300	5	without layer
33	2000	5	with layer
34	2000	2	without layer
35	2000	2	with layer
36	1300	5	with layer

3.5.1 Tensile Shear Test

Tensile testing is an important test used to determine the best type of material for a particular application. For this test the material is molded to a standardized sample type and loaded into the machine's grips. Tensile testing can give important measurements such as the ultimate tensile strength (the maximum amount of strength a material can take) and the amount of elongation that occurs before breaking. In this study according to (AWS C1.1M/C1.1:2012) as shown in Figure 26. The standard the tensile shear specimen prepared 25-mm wide and 100-mm long. The weld was creating at the center of the overlapping 25-mm region as illustrated in Figure 27. After get successful sound weld results next step to evaluation of mechanical properties. The load rate was set at 3 mm/min for all runs. The joint efficiency (η) of AA5052 with CFRP was obtained by applying the formula as below [233].

$$\text{Efficiency } (\eta) = \frac{\text{Tensile shear load of weld joint}}{\text{Tensile shear load base metal}} * 100\% \quad (1)$$

Figure 26: Universal tensile test machine (INSTRONE -3385H).

Figure 27: FSSW of AA5052 welded samples.

3.5.2 Micro Hardness

The Vickers method is based on an optical measurement system. The Microhardness test procedure, according to ASTM E384-11e1 standard as shown in Figure 28, specifies a range of light loads using a diamond indenter to make an indentation which is measured and converted to a hardness value. The hardness values for welded metals for this experiment were measured by utilizing Vickers test of 0.5 HV, force 4.903 N and dwell time 10 sec. It is very useful for testing on a wide type of materials, but test samples must be highly polished to enable measuring the size of the impressions. A square base pyramid shaped diamond is used for testing in the Vickers scale. Since the test indentation is very small in a Vickers test, it is useful for a variety of applications: testing very thin materials like foils or measuring the surface of a part, small parts or small areas, measuring individual microstructures, or measuring the depth of case hardening by sectioning a part and making a series of indentations to describe a profile of the change in hardness. Additionally, the sample preparation will need to make the specimen's surface smooth to permit a regular indentation shape and good measurement, and to ensure the sample can be held perpendicular to the indenter.

Figure 28: Tukon microhardness tester machine.

3.6 Temperature Measurement

In this study, temperature evolution on the top surfaces of aluminum was monitored during friction stir spot welding by data accusation system (Thermometer PCE-T390) as illustrated in Figure 29. The maximum process temperature was considered as the highest temperature measured on the top surfaces of aluminum sheets.

Figure 29: Temperature recorded of the weld joint with thermometer PCE-T390.

3.7 Metallographic Inspection

Variation in microstructure and grains orientation provides different mechanical properties for different material, therefore different approached being considered to get the best results in this research. Scanning Electron Microscopy (SEM-EDS) for metallurgical analysis and optical Microscopy (OM) for fracture analysis will be used to get the results.

3.7.1 SEM-EDS Analysis

The metallurgical analysis of weld joint by scanning electron microscopy (SEM-EDS) provides valuable information about the joints characteristics. Weld nugget/ stir zone, actual weld depth and hook formation and some other geometrical information are possible to visualize through the cross section of the weld joint image as shown in Figure 30. For sample preparation of microstructural analysis, all specimens are cut in the middle of the pin hole region by using semi-automatic cast iron DK 6673 EDM

wire cutting machine that uses water coolant in order to avoid any heat input into specimens. After the cutting process is done burrs and contamination are removed from the surfaces. To facilitate the grinding and polishing processes; cold mounting of all specimens was obtained by using epoxy and resin. The percentage of epoxy hardener and epoxy resin were 50 percent and mixed it very well before pouring into the mold. A different number of sand paper (220, 500, 1000, 2400, 4000) were used for the grinding of all specimens. After grinding all specimen were washed with distilled water. Polishing of all specimen were carried out by using DP-Paste, P size of 1 µm polishing paste, and distilled water were used until scratch less surface appeared. Polishing processes have been carried out according to Voort. (1999), and killer reagent solution of H_2O (95ml) + HNO_3 (2.5 ml) + HCl (1.5 ml) + HF (1 ml) were used to etch the all specimens as shown in Figure 30.

Figure 30: (a) Cold mount prepared samples, (b) EDM wire cutting machine, (C) Grinding process of samples, (d) Polishing machine

3.7.2 Metallurgical Microscope

The optical microscope exposes the stir zone and its cross section. The optical microscope displays the heat penetration into the lower sheet under the pin hole of the tool. The welded samples for this inspection process are prepared in the same manner for SEM analysis. Optical microscope used in this study can be seen in Figure 31.

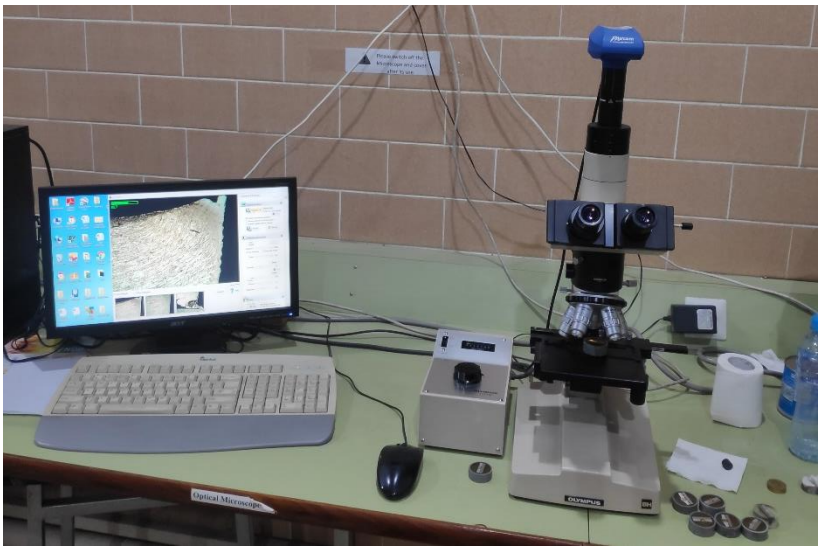

Figure 31: Olympus optical microscope

Chapter 4

FRICTION STIR SPOT WELDING OF AA5052 WITH ADDITIONAL CFRP COMPOSITE INTERLAYER

4.1 Introduction

The results and analysis of the FSSW process of AA5052 with carbon fiber interlayer using different welding parameters such as rotation speed and dwell time carried out is presented in detail in this chapter. However, mechanical testing, such as the shear-tensile test and Vickers microhardness test were covered. Also temperature profile was evaluation. Metallographic inspection using the digital optical microscope and the scanning electron microscope (SEM) coupled with Energy Dispersive X-ray Spectroscopy (EDS) test were investigated.

4.2 Temperature Evaluation

Figure 32 shows peak temperature of aluminum and CFRP interlayer at different rotational speed and dwell time. The peak temperature was about 298.5°C at rotational speed 2,000 rpm and dwell time 5 s, while the minimum temperature was 216.9 °C at rotational speed 850 rpm and dwell time 2 s.

Generally, Al_4C_3 compound could not be formed due to low temperature during the FSSW processes. Also, it was clear that the increase of dwell time from 2 to 5 s at all rotating speeds directly affected temperature, dramatically increasing it by up to 10%. Heat generation at the surface of aluminum was not high enough to melt the interlayer

at the interface in the whole overlapped area. This was due to the lower thermal conductivity of CFRP around 0.19 W/m K which is than aluminum [120].

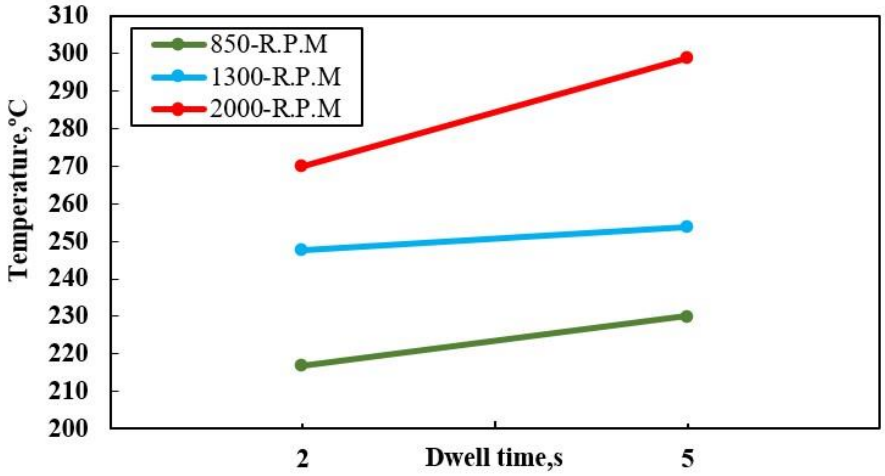

Figure 32: Evolution of friction spot joining process temperature.

4.3 Tensile Shear Load

The results of tensile shear load of AA5052 FSSW joints are showed in Figure 33. Maximum tensile of 1779.6 N was produced at rotational speed 2,000 rpm and dwell time 2 s with 14.6% joint efficiency, while minimum tensile occurred at 850 rpm and dwell time 2 s was 1,373 N. In addition, the results showed that increase of rotational speed from 850 to 2,000 rpm at 2 s dwell time with 39.5% improvement in tensile shear load was obtained. High heat input was developed due to high dwell time, which led to initiate the cracks in the weld interface and reduce the tensile shear load [87]. The maximum strain of 0.03827 mm/mm was founded at rotational speed of 2000 rpm and 2 s of dwell time. The material around the tool is softened and plastic ally deformed to high strains during the plunge and dwell stages, and the tool movement in the vertical direction facilitates the flow of plasticized material in both circumferential and axial directions, which also helps to disrupt the oxide layer at the joint interface as showed in Figure 34. The maximum elongation of 8% was founded at rotational speed

of 850 rpm and 2 s of dwell time. Large elongation could be due to large joint area and increased amount of CFRP attached to aluminum surface [122].

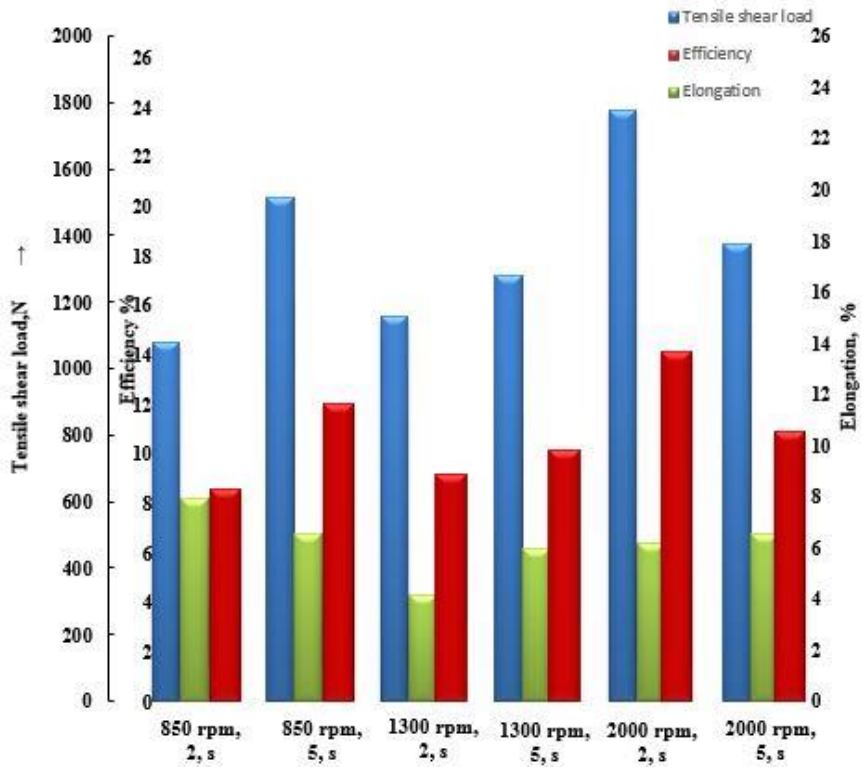

Figure 33: Tensile shear load (N), elongation and efficiency % of FSSW.

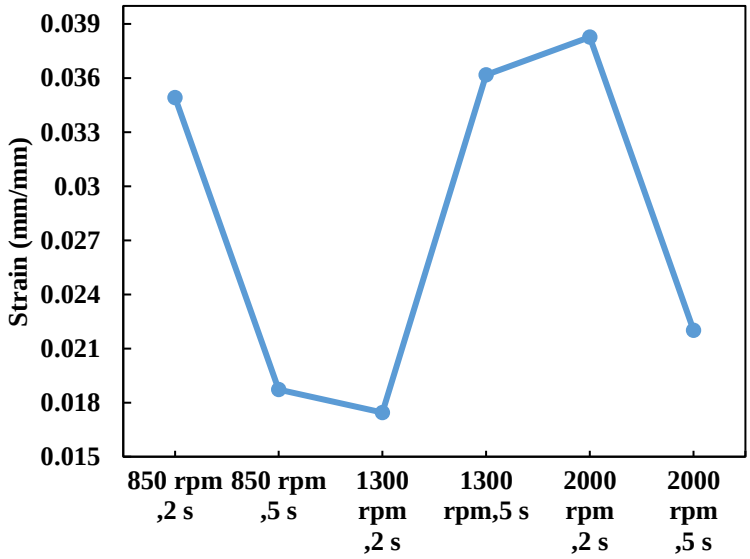

Figure 34: Strain (mm/mm) of FSSW with CFRP interlayer

4.4 Microhardness

Rotational speed and dwell time are significant parameters in FSSW processes, such that increase of dwell time from 2 to 5 s at all rotational speeds directly increased microhardness. Microhardness profile is illustrated in Figure 35. Maximum microhardness value was 58 HV which was obtained at 2,000 rpm rotating speed and 5 s dwell time in keyhole, whereas minimum value was 24.5 HV obtained at 1,300 rpm rotational speed and 2 s dwell time in stir zone (SZ).

The graph showed the highest microhardness in keyhole area rather than SZ and TMAZ. In keyhole area, 29% improvement was achieved by increasing rotational speed and dwell time. This was due to mixing and incorporating CFRP and aluminum during FSSW processes. Hardness test results provided further support to the fact that large amounts of CFRP were uniformly dispersed in the matrix over large region. However, heat generation during FSSW minimized microhardness in TMAZ region. Large amounts of geometrically necessary dislocations (GNDs) [235,236] induced during FSSW are thought to be an important reason of strengthening.

The thermal expansion coefficient (TEC) between AA5052 (23.8X10-6 K-1) and CFRP (5.5X10-6 K-1) are highly different and along transverse and longitudinal directions, respectively. The mismatch of CTE led to the generation of GNDs during FSSW [195]. Hence, hardness in SZ and TMAZ could be attributed to the comprehensive effect of variations in grain size and strengthening of precipitates [107].

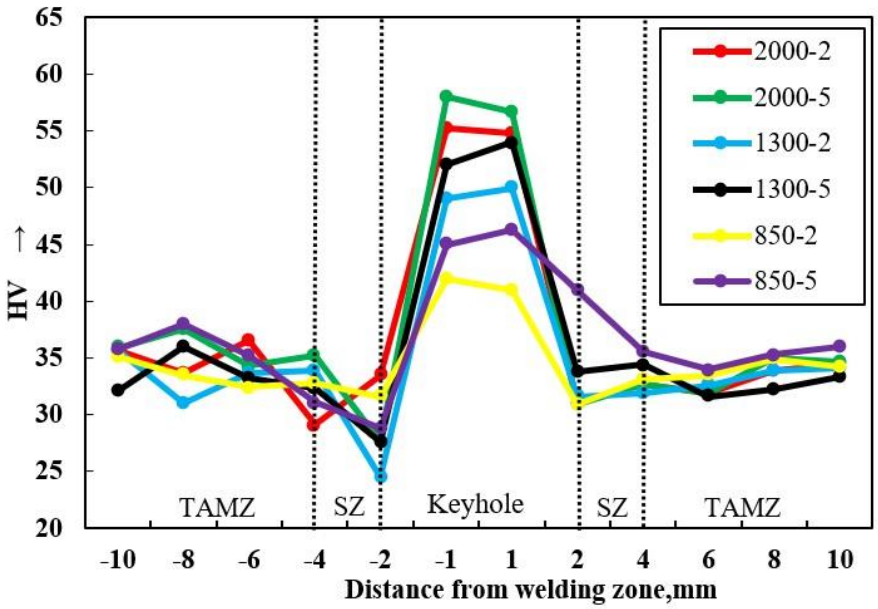

Figure 35: Micro hardness distributions of welds at different rotational speed and dwell time.

4.5 Microstructure

The microstructure of AA5052 with CFRP interlayer was presented in this study. Weld microstructure analysis are different from sample to the other sample according to welding parameters such as dwell time, rotational speed, pin length , type of metal and thermal conductivity [87]. Nub was slightly inserted into thermoplastic composite part, which consequently increased mechanical interlocking between joining partners and contributed to joint mechanical strength under shear loading [126].

The samples of rotational speed 850 rpm and dwell times 2 and 5 s had lower mechanical performance compared with those at 2,000 rpm. The main reason for this was low heat input during FSSW process, which was not enough to melt interlayer to improve microhardness, as shown in Figure 36 (a and b). In the cross section joint of 1,300 rpm and 5 s, crack was observed under tool pin after welding. Cracks on right and left sides rapidly extended along the top surface to pull out the entire joint from

the upper plate. In the hook defect, the crack initiation was identified and extended along the hook toward the top surface to pull out stir zone; meanwhile, cracks at hook defect on the left side extended along the hook toward the bottom of stir zone. The joint broke along the interface and only a small part was pulled out. Microcracks in stirring zone were clear and their number was increased by increasing rotational speed and dwell time, as showed in Figure 36(c). In cross section joint at rotation speed 2,000 rpm and dwell time 2 s, interlayer was melted and squeezed out of the center to the edges of the joint. This was due to high temperatures (about 298.5°C) during welding process which led to the melting of interlayer at the middle of specimen. This occurred due to lower molten viscosity associated with higher frictional energy generation in this region [120]. The molten CFRP interlayer could flow into incision and crack on the surface of specimens. It results in an increase in tensile shear load due to micro-mechanical interlocking between plates, as showed in Figure 36 (d) [237].

It has been observed in conventional friction stir spot welding the microstructural properties of grain size and precipitates, relies on the weld structure which is symmetrical with motion of the tool axis. The most prominent zone, stir zone or nugget and TMAZ are produced in a sequence from the keyhole periphery approaching to the base metal. In friction stir spot welding tool penetration produce rapid strain rates due to the tool rotation. In traditional FSSW method, a fully fine equaled grains developed in the stir zone area, at the end of penetration procedure when tool is entirely infiltrated into the sheets. Even in some cases cracks were observed under the tool pin and confirmation of such cracks was acclaimed in Al7075 refill friction stir spot welding, as stated by Shan et al. [15]. The creation of glistening surface during FSSW process is a sign of liquid film formation and indication the merger of material and welding

parameters may be prone to liquation and cracking. Local melting in metal persuaded due to plastic deformation and high temperature, and it was argued that liquation and solidification happened frequently based on fluctuating temperature, resulting a non-equilibrium solidus temperature.

This paper (SEM-EDS) analyzed the welds produced at rotational speed 2,000 rpm and dwell time 2 s. similar aluminum alloys made strong bonds with CFRP. It is necessary to uniformly distribute CFRP in the matrix for fabricating aluminum alloys with CFRP and the results showed that the concentration of aluminum and carbon elements confirmed chemical bonding between aluminum and molten CFRP interlayer. Also, SEM-EDS analysis was performed to the compositions, to take place and form intermetallic compound. Dwell time was the main effect parameter to provide time for the diffusion. Figure 37 presents an SEM-EDS mapping microanalysis to identify the chemical intermetallic composition of the phases present in the welding joint and disruptions of carbon particles into the matrix, which might significantly affect structures and their properties.

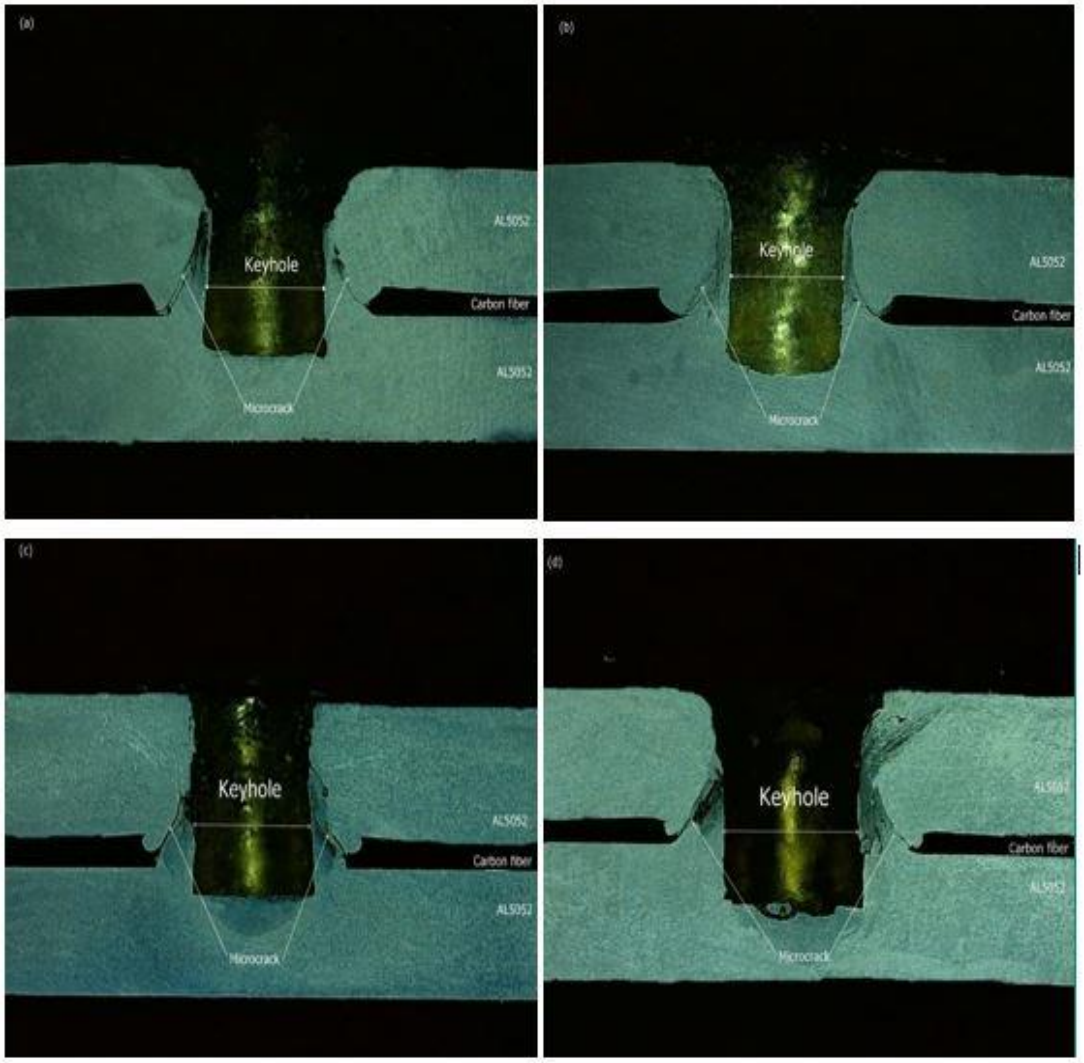

Figure 36: Cross-section of the welding of samples (a) 850 rpm and 2 s. (b) 850 rpm and 5 s. (c) 1300 rpm and 5 s. (d) 2000 rpm and 2 s.

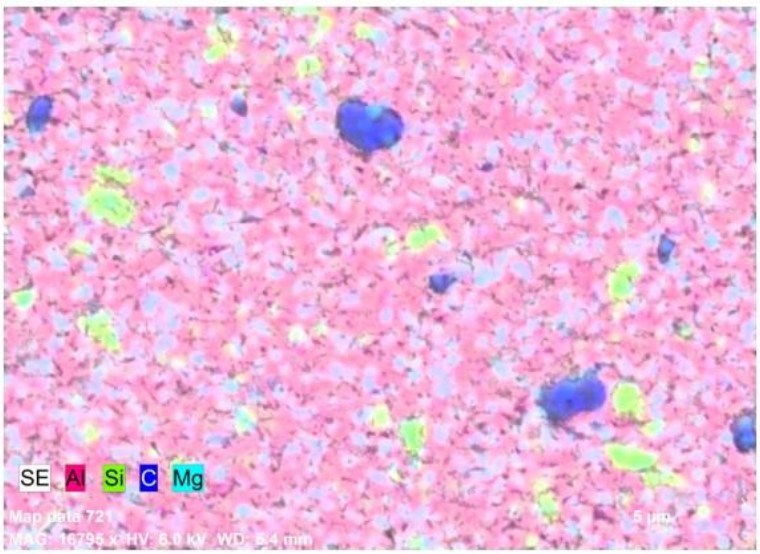

Figure 37: Element distribution of Al and CFRP joint.

Moreover, aluminum carbide (Al4C3) was not observed because of low heat input during welding processes (Max. 298.5°C). Contact and bonding between CFRP and AA5052 was high due to thermal-mechanical effect. The presence of Al, Mg, and C elements was proved, as illustrated in Figure 38, which indicated the presence of strong bonding, and there may be mechanical interlocking leading to high adhesive forces at joint areas which was due to the presence of carbon molecular bonding [238].

Also, Figure 38 shows ternary intermetallic compound (Al–Si–C) and these elements mixed together due to heat input during friction processes between aluminum and CFRP [239,240]. These compounds might increase microhardness by about 58% in keyhole rather than in SZ and TMAZ [241].In addition, more carbon fiber increased microhardness. On the other hand, more fiber reduced the distance between aluminum and fibers and increased stress, which decreased the strength of composites [242].

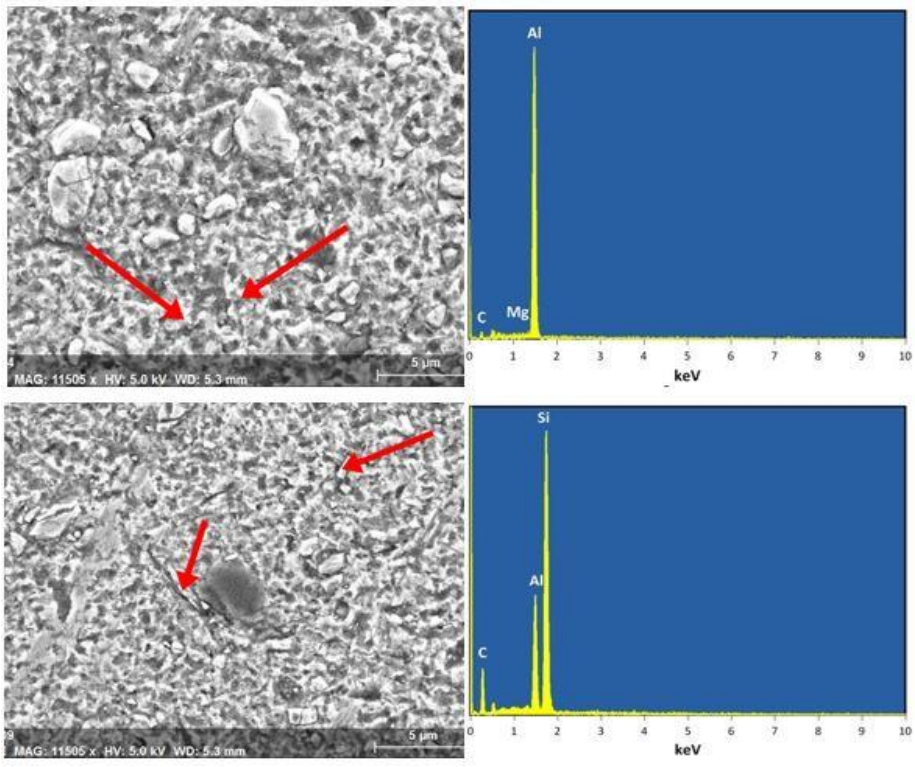

Figure 38: SEM-EDS analyses of friction stir spot welding zone: 2000 rpm and 2 second dwell time.

Chapter 5

FRICTION STIR SPOT WELDING OF AA5052

5.1 Introduction

The results and analysis of the FSSW process of similar AA5052 using different welding parameters such as rotation speed and dwell time carried out is presented in detail in this chapter. However, mechanical testing, such as the shear-tensile test and Vickers microhardness test were covered. Also, temperature profile was evaluation. Metallographic inspection using the digital optical microscope were investigated.

5.2 Temperature Evaluation

As shown in Figure 39, peak temperature of aluminium at different rotational speed and dwell time. The peak temperature was about 303.7 ºC at rotational speed 2000 rpm and 5 second dwell time, while the minimum temperature was 176 ºC at rotational speed 850 rpm and 2 second dwell time. Also, it clear that increase dwell time from 2 second to 5 second in all different rotating speed directly effect of temperature and dramatically increase up to 31.8 %.

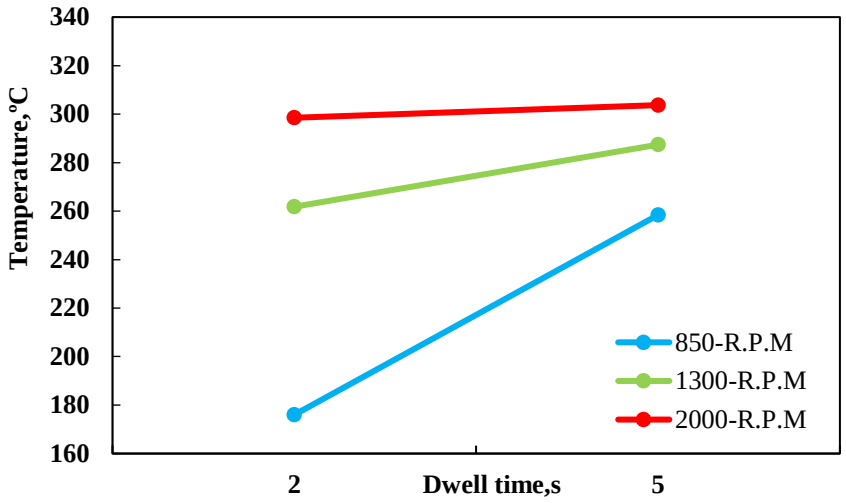

Figure 39: Evolution of friction spot joining process temperature.

5.3 Tensile Shear Load

The results of tensile shear load of AA5052 FSSW joints are showed in Figure 40. Maximum tensile shear load produced at rotational speed 1300 rpm with 2 second dwell time to be 2439.1 N with 19.4 % joint efficiency, while minimum tensile occurred at 850 rpm and dwell time 5 second dwell time to be 1264.3 N.

Besides that, the result showed that increase the dwell time from 2 second to 5 second at different rotating speed, the tensile shear decreased and could promote the nugget thickness; in all this process dwell time is of great importance in attaining a nugget with larger size [243-245]. Tensile shear load increased when tool rotational speed and dwell time were increased form 850-1300 rpm and 2-5 second respectively, but increased rotational speed at 2000 rpm and dwell time caused to decrease tensile shear load due to frictional energy generation and plasticized material in the stirring zone [136].

Also, tensile decreased due to heat input which leads to increase grain size [246] , also residual stress reduce tensile shear load at high rotation speed especially for aluminum [93]. On the other hand, increase of dwell time from 2 to 5 second a 41 % decline in tensile shear load at high to low rotational speeds which causes to increase heat input that led to overheat the material in weld region, which induced the grain growth and eventually decreased tensile shear load. The microcracks formation in stir zone caused to decrease the tensile. In low dwell time and rotating speed generate smooth grain in the upper sheet mainly at stirring zone and more heat input during the friction stir spot welding, develops the stirring zone [93]. The maximum elongation about 13.9% at 2 second dwell time and rotational speed at 2000 rpm. The large elongation could be due to the large joint area [122]. The maximum strain of 0.04845 mm/mm was founded at rotational speed of 1300 rpm and 5 s of dwell time. Frictional heat and localized softening leads to high plastic deformation at high strain rates, which provides another heat generation mechanism as showed in Figure 41.

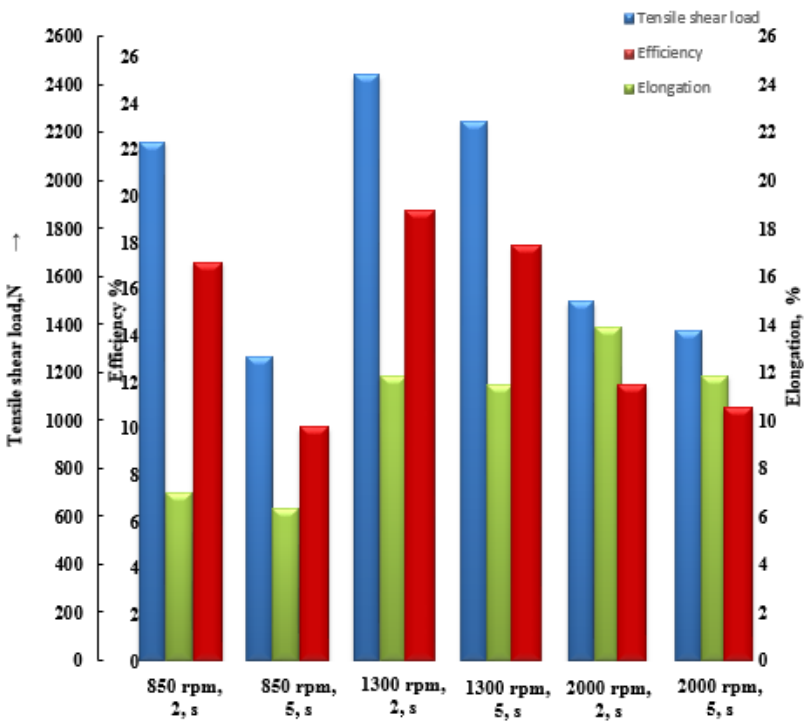

Figure 40: Tensile shear load (N), elongation and efficiency % of FSSW.

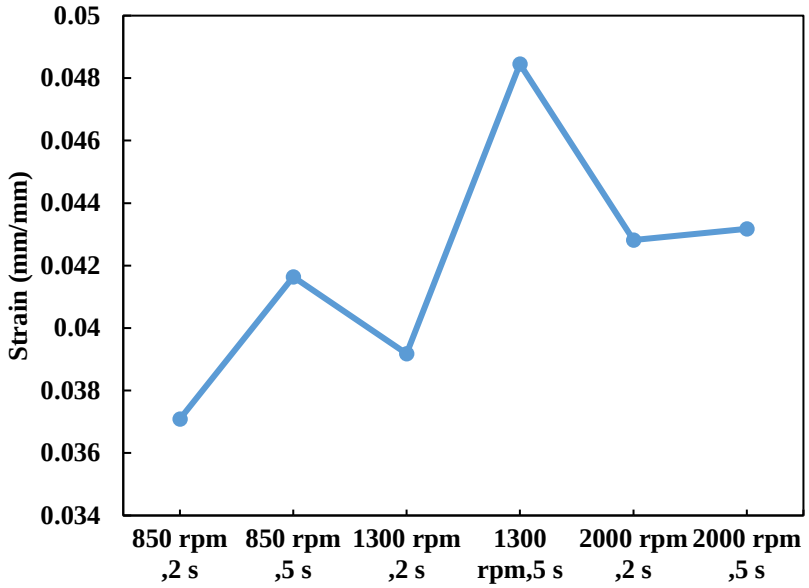

Figure 41: Strain (mm/mm) of FSSW without CFRP interlayer

5.4 Microhardness

The rotational speed and dwell time are significant parameters in FSSW processes,

increase dwell time from 2 to 5 second in all rotational speed directly decrease the micro hardness.

The micro hardness profile of AA5052 joints on the top and bottom were illustrated in Figure 42. The highest micro hardness of 37.2 HV was obtained at 850 rpm rotating speed and 2 second dwell time in thermal mechanical affect zone (TMAZ). On the other hand, the minimum result was obtained about 23 HV at 5 second dwell time and 1300 rpm rotating speed in stirring zone.

Moreover, the highest microhardness was in (TMAZ) and dramatically decreased in (SZ). This increase in hardness may be due to the increased thermomechanical effect of the shoulder onto the aluminum interface. The maximum microhardness in (TMAZ) and (SZ) area rather than key hole due to increase grain size in the former [181,209]. There is slight increase in (TMAZ) compared with (SZ) because of plastic deformation causes strain hardening and influence of shoulder on interface [87,136].

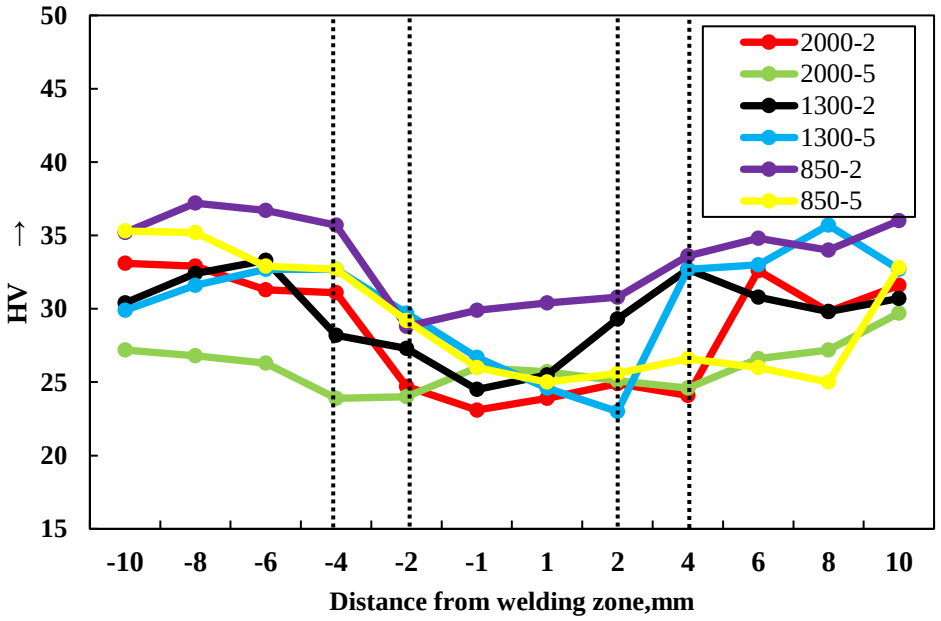

Figure 42: Micro hardness distributions of welds at different rotational speed and dwell time

5.5 Microstructure

In this study an optical microscope were applied to provide and investigate the cross section of welding samples in different rotational speed and dwell time. The tool was penetrated at high rotational speed and dwell time, the material around the pin penetrate into lower sheet and strong metallurgical bonding between the top and bottom work piece was completed and easily observed at the weld of cross-section as shown in Figure 43. The nugget area around the pin was clearly observed in different welding parameters and the area in low rotational speed is wider than high tool rotational speed as shown in Figure 43 and the nugget area was characterized by plasticized material providing the FSSW processes. In an optical microscope images, show that varying rotational speed from 850-2000 rpm caused the tool indentation inside the top sheet and bending around the tool. The cross-section of samples (e) and (f) had large bonding compared to the other samples.

In the cross-section of joints, the regions are mainly stir zone and thermomechanical affected zone. The thermomechanical affected zone in similar joints configuration could be defined by the grains oriented in material flow direction and finer structure. There are mainly three factors by grain size variation of the SZ at different welding processes parameters: high temperature during the welding processes caused to increase grain size, grain refining by dynamic recrystallization and cooling rate at temperature profile [247,248]. According to low deformation and temperature, the dynamic recrystallization is not occurred in TMAZ. This zone comprises of the stretched coarse grains parallel to the blend zone boundary. Deformation of grains in this zone is owing to the shear stress connected by the material flow. The material flow

increase by increase the heat input during the processes. Thus, as a result in the processes the soft and paste materials are transmitted as burs into the joint edges [249].

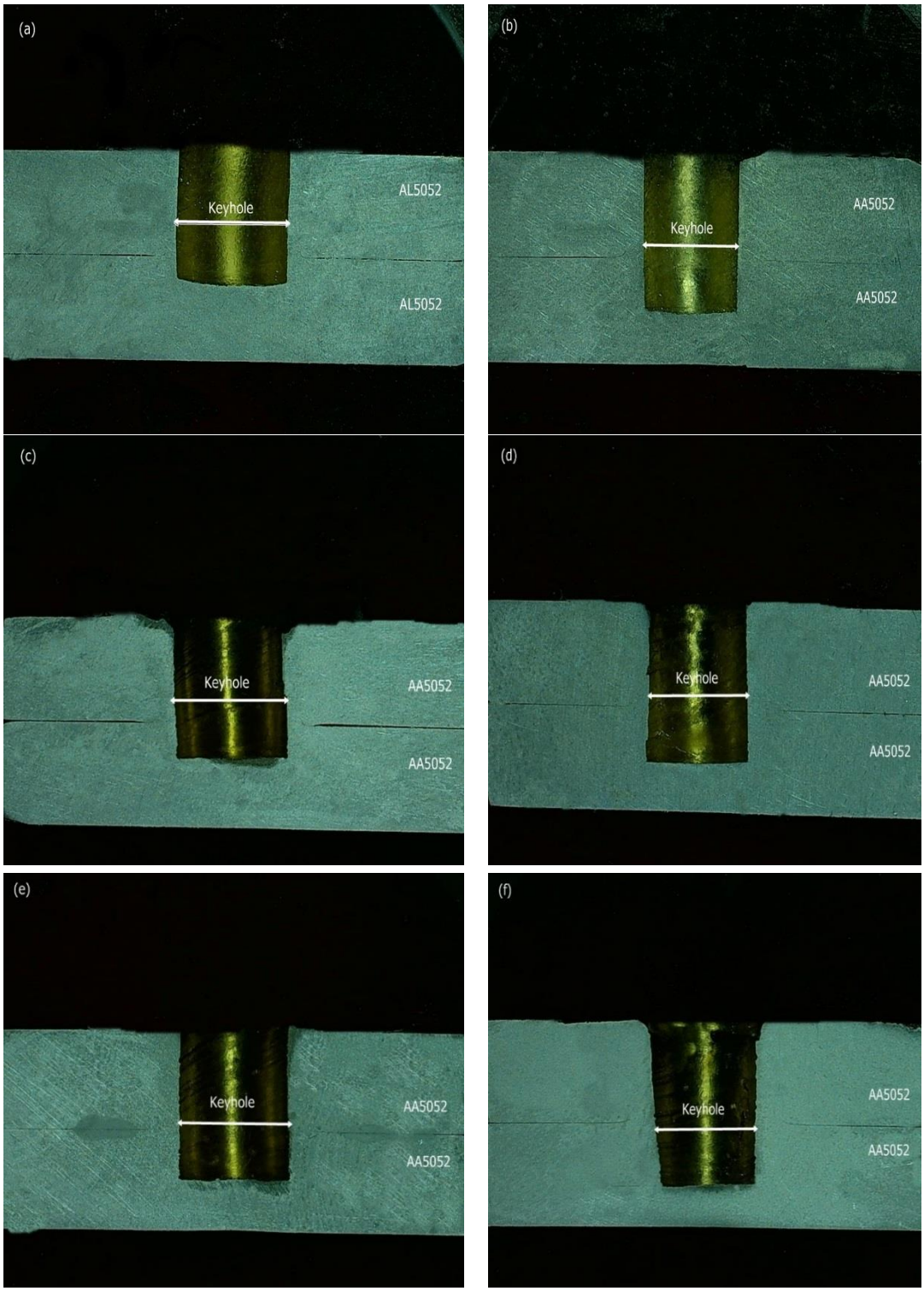

Figure 43: Cross-section of the welding of samples (a) 850 rpm and 2 s. (b) 850 rpm and 5 s. (c) 1300 rpm and 2 s. (d) 1300 rpm and 5 s. (e) 2000 rpm and 2 s. (f) 2000 rpm and 5 s.

Chapter 6

METAMODELING

6.1 Introduction

The demand of aluminium alloys is increasing in the area of aerospace, shipbuilding, automotive, transport, military and other many industries owing to their unique features, i.e., high strength to weight ratio, high formability, excellent corrosion resistance [250]. Friction stir spot welding process is a suitable to connect two plates. FSSW process omitted arc- welding problems of aluminium alloys without change of phase of base metal or without reaching melting point. This revolutionary technique has a capability of joining thin and thick materials with a less skilled operator.

In recent years, many researches have been applied machine learning and consider as part of Artificial Intelligent. It is a method, which is accesses computers to do work come from data collected, experience and experimental. The algorithm performance could be improved by increased number of specimens [17]. Machine learning algorithms can learn from the data obtained during welding process. It is therefore critical to choose the reliable data and suitable machine learning algorithm to enable the real time monitoring effectively [251]. Our methods can analyses large volumes of data gathered in the manufacturing environment, including historic data , welding machine configurations, manufacturing specifications, and the quality estimates of previously welded spots [252]. In this dissertation, we address this problem by developing machine learning based methods to predict welding quality before the

actual welding happens. Also to investigate the capability of artificial neural network (ANN), support vector machine (SVM), multi linear regression (MLR) and adaptive neuro-fuzzy inference system (ANFIS) in evaluation of tensile shear load by FSSW.

6.2 Modeling of FSSW Process

In this chapter, ANN, SVM, MLR and ANFIS approaches are employed to develop different regression models for a better understanding of FSSW process. Tensile shear load is considered as a performance parameter for all modeling techniques. Before the modeling process, the results could be divided into training data and testing data sets. In current research work, 70 % of data is selected randomly for training data set and 30 % data for testing data set. Primarily, the training data set is used for developing a different regression model by using ANN, SVM, MLR and ANFIS approaches. Subsequently, the testing data set is applied to check the completeness of each developed model.

6.2.1 Artificial Neural Network (ANN)

Many studied have been reported that suitable method for data processing systems was artificial neural networks. In general, the neurons are inspired by the human brain. Through previous experiments, it was found that neurons can learn from previous experiences and through them improve their performance [253]. The ANN could be classified as a network comprised several processors which are named neurons. Each neuron includes a numerical data and would be known as weights [254]. In order to build a useful neural network, 3 steps should be considered: Select a suitable architecture for the artificial neural network, using necessary training data for network, and the accuracy network use different test data. Figure 44 illustrated the ANN method.

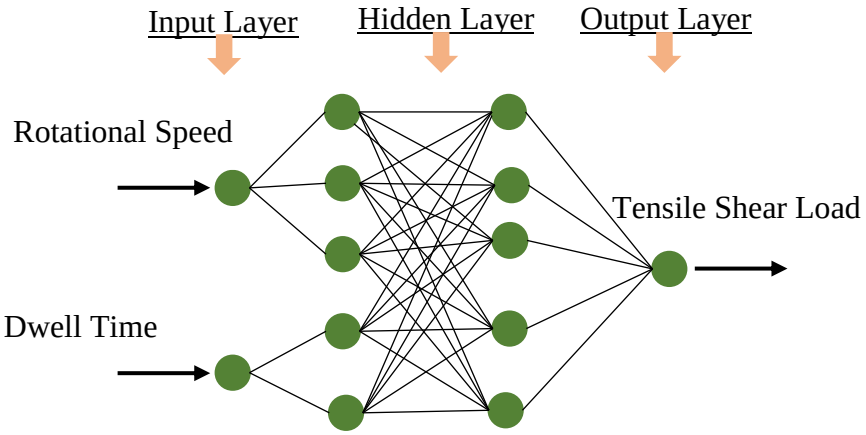

Figure 44: The architecture of the ANN

ANN is contain three main processes and classified to be: Training processes to decrease the error function, in validation the ANN to construct the method and finally training processes. The test processes is applied to anticipate the accuracy of the machine algorithm. Neural networks are divided in two layers. The input layers have input data of the study whereas the results as output layer. ANN method has hidden layer between input and output. During the processes , could apply any number of hidden layers and might be any number of nonlinear relationship [255]. All layer have a vector with any number of R of neurons, and the output of the layer is a vector of length R containing the output from all neuron in that layer. [256]. Satpathy et al. [257] investigated the tensile shear load by experimentation and ML methods. The ANN tool was applying and presented the prediction. In ANN, the number of neurons, learning rate, and momentum factor are tuned as 10, 0.08 and 0.6 respectively. The average absolute errors of tensile shear was obtained as 0.15%. Maleki et al. [258] evaluated the effective welding parameters of AA7075-T6 by FSW applying ANN. The network recognized on back broadcast (BP) algorithm. In this study, the input parameters are TRS, TS, axial force, pin diameter, shoulder diameter and tool hardness of ANN method. Khourshid et al [259] investigated the mechanical properties to expression the

feasibility of FSW of Al 6061 on pipe. To achieve the TS, the %EL and hardness of FSW weld of AA6061 aluminum ANN and RSM implanted. The ANN and RSM results show that model proved prosperous in term of settlement with experimental result ratio of 93.5% and 90% respectively.

6.2.2 ANNs Results

6.2.2.1 Tensile Shear Load

In this work, a standard multilayer feed forward neural network (nftool) model were used to train the model. A two layer feed forward network with sigmoid hidden neurons with linear output neurons which can solve multidimensional mapping problems. In this model tool rotational speed and dwell time used as input parameter and tensile shear load data used as target output data. Input data was distributed into three categories 70 percent data from input data used for training, 15 percent kept for validation and remaining data used for testing. In this model 10 hidden neurons were applied to train the model. The neural network architecture are shown in Figure 45. A full factorial design of experiment were applied with two factor (rotational speed and dwell time), in which rotational speed has three level and dwell time has two level. Each factor were replicate three time and fully randomized. In this work the total number of specimen were 36. The set of specimens are divided into two categories: first category similar metal of AA5052 with additional interlayer of carbon fiber reinforced polymer (CFRP), second category similar metal of AA5052 without any additional interlayer.

In this section total 18 specimen were used to train the model. Rotational speed and dwell time used as input data and tensile shear load output data used as target output

data. In this model out of 18 samples 12 were used for training, from remaining data half used for validation and testing.

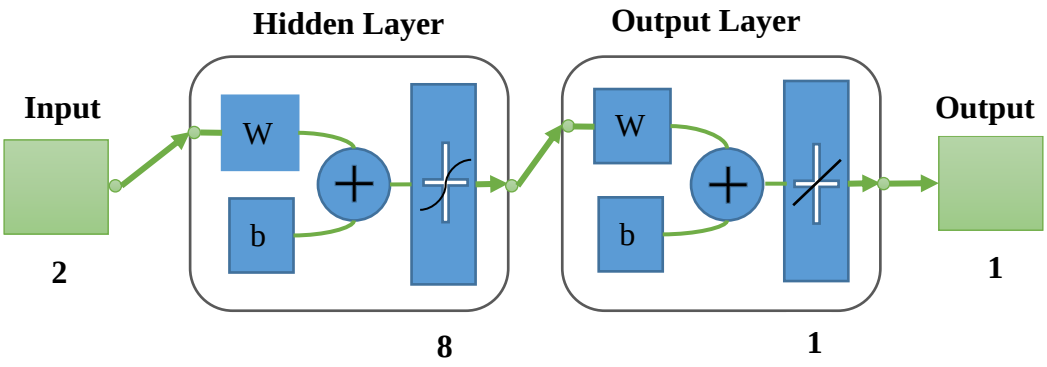

Figure 45: Neural network architecture

The network were trained by using Levenberg-Marquardt backpropagation algorithm to train the input data. Multiple time model.

The Figure 46 shows the experimental and predicted results of AA 5052 with additional CFRP interlayer. The result show that correlation coefficient of training data is 0.99026. Also, the coefficient of validation and test are 0.9933 and 0.98595 respectively. The closeness of correlation training data and validation data indicates that the prediction efficiency of the model is acceptable. The overall value of the model was found to be 0.97715 which indicate the good prediction efficiency of the ANN model.

On the other hand, the experimental and predicted results of AA 5052 without interlayer show that correlation coefficient of training data is 0.98507. Also, the coefficient correlation vale of R-square for validation and testing are 0.99142 and 0.99064 respectively. The closeness of correlation training data and validation data indicates that the prediction efficiency of the model is acceptable. The overall

correlation coefficient value of R-square of the model was found to be 0.98794 as shown in Figure 47.

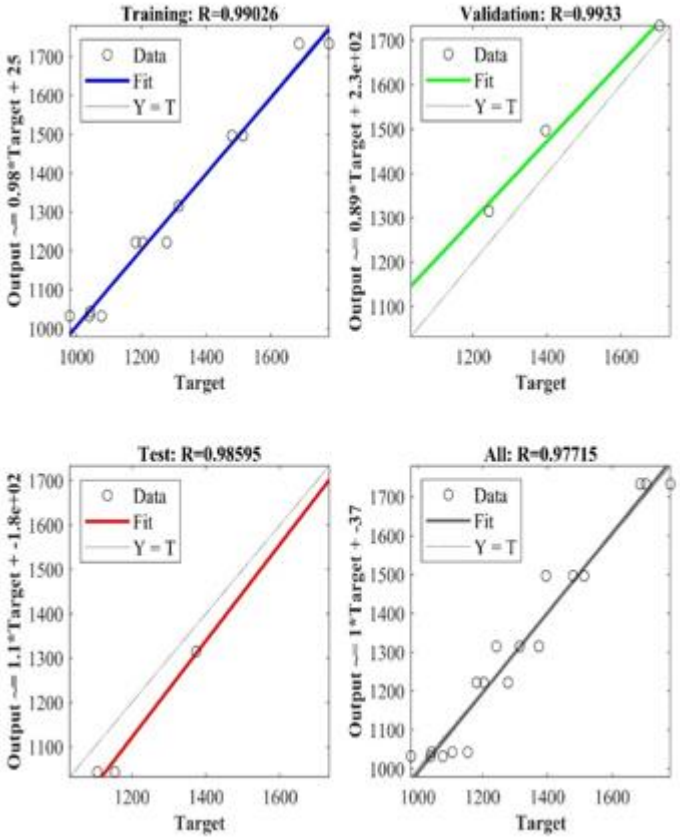

Figure 46: ANNs result for AA5052 with CFRP

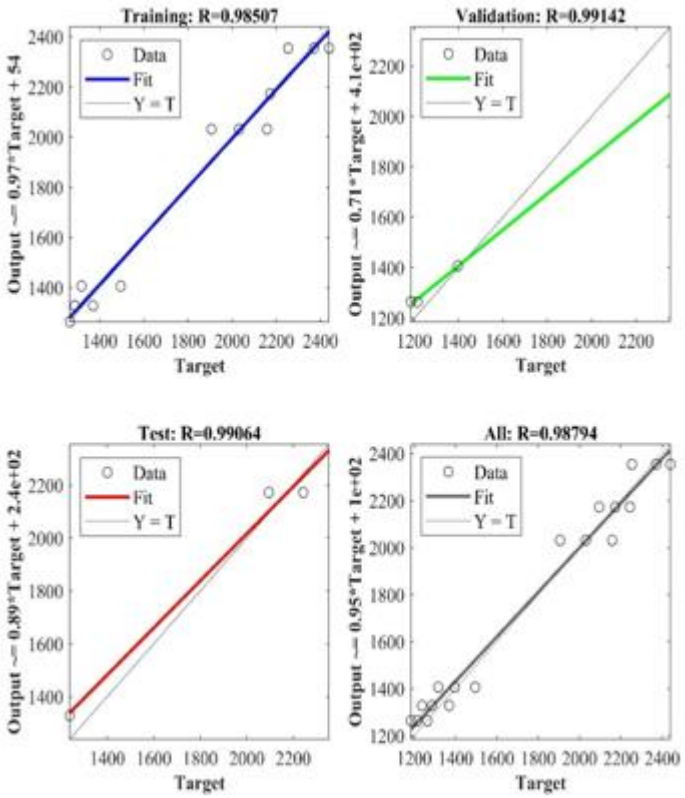

Figure 47: ANNs result for AA5052 without interlayer

6.2.2.2 Temperature Evaluation

In this work, a standard multilayer feed forward neural network (nftool) model were used to train the model. A two layer feed forward network with sigmoid hidden neurons with linear output neurons which can solve multidimensional mapping problems. In this model tool rotational speed and dwell time used as input parameter and temperature data used as target output data. Input data was distributed into three categories 70 percent data from input data used for training, 15 percent kept for validation and remaining data used for testing. In this model 10 hidden neurons were applied to train the model. In this work the total number of specimen were 12. The set of specimens are divided into two categories: first category similar metal of AA5052 with additional interlayer of carbon fiber reinforced polymer (CFRP), second category similar metal of AA5052 without any additional interlayer.

In this section total 6 specimen were used to train the model. Rotational speed and dwell time used as input data and temperature output data used as target output data. In this model out of 6 samples 4 were used for training, from remaining data half used for validation and testing.

The network were trained by using Levenberg-Marquardt backpropagation algorithm to train the input data. Multiple time model.

The Figure 48 shows the experimental and predicted results of AA 5052 with additional CFRP interlayer. The result show that correlation coefficient of training data is 0.999867. The closeness of correlation training data and validation data indicates that the prediction efficiency of the model is acceptable. The overall value of the model was found to be 0.99393 which indicate the good prediction efficiency of the ANN model.

On the other hand, the experimental and predicted results of AA 5052 without interlayer show that correlation coefficient of training data is 0.99902. The closeness of correlation training data and validation data indicates that the prediction efficiency of the model is acceptable. The overall correlation coefficient value of R-square of the model was found to be 0.9959 as shown in Figure 49.

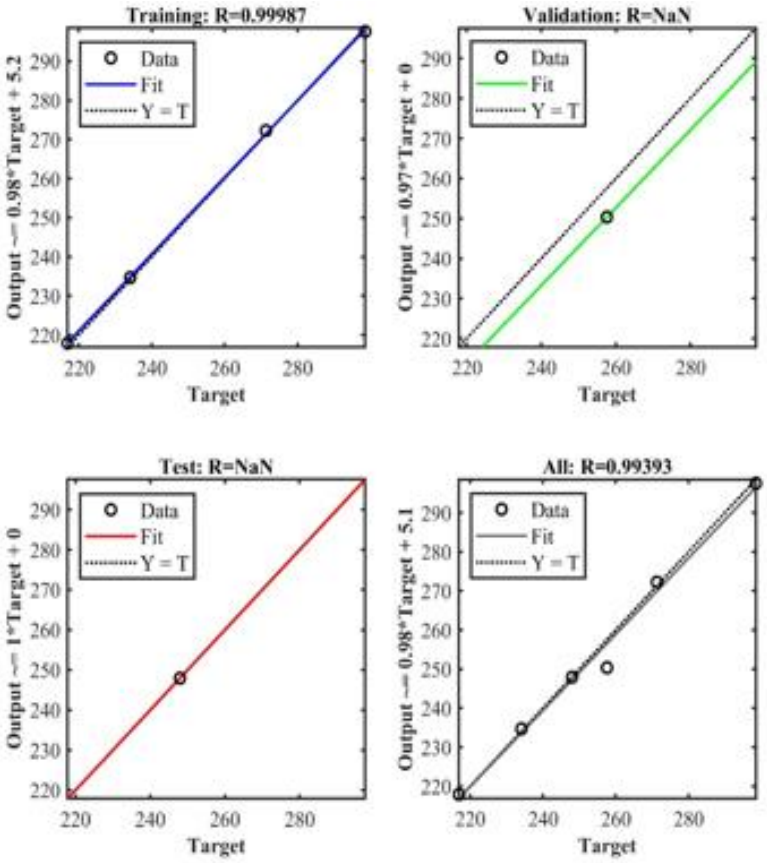

Figure 48: ANNs result for AA5052 with CFRP

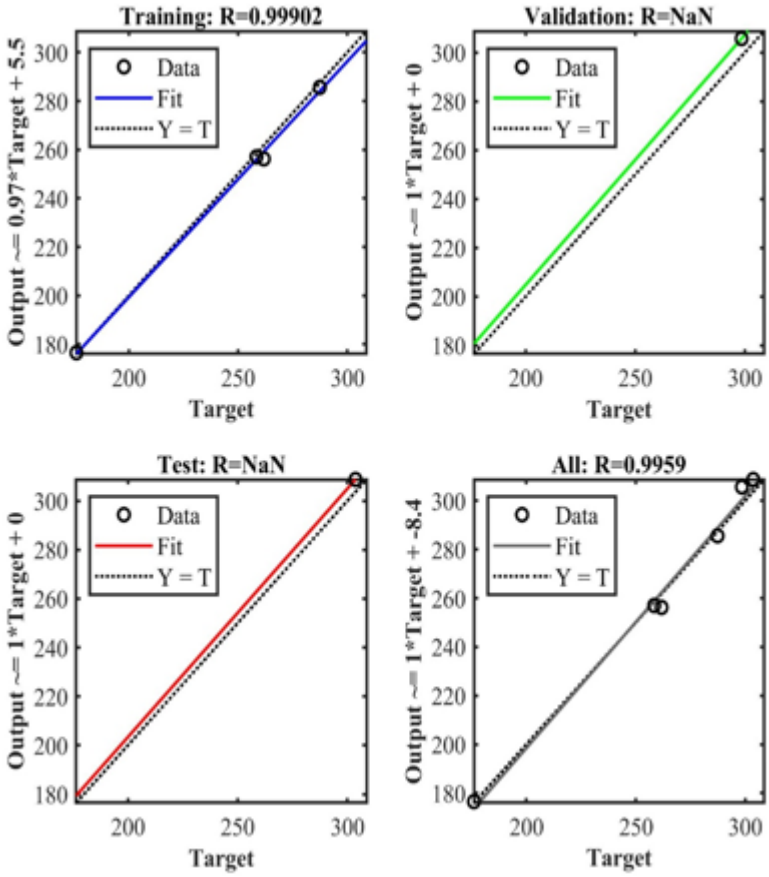

Figure 49: ANNs result for AA5052 without interlayer

6.2.3 Support Vector Machine (SVM) and Support Vector Regression (SVR)

In recent decades, rapid advances in information processing systems have triggered, some complex studies, which contain a number of information, need systems to help make the appropriate decision. The study and construction of algorithms that are able to learn from to make predictions according to small experimental data are explored at sub-field science of computer by machine learning (ML). In supervised learning, given a set of N input vectors Xn and the corresponding targets tn, the goal is to learn a model of the according of the targets on the inputs in order to predict the main goal in case of unobserved inputs [260].

Support vector machines (SVMs) are supervised learning models with associated learning algorithms that analyze data and recognize patterns, used for classification

and regression analysis. Structural risk minimization alongside with minimization of empirical risk is the main advantage of the SVMs over the neural networks resulting in a better generalization capability in many practical applications [261]. Based on regression in Support vector machine, acccording to small data was obtined to estimate a function from of equation.

The input space is plotted into ∅ (x) and then LOR is presented.

$$y = f(x) = w^T \emptyset(x) + W_o \quad (2)$$

The vector of weights W and the bias W0 are expected according on fundamental risk decresing values [262], by calculating the following equations:

$$\min\{R(w) = \frac{1}{2}w^2 + C.\sum_{i=1}^{n} \xi_i + \xi^*_i\} \quad (3)$$

where C is the regularization factor, ε is the inconsiderateness parameter and εi and εi* are loose variables, calculated based on the Vapnik's ε-insensitive loss function, as:

$$\xi = \left|y - f(x)\right|_\varepsilon = \max\{0. \left|y - f(x)\right| - \varepsilon\} \quad (4)$$

The conception of ε -thoughtlessness in SVM-based regression.

$$f(x) = y(x_i, w) = \sum_{i=1}^{n} w_i K(x, x_i) + W_o \quad (5)$$

where N is the number of training testers and K(x, xi) is considered as:

$$K(x_k . x_i) = \varphi(x_k).\varphi(x_i), (k. i = 1 \ldots N) \quad (6)$$

The Gaussian radial basis function (RBF) kernel is the most general Kernel function in SVM and other kernel techniques, expressed as:

$$K(x, x_i) = \exp\{-\frac{x - x_i^2}{2\,\sigma^2}\} \quad (7)$$

SVM makes non-probabilistic point predictions. Ideally, estimation of a conditional distribution of the outputs P (t|x) is desired in order to capture the uncertainty in prediction [263]. The main part to estimate the regularization parameter C causes a

trade-off between the error, margin, and the thoughtlessness parameter ε, as the margin of tolerance in function approximation. The kernel function K (x, xi) must satisfy the mercer's condition.

Support vector regression mainly is a linear machine of one output and working in dimension space formed by nonlinear of N dimensional input vector into a K-dimensional feature space. SVR is a controlled learning method for solving regression problems via structural risk minimization [264,265].

The dateset $\{(x_1,y_1), \ldots, (x_n , y_n)\}$ and each input value has a numerical target value regression to predict accurate value. The general function of SVR method is given as [266].

$$f(x) = \big(w \times \emptyset(x)\big) + b, \tag{8}$$

The aim of SVR is to find the w and b values by reducing the x values to those that indicate the lowest regression risk. The relevant equation is given as:

$$R_{reg}(f) = c \sum_{i=0}^{n} T(f(xi) - yi) + \frac{1}{2} \, ||w^2||. \tag{9}$$

Here, ` is the cost function and c is a constant that determines the penalties for prediction errors. The equation for the vector w is given as:

$$w = \sum_{i=1}^{n} (\alpha_i - \alpha_i^*) \emptyset(x_i) \tag{10}$$

Then, combining equations (1) and (3) produces:

$$f(x) = \sum_{i=1}^{n} (\alpha_i - \alpha_i^*) \emptyset(x_i) \, \emptyset(x) + b$$

$$= \sum_{i=1}^{n} (\alpha_i - \alpha_i^*) k(x_i, x) + b \tag{11}$$

The objective of this work is to propose a model for prediction the mechanical property of friction stir welded join which focus on the tensile shear load based on the governing

parameters. The governing parameters will be considered as the input to the proposed prediction system model and then fed into the (SVM) and (SVR) in order to produce predicted tensile strength.

6.2.4 SVR Results

6.2.4.1 Tensile Shear Load

In this work MATLAB 2019a commercially available tool platform were used to develop the model. In MATLAB app section under machine learning and deep learning (Regression learner) tool used to train the input data. In regression learner app platform all support vector machine model was run to train the model. In this method 10 cross validation technique used to train the model, each time 10 percent data will be used for testing and remaining used to train the model. Until all data will be used to train and test the model it will run. Gaussian kernel function was selected to train the model. First category with CFRP interlayer data were trained. Fine Gaussian SVR kernel function provided more reliable prediction than any other model. The following Figure 50 will show the prediction results of SVR model with function Root Mean Square Error (RMSE) of 69.817, and the R-square value was 0.92. On the other hand the results without CFRP interlayer show that RMSE was 105.16 and R-square value was 0.93 as shown in Figure 51.

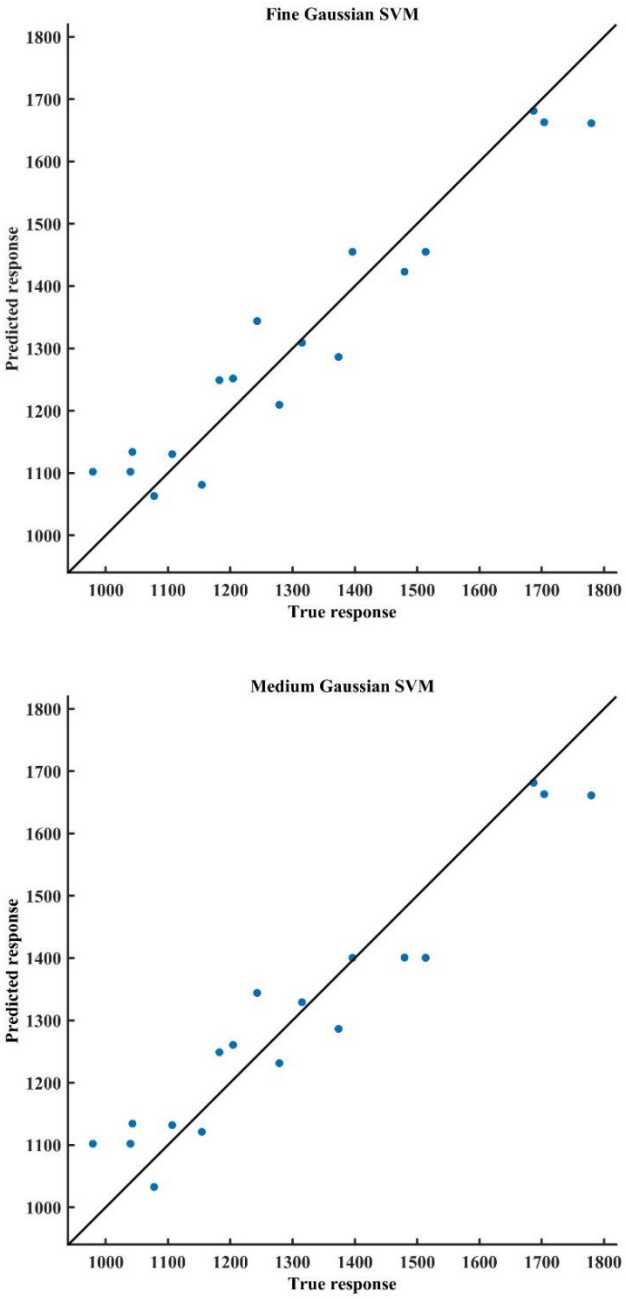

Figure 50:SVM results of fine gaussian regression model result of actual vs predicted with CFRP

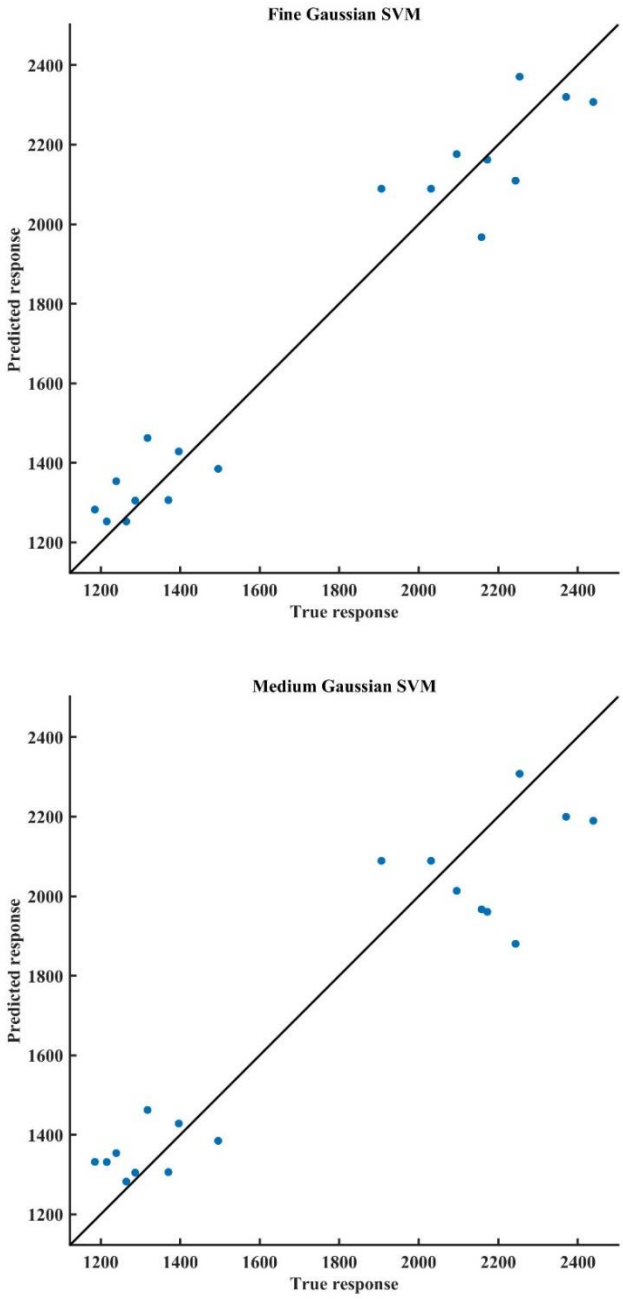

Figure 51: SVM results of fine & medium gaussian regression model result of actual vs predicted without CFRP

6.2.4.2 Temperature Evaluation

In this work MATLAB 2019a commercially available tool platform were used to develop the model. In MATLAB app section under machine learning and deep learning (Regression learner) tool used to train the input data. In regression learner app platform all support vector machine model was run to train the model. In this method

5 cross validation technique used to train the model, each time 10 percent data will be used for testing and remaining used to train the model. Until all data will be used to train and test the model it will run. Gaussian kernel function was selected to train the model. First category with CFRP interlayer data were trained. Quadratic SVM use for this model. The following Figure 52 will show the prediction results of SVM model with function Root Mean Square Error (RMSE) of 12.929, and the R-square value was 0.83. On the other hand the results without CFRP interlayer show that RMSE was 30.613 and R-square value was `0.62as shown in Figure 53.

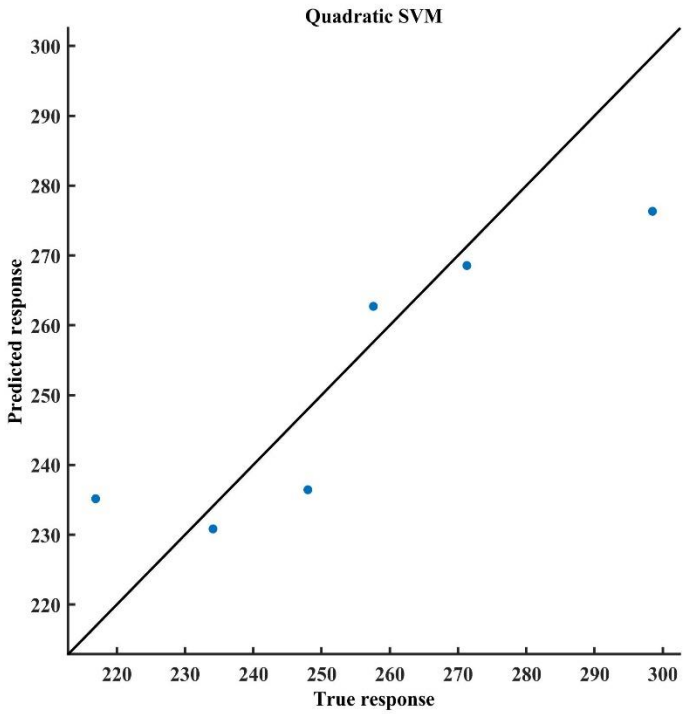

Figure 52: SVM results of quadratic model result of actual vs predicted with CFRP

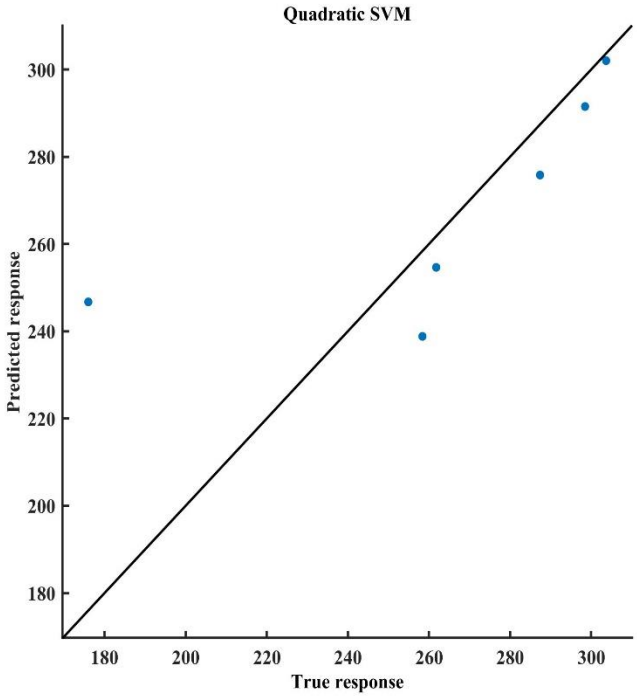

Figure 53: SVM results of quadratic result of actual vs predicted without CFRP

6.2.5 Adaptive Neuro-Fuzzy Inference System (ANFIS)

ANFIS is an advanced fuzzy inference system (FIS) with learning capacity like ANN. Due to this fact, neural network training algorithm can make a change in this FIS structure and fine tunes the predicted output [267]. ANFIS constructs an input– output mapping based on human knowledge and generates input–output data pairs by using a hybrid algorithm. According to Jang, the ANFIS is a neural network that is functionally similar to the Takagi–Sugeno– Kang (TSK) type inference model [268]. It decreases significant computational efforts like in the conventional feed forward neural network algorithm and found numerous applications in the control sector [269]. ANFIS model consists of five main layers as shown in Figure 54 and summarized as follows:

In the Layer 1, the inputs x and y are subjected to generalized Gaussian membership function to produce a new output O_{1i} which can be expressed by the following equations:

$$O_{1i} = \mu_{Ai}(x),\ i = 1, 2\ ,\ O_{1i} = B_{i-2}(y)\ ,\ i = 3, 4 \tag{12}$$

$$\mu(x) = e^{-\left(x-\frac{\rho i}{\sigma i}\right)2} \tag{13}$$

where A_i and B_i denote the membership values of the μ. ρ_i and ρ_i denote the set of hypothesis parameters. In the second, the output of each node is calculated as follows:

$$O_{2i} = \mu_{Ai}(x)\ x\ \mu_{Bi-2}(y) \tag{14}$$

Then, the output of the second layer is normalized in Layer 3 using the following equation:

$$O_{3i} = \hat{W}_i = \frac{\omega i}{\sum_{wi}^{2} \omega i} \tag{15}$$

Then, the output of layer 3 is passed through the adaptive nodes of Layer 4 as follows:

$$O4,i = \hat{W}_i f_i = \hat{W}_i(p_i x + q_i y + r_i) \tag{16}$$

where p, q and r denote the consequent parameters of the i-th node.

Finally, the overall output of the model is calculated as follows:

$$O_5 = \sum_i \hat{W}ifi \tag{17}$$

ANFIS method were applying by many researches for optimization and prediction. Dewan et al. [270] studied the prediction of tensile shear strength of friction stir weld joints with ANFIS. There are 1200 different ANFIS models were developed by varying number of membership function. The results show that the ANFIS model with three input variables resulted in lowest root mean square error and mean absolute percentage error of 29.7 MPa and 7.7% respectively.

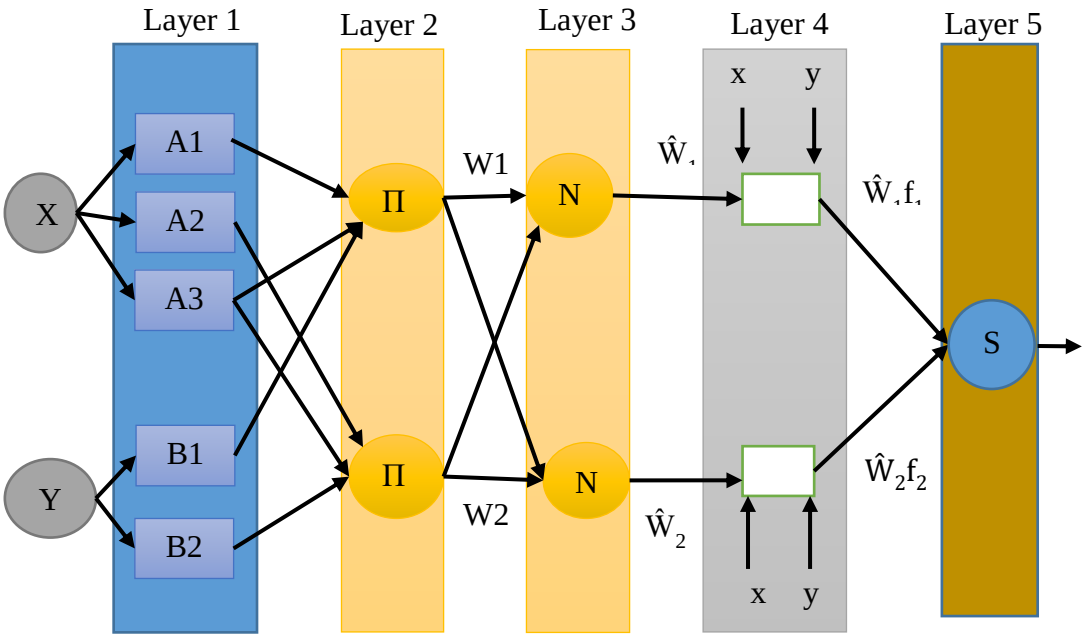

Figure 54: The structure of ANFIS for two inputs and two rules.

6.2.6 ANFISs Results

6.2.6.1 Tensile Shear Load

An adaptive neuro-fuzzy inference system (ANFIS) is a fuzzy system, train Sugeno system using neuro-adaptive learning technique, in which membership function parameters have been tuned by using either a back propagation algorithm alone or in combination with a least squares type of method. These adjustment allow the fuzzy system to learn from the data they are modeling. The network structure of fuzzy inference system (FIS) is similar to that of neural network, which maps inputs through input membership function and associated parameters, and then through output membership function and associated parameters to outputs, which used to interpret the input/output data. In this work, neuro-fuzzy designer tool was used to train the model data set. In this model hybrid learning algorithm was use to tune the input parameters of a Sugeno-type fuzzy inference system. Algorithm uses the combination of the least-square and back-propagation gradient descent method to model the training data. Fuzzy-inference system (FIS) was generated by using Grid partition method. In which

one input parameter rotational speed has three membership function and dwell time has two membership function. The membership type (gaussmf) was selected with linear output type. The structure of FIS model can be seen in Figure 55.

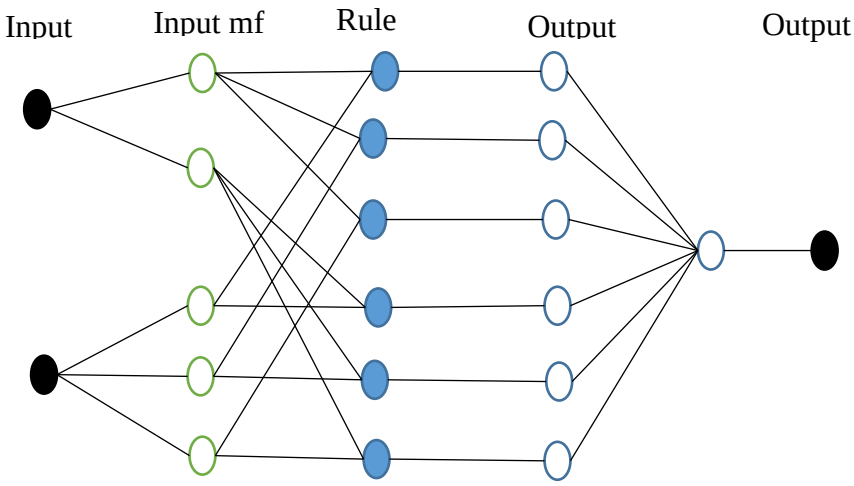

Figure 55: ANFIS system with fuzzy rules and membership function

The fuzzy-inference system was trained by using hybrid optimization method with error tolerance of 0.005 and the number of epochs was 250. This ANFIS model was applied on both categories of data sets.

6.2.6.2 Temperature Evaluation

An adaptive neuro-fuzzy inference system (ANFIS) is a fuzzy system, train Sugeno system using neuro-adaptive learning technique, in which membership function parameters have been tuned by using either a back propagation algorithm alone or in combination with a least squares type of method. These adjustment allow the fuzzy system to learn from the data they are modeling. The network structure of fuzzy inference system (FIS) is similar to that of neural network, which maps inputs through input membership function and associated parameters, and then through output membership function and associated parameters to outputs, which used to interpret the input/output data. In this work, neuro-fuzzy designer tool was used to train the model

data set. In this model hybrid learning algorithm was use to tune the input parameters of a Sugeno-type fuzzy inference system. Algorithm uses the combination of the least-square and back-propagation gradient descent method to model the training data. Fuzzy-inference system (FIS) was generated by using Grid partition method. In which one input parameter rotational speed has three membership function and dwell time has two membership function. The membership type (gaussmf) was selected with linear output type. The structure of FIS model can be seen in Figure 56.

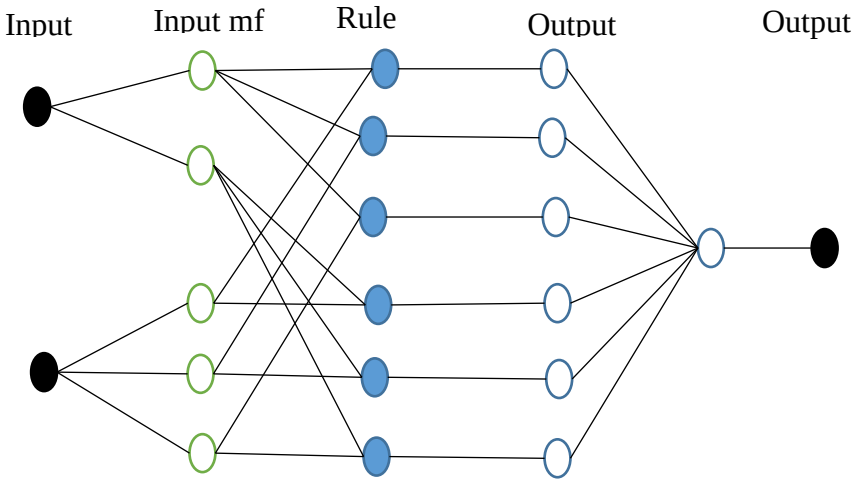

Figure 56: ANFIS system with fuzzy rules and membership function

The fuzzy-inference system was trained by using hybrid optimization method with error tolerance of 0.05 and the number of epochs was 50. This ANFIS model was applied on both categories of data sets.

6.2.7 Multi Linear Regression (MLR)

The optimization and modeling of industrial processes has been made by applying multi linear regression models (MLR). During the design of experimental is a set of tests where we delivery introduce a controlled changes in the input variables of the process under study, for predict and understand the output variable behavior [271].

Training data is analyzed to form a fitted regression line around the data points. This regression line is a line segment which passes as close as possible from various data points [272]. The general equation for the linear regression model is represented as:

$$Y_i = \beta_0 + \beta_1 x_i \quad (18)$$

Where β_0 and β_1 are the regression coefficients. Here β_0 is interpreted as the line intercept and β1 as the slope of the regression line. The actual value of Y_i may vary from the expected value by e_i, the random error, as given by:

$$Y_i = \beta_0 + \beta_1 x_i + e_i \quad (19)$$

The objective of the fitted regression line is to minimize these errors. These errors are generally distributed around the regression line. The ordinary least squares method is an unbiased estimator for the coefficient β_0 and β_1 as it has a low variance, as given by:

$$\beta^{\wedge} = \frac{\sum_{i=1}^{n}(Y_i - \bar{Y})(x_i - \bar{x})}{\sum_{i=1}^{n}(x_i - \bar{x})^2} \quad (20)$$

$$\beta^{\wedge}_i = \bar{Y} + \beta_1 x_i + e_i \quad (21)$$

The relationship between input and output values are expressed in regression models and input values could be more than one.

The multiple regression model is a parametric model. To obtain the results, linear and nonlinear regression model by some application such as statistic and machine learning. Elatharasan et al. [273] studied the modeling and optimization of AA6061-T6 and AA7075-T6 by FSW parameters to predict the ultimate tensile load. The results show that 95% was confidence level. Srinivasa et al. [274] applied regression model. Optimization of FSW process parameters obtained by using response surface plots for maximize hardness, tensile strength, % elongation, impact strength and bending strength. The R^2 values for the predicted model were equal to hardness 83.90%,

ultimate Tensile strength 95.47%, elongation 86.47%, bending strength 90.73% and impact strength 93.78%.

6.2.8 MLR Results

6.2.8.1 Tensile Shear Load

In this section of research, multiple linear regression model was examined. MLR (cf-tool) equation was fitted using the data experiments for tensile shear load. The number of experiments are 6 for with CFRP and same as without CFRP.

The MLR equation consists of constant and linear expressions. The equation below shows the linear regression obtained as a result of the regression analysis in the case of with CFRP.

$$f(x, y) = 863.3 + 355.7x - 0.6097y - 0.2447xy + 0.0006002y^2$$

In this formula, (x, y) , as a function x and y stand for dwell time and rotational speed , which used to predict the tensile shear load at given parameters.

The performance of MLR evaluated by correlated coefficient R-square value 0.9997, root mean square error (RMSE) value 10.24. The graph of the estimates obtained from the model with the data set used in the training and testing phase is presented in Figure 57.

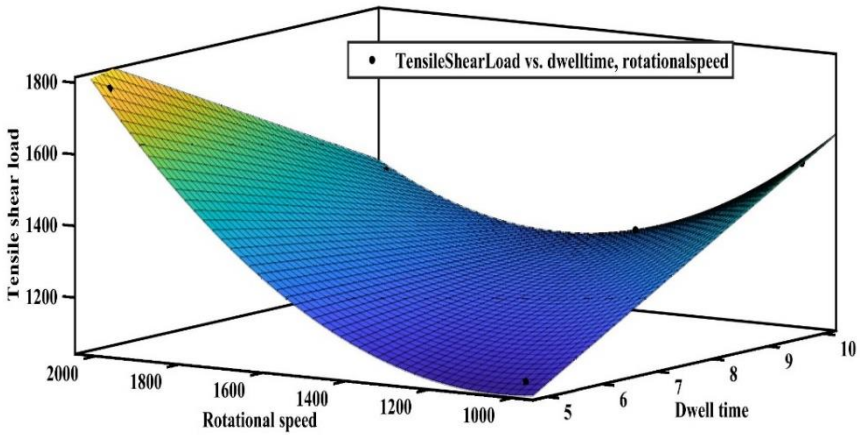

Figure 57: Graphical representation of MLR model results with CFRP interlayer

The second part of the data set, the MLR equation consists of constant and linear expressions. The equation below shows the linear regression obtained as a result of the regression analysis in the case of without CFRP.

$$f(x,y) = -601 - 420a + 5.723b + 0.2063ab - 0.002346b^2$$

In this formula,(x,y), a and b represented as function of dwell time and rotational speed to predict the results. The performance of the developed model is measured by using correlated coefficient R-square value, which is obtained as 0.9599, and RMSE value was 227.7. Figure 58 shows the MLR results obtained at certain welding parameters.

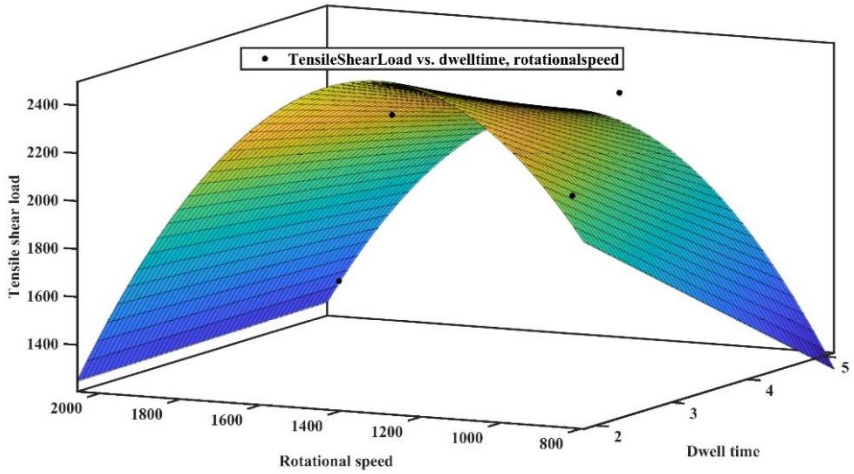

Figure 58: Graphical representation of MLR model results without CFRP interlayer

6.2.8.2 Temperature Evaluation

In this section of research, multiple linear regression model was examined. MLR (cf-tool) equation was fitted using the data experiments for temperature. The number of experiments are 6 for with CFRP and same as without CFRP.

The MLR equation consists of constant and linear expressions. The equation below shows the linear regression obtained as a result of the regression analysis in the case of with CFRP.

$$f(x,y) = 155 + 0.07654x + 1.332y - 0.00001288x^2 + 0.003375xy$$

In this formula, (x, y) , as a function x and y stand for dwell time and rotational speed , which used to predict the temperature at given parameters.

The performance of MLR evaluated by correlated coefficient R-square value 0.9894, root mean square error (RMSE) value 6.595. The graph of the estimates obtained from the model with the data set used in the training and testing phase is presented in Figure 59.

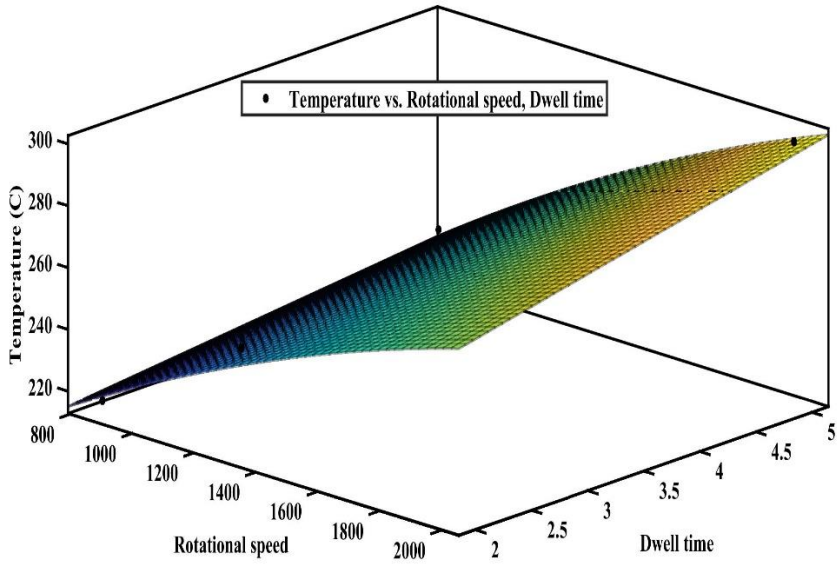

Figure 59: Graphical representation of MLR model results with CFRP interlayer

The second part of the data set, the MLR equation consists of constant and linear expressions. The equation below shows the linear regression obtained as a result of the regression analysis in the case of without CFRP.

$$f(x,y) = -124.4 + 42.01a + 0.3697b - 0.02128ab - 0.000078b^2$$

In this formula,(x,y), x and y represented as function of dwell time and rotational speed to predict the results. The performance of the developed model is measured by using correlated coefficient R-square value, which is obtained as 0.9791, and RMSE value was 15.23. Figure 60 shows the MLR results obtained at certain welding parameters.

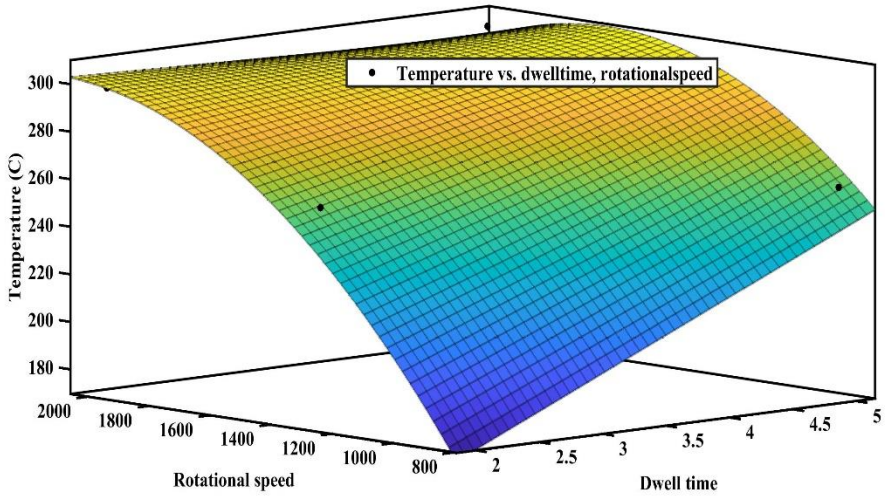

Figure 60: Graphical representation of MLR model results without CFRP interlayer

6.3 Discussion

In this research tensile shear load and temperature prediction including different dwell time and rotational speed were used as input to predict tensile shear load and temperature values (dependent value) by machine learning techniques. For the prediction models, four different models are created to estimate the tensile shear load. These models are artificial neural network (ANN), support vector regression (SVR), Adaptive Neuro-Fuzzy Inference System (ANFIS) and multilinear regression (MLR). The table 6 presented an actual and prediction tensile shear load results of specified models with CFRP interlayer and table 7 presented an actual and prediction results of specified models without CFRP interlayer. Also, table 8 presented an actual and prediction temperature results of specified models with CFRP interlayer and table 9 presented an actual and prediction results of specified models without CFRP interlayer

The performance of model will be evaluated by calculating the error between actual results and predicted results which is calculated by following equation.

$$Prediction\ error\% = \frac{|Actual\ value - predicted\ vslue|}{Actual\ value} \times 100 \quad (22)$$

The production values of tensile shear load in case of CFRP interlayer, the result show the minimum error was 0.333 % on the MLR model whereas the maximum was obtained 4.38 % in the ANN model. The case of without interlayer, the result show the minimum error was 4.3 % on the ANFIS model whereas the maximum was obtained 4.92 % in the SVM medium gaussian model. The production values of temperature in case of CFRP interlayer, the result show the minimum error was 0.697 % on the ANN model whereas the maximum was obtained 1.406 % in the SVM model. The case of without interlayer, the result show the minimum error was 0.803 % on the ANFIS model whereas the maximum was obtained 3.449 % in the SVM model.

Furthermore, estimation in numerical research measuring the Root Mean Square Error (RMSE) is a suitable technique .The RMSE equation described below:

$$RMSE = \sqrt{\frac{1}{N}\sum_{i=1}^{N}(p_i - t_i)^2} \quad (23)$$

Here N represent of training data completed, p_i is the estimation of required information, and $t_i$is the actual value. RMSE have been presented method to predict tensile shear load in this research. The results presented that, RMSE of tensile shear load was maximum in medium gaussian 111.797 and minimum in MLR with 7.41324. On the other hand, the RMSE of tensile shear load was maximum in medium gaussian 220.851 and minimum in ANFIS with 147.536.

Table 6: Actual vs prediction tensile shear load results with CFRP and average prediction error

Rotational speed	Dwell time	Tensile shear load	SVM		ANFIS	ANN	MLR
			Fine Gaussian	Medium Gaussian			
850	2	1077.7	1050.092	1050.044	1032.4	1032	1074.1
850	5	1513.6	1452.104	1423.853	1463.3	1497	1517.2
1300	2	1154.3	1126.695	1126.697	1101.9	1043	1160.2
1300	5	1278.7	1232.014	1239.17	1222.6	1222	1272.9
2000	2	1779.6	1676.365	1676.367	1731.7	1733	1777.3
2000	5	1373.7	1307.523	1328.516	1319.3	1315	1376.2
		Prediction error %	4.05	3.84	3.85	4.38	0.30

Table 7: Actual vs prediction tensile shear load results without CFRP and average prediction error

Rotational speed	Dwell time	Tensile shear load	SVM		ANFIS	ANN	MLR
			Fine Gaussian	Medium Gaussian			
850	2	2158.02	1971.6	2014.43	2031.7	2031.6	2079.2
850	5	1264.3	1250.8	1280.73	1221.7	1221.5	1345.3
1300	2	2439.2	2319.3	2305.13	2355.2	2353.9	2570.5
1300	5	2243.59	2161.1	2029.73	2171.1	2169.8	2115.1
2000	2	1495.55	1430.3	1429.9	1410.2	1392.6	1446.2
2000	5	1370.23	1305.1	1304.8	1305.1	1288.2	1424
		Prediction error %	4.84	4.9	4.3	4.83	4.7

Table 8: Actual vs prediction temperature results with CFRP and average prediction error

Rotational speed	Dwell time	Temperature	SVM Quadratic	ANFIS	ANN	MLR
850	2	216.9	223.7358748	216.8352	217.9	219.1547
850	5	234.1	236.0162827	234.0349	234.7	231.757
1300	2	248	244.3981237	247.4025	247.9	244.1738
1300	5	257.6	260.3523413	256.9999	250.4	261.3323
2000	2	271.3	274.0681121	262.5494	272.2	272.724
2000	5	298.5	295.7371448	289.7103	297.6	296.97
		Prediction error %	1.406	1.116	0.697	1.011

Table 9: Actual vs prediction temperature results without CFRP and average prediction error

Rotational speed	Dwell time	Temperature	SVM Quadratic	ANFIS	ANN	MLR
850	2	176	203.083047	175.9508235	176.5	181.334
850	5	258.4	255.4313165	258.350105	257	253.1
1300	2	261.8	258.8222936	261.3467696	256.2	253.082
1300	5	287.4	290.3867683	286.9401197	285.6	296.12
2000	2	298.5	301.4764611	291.8618208	305.7	301.9
2000	5	303.7	300.7105883	296.9644409	308.8	300.25
		Prediction error %	3.449	0.803	1.275	2.286

Chapter 7

CONCLUSION

7.1 Introduction

The current study demonstrated that similar aluminum alloys 5052 with additional CFRP interlayer were successfully joined by applying friction stir spot welding. The effect of tool rotational speed and dwell time are significantly effects on mechanical performance and microstructure was evaluated. Through research and investigations, the following results were reached.

7.2 Conclusion

- The maximum tensile shear load was obtained at rotational speed 2,000 rpm and 2 s dwell time with joint efficiency of 14.6%. The increase of tensile load due to heat input melted CFRP interlayer and squeezed out of the center, whereas low rotational speed had low value of tensile shear load. Consequently, this decrease in tensile shear load may be due to the formation of microcracks within the stir zone. On the other hand the joints without interlayer, maximum tensile shear load was obtained at rotational speed 1300 rpm and 2 second dwell time with joint efficiency of 19.4%. Tensile shear load increased by increase the from 850 to 1300 rpm, but the value dwindle when the rotational speed increase to 2000 rpm this scenario due to fine grans and dynamic recrystallized.
- The maximum hardness was observed at rotational speed 2,000 rpm and 5 s dwell time, which gradually reduced by decreasing rotational speed and dwell

time. The increase in key hole area was due to plastic deformation rather than SZ and TMAZ. Carbon fiber interlayer and welding parameters showed significant effect on microhardness result. This was due to highly different coefficients of thermal expansion, mixing, and incorporating between AA5052 sheets and CFRP interlayer whereas the joints without interlayer, maximum microhardness was obtained at 850 rpm and 2 second dwell time in thermal mechanical affect zone. In the TMAZ area, 49 % improved in increased compared to SZ, this increase due to the increased thermomechanical effect of the shoulder tool into welded sample.

- In the microstructural, the main discrete regions observed in FSSW joints are SZ and TMAZ. Interlayer was melted and squeezed out of the center of edge joint due to high heat input during the processes. Scanning electron microscope showed welding defects such as cracks which were clearly observed on the left and right sides of keyhole and were increased by increasing welding parameters while the sample without interlayer microstructure, the regions are mainly (SZ) and (TMAZ), the (SZ) much fine than (TMAZ). Also, nugget was characterized by plasticized material during the friction stir spot welding processes. Deformation of grains in this zone is owing to the shear stress connected by the material flow. Also, SEM-EDS analysis was applied to observe the intermetallic compound and their element distribution. The elements such as Al, Mg, and C increase the mechanical performance.
- The CFRP interlayer had an effective role in terms of micro hardness especially in welding area. It was more bonding rather than the other area. This due union of the carbon with aluminuim alloy.

- The machine learning tool were applied for tensile shear load prediction of similar AA5052 with and without CFRP interlayer by. Four different supervised machine learning tool, artificial neural network, adaptive neuro-fuzzy inference system, support vector machine regression and multi linear regression model were applied to train the model by using provided input data. The predict results of all these model were evaluated by calculating the prediction error of these model with actual experimental results. The prediction error percentage shows the prediction accuracy of the each model. The better prediction was multi linear regression models with CFRP interlayer samples rather than the other module. On the other hand the samples without CFRP interlayer, the ANFIS method has better prediction.

7.3 Future Recommendations

- Applying welding quality control technology. i.e., strain gage rosette (SGR) in order to investigate strain value near the SZ periphery.
- Instead of single spot joint on a joint to predict the behavior of their properties, Multiple Spot weld point could be made.
- It is recommended that should consider further characterization of the mechanical properties for the samples through a three-point bending test.

REFERENCES

[1] Cinar, Z.; Asmael, M.; Zeeshan, Q.; Safaei, B. Effect of Springback on A6061 Sheet Metal Bending: A Review. *Jurnal Kejuruteraan* 2021, *33*, 13-26.

[2] Lapčík, L.; Vašina, M.; Lapčíková, B.; Hui, D.; Otyepková, E.; Greenwood, R.W.; Waters, K.E.; Vlček, J. Materials characterization of advanced fillers for composites engineering applications. *Nanotechnology Reviews* 2019, *8*, 503-512.

[3] Toros, S.; Ozturk, F.; Kacar, I. Review of warm forming of aluminum–magnesium alloys. *Journal of materials processing technology* 2008, *207*, 1-12.

[4] Jung, J.; Cho, Y.J.; Kim, S.-H.; Lee, Y.-S.; Kim, H.-J.; Lim, C.-Y.; Park, Y.H. Microstructural and mechanical responses of various aluminum alloys to ballistic impacts by armor piercing projectile. *Materials Characterization* 2020, *159*, 110033.

[5] Howeyze, M.; Arabi, H.; Eivani, A.; Jafarian, H. Strengthening of AA5052 aluminum alloy by equal channel angular pressing followed by softening at room temperature. *Materials Science and Engineering: A* 2018, *720*, 160-168.

[6] Yogesha, K.; Joshi, A.; Kumar, N.; Jayaganthan, R. Effect of cryo groove rolling followed by warm rolling (CGW) on the mechanical properties of 5052 Al alloy. *Materials and Manufacturing Processes* 2017, *32*, 1336-1344.

[7] Saju, T.P.; Narayanan, R.G. Dieless friction stir lap joining of AA 5050-H32 with AA 6061-T6 at varying pre-drilled hole diameters. *Journal of Manufacturing Processes* 2020, *53*, 21-33.

[8] Engler, O.; Kuhnke, K.; Westphal, K.; Hasenclever, J. Impact of chromium on the microchemistry evolution during solidification and homogenization of the Al-Mg alloy AA 5052. *Journal of Alloys and Compounds* 2018, *744*, 561-573.

[9] Hassanpour, H.; Jamaati, R.; Hosseinipour, S.J. A novel technique to form gradient microstructure in AA5052 alloy. *Materials Science and Engineering: A* 2020, *777*, 139075.

[10] Sahmani, S.; Safaei, B. Large-amplitude oscillations of composite conical nanoshells with in-plane heterogeneity including surface stress effect. *Applied Mathematical Modelling* 2021, *89*, 1792-1813.

[11] Behdinan, K.; Moradi-Dastjerdi, R.; Safaei, B.; Qin, Z.; Chu, F.; Hui, D. Graphene and CNT impact on heat transfer response of nanocomposite cylinders. *Nanotechnology Reviews* 2020, *9*, 41-52.

[12] Heggemann, T.; Homberg, W. Deep drawing of fiber metal laminates for automotive lightweight structures. *Composite Structures* 2019, *216*, 53-57.

[13] Asmael, M.; Safaei, B.; Zeeshan, Q.; Zargar, O.; Nuhu, A.A. Ultrasonic machining of carbon fiber–reinforced plastic composites: a review. *The International Journal of Advanced Manufacturing Technology* 2021, 1-42.

[14] Sharma, A.; Sharma, V.M.; Gugaliya, A.; Rai, P.; Pal, S.K.; Paul, J. Friction stir lap welding of AA6061 aluminium alloy with a graphene interlayer. *Materials and Manufacturing Processes* 2020, *35*, 258-269.

[15] Shen, Z.; Ding, Y.; Gerlich, A.P. Advances in friction stir spot welding. *Critical Reviews in Solid State and Materials Sciences* 2020, *45*, 457-534.

[16] Ilman, M.N. Microstructure and mechanical properties of friction stir spot welded AA5052-H112 aluminum alloy. *Heliyon* 2021, *7*, e06009.

[17] Nasir, T.; Asmaela, M.; Zeeshana, Q.; Solyalib, D. Applications of Machine Learning to Friction Stir Welding Process Optimization. *Jurnal Kejuruteraan* 2020, *32*, 171-186.

[18] Feng, Z.; Santella, M.; David, S.; Steel, R.; Packer, S.; Pan, T.; Kuo, M.; Bhatnagar, R. Friction stir spot welding of advanced high-strength steels–a feasibility study. *SAE Transactions* 2005, 592-598.

[19] Peters, S.T. *Handbook of composites*; Springer Science & Business Media: 2013.

[20] Kodokian, G.-K. Adhesive bonding of thermoplastic fibre-composites. Imperial College London (University of London), 1989.

[21] Amancio-Filho, S.; dos Santos, J. Method for joining metal and plastic workpieces. *European Patent No. EP2329905B1* 2012.

[22] Ren, S.; Ma, Z.; Chen, L. Effect of welding parameters on tensile properties and fracture behavior of friction stir welded Al–Mg–Si alloy. *Scripta Materialia* 2007, *56*, 69-72.

[23] Zhang, Q.; Zhang, L.; Liu, W.; Zhang, X.; Zhu, W.; Qu, S. 3D rigid viscoplastic FE modelling of continuous drive friction welding process. *Science and Technology of Welding and Joining* 2006, *11*, 737-743.

[24] Zhao, H.; Shen, Z.; Booth, M.; Wen, J.; Fu, L.; Gerlich, A. Calculation of welding tool pin width for friction stir welding of thin overlapping sheets. *The International Journal of Advanced Manufacturing Technology* 2018, *98*, 1721-1731.

[25] Shen, Z.; Chen, Y.; Haghshenas, M.; Nguyen, T.; Galloway, J.; Gerlich, A. Interfacial microstructure and properties of copper clad steel produced using friction stir welding versus gas metal arc welding. *Materials Characterization* 2015, *104*, 1-9.

[26] Sathiya, P.; Aravindan, S.; Haq, A.N. Some experimental investigations on friction welded stainless steel joints. *Materials & Design* 2008, *29*, 1099-1109.

[27] Woo, I.; Aritoshi, M.; KIkUCHI, Y. Metallurgical and mechanical properties of high nitrogen austenitic stainless steel friction welds. *ISIJ international* 2002, *42*, 401-406.

[28] Li, Y.; Lu, J. Lightweight structure design for wind energy by integrating nanostructured materials. *Materials & Design* 2014, *57*, 689-696.

[29] Murray, R.E.; Roadman, J.; Beach, R. Fusion joining of thermoplastic composite wind turbine blades: Lap-shear bond characterization. *Renewable Energy* 2019, *140*, 501-512.

[30] Dursun, T.; Soutis, C. Recent developments in advanced aircraft aluminium alloys. *Materials & Design (1980-2015)* 2014, *56*, 862-871.

[31] Zhang, J.; Chaisombat, K.; He, S.; Wang, C.H. Hybrid composite laminates reinforced with glass/carbon woven fabrics for lightweight load bearing structures. *Materials & Design (1980-2015)* 2012, *36*, 75-80.

[32] Singh, R.; Kumar, R.; Feo, L.; Fraternali, F. Friction welding of dissimilar plastic/polymer materials with metal powder reinforcement for engineering applications. *Composites Part B: Engineering* 2016, *101*, 77-86.

[33] Hamm, L.; Krautkrämer, B.; Malik, R.; Peitz, V.; Plank, R.; Solfrank, P. Werkstoffe und Fertigungsverfahren. In *Vieweg Handbuch Kraftfahrzeugtechnik*, Springer: 2016; pp. 1163-1255.

[34] Min, J.; Li, Y.; Li, J.; Carlson, B.E.; Lin, J. Friction stir blind riveting of carbon fiber-reinforced polymer composite and aluminum alloy sheets. *The International Journal of Advanced Manufacturing Technology* 2015, *76*, 1403-1410.

[35] Mitschang, P.; Velthuis, R.; Didi, M. Induction spot welding of metal/CFRPC hybrid joints. *Advanced engineering materials* 2013, *15*, 804-813.

[36] Wang, T.; Li, L.; Pallaka, M.R.; Das, H.; Whalen, S.; Soulami, A.; Upadhyay, P.; Kappagantula, K.S. Mechanical and microstructural characterization of AZ31 magnesium‐carbon fiber reinforced polymer joint obtained by friction stir interlocking technique. *Materials & Design* 2020, *198*, 109305.

[37] Wang, X.; Morisada, Y.; Fujii, H. Flat friction stir spot welding of AZ31B magnesium alloy using double side adjustable tools: microstructure and mechanical properties. *Science and Technology of Welding and Joining* 2020, *25*, 644-652.

[38] Amancio-Filho, S.T.; Dos Santos, J.F. Joining of polymers and polymer–metal hybrid structures: recent developments and trends. *Polymer Engineering & Science* 2009, *49*, 1461-1476.

[39] Haghshenas, M.; Khodabakhshi, F. Dissimilar friction-stir welding of aluminum and polymer: a review. *The International Journal of Advanced Manufacturing Technology* 2019, *104*, 333-358.

[40] Alia, C.; Arenas, J.M.; Suárez, J.C.; Ocana, R.; Narbón, J.J. Mode II fracture energy in the adhesive bonding of dissimilar substrates: carbon fibre composite to aluminium joints. *Journal of Adhesion Science and Technology* 2013, *27*, 2480-2494.

[41] Khodabakhshi, F.; Haghshenas, M.; Chen, J.; Shalchi Amirkhiz, B.; Li, J.; Gerlich, A. Bonding mechanism and interface characterisation during dissimilar friction stir welding of an aluminium/polymer bi-material joint. *Science and Technology of Welding and Joining* 2017, *22*, 182-190.

[42] Chowdhury, S.; Chen, D.; Bhole, S.; Cao, X.; Wanjara, P. Lap shear strength and fatigue behavior of friction stir spot welded dissimilar magnesium-to-aluminum joints with adhesive. *Materials Science and Engineering: A* 2013, *562*, 53-60.

[43] Fink, A.; Camanho, P.; Andrés, J.; Pfeiffer, E.; Obst, A. Hybrid CFRP/titanium bolted joints: Performance assessment and application to a spacecraft payload adaptor. *Composites Science and Technology* 2010, *70*, 305-317.

[44] Yan, B.; Zhu, S.; Tong, M.; Pan, S. Experimental study on the mechanical properties of laminates made of thin carbon fiber plies. *Composite Structures* 2020, 112336.

[45] Pramanik, A.; Basak, A.; Dong, Y.; Sarker, P.; Uddin, M.; Littlefair, G.; Dixit, A.; Chattopadhyaya, S. Joining of carbon fibre reinforced polymer (CFRP) composites and aluminium alloys–A review. *Composites Part A: Applied Science and Manufacturing* 2017, *101*, 1-29.

[46] Boucherit, A.; Abdi, S.; Aissani, M.; Mehdi, B.; Abib, K.; Badji, R. Weldability, microstructure, and residual stress in Al/Cu and Cu/Al friction stir

spot weld joints with Zn interlayer. *The International Journal of Advanced Manufacturing Technology* 2020, *111*, 1553-1569.

[47] Davies, P.; Cantwell, W.; Jar, P.-Y.; Bourban, P.-E.; Zysman, V.; Kausch, H. Joining and repair of a carbon fibre-reinforced thermoplastic. *Composites* 1991, *22*, 425-431.

[48] Jiang, B.; Chen, Q.; Yang, J. Advances in joining technology of carbon fiber-reinforced thermoplastic composite materials and aluminum alloys. *The International Journal of Advanced Manufacturing Technology* 2020, 1-19.

[49] Wise, R. New technique for joining dissimilar materials. *Welding Review International* 1993, *2*, 40-42.

[50] Wang, S.; Liang, W.; Duan, L.; Li, G.; Cui, J. Effects of loading rates on mechanical property and failure behavior of single-lap adhesive joints with carbon fiber reinforced plastics and aluminum alloys. *The International Journal of Advanced Manufacturing Technology* 2020, *106*, 2569-2581.

[51] Lin, P.-C.; Lin, J.-W.; Li, G.-X. Clinching process for aluminum alloy and carbon fiber-reinforced thermoplastic sheets. *The International Journal of Advanced Manufacturing Technology* 2018, *97*, 529-541.

[52] Messler Jr, R.W. Joining composite materials and structures: some thought-provoking possibilities. *Journal of Thermoplastic Composite Materials* 2004, *17*, 51-75.

[53] Zhu, W.; Xiao, H.; Wang, J.; Fu, C. Characterization and properties of AA6061-based fiber metal laminates with different aluminum-surface pretreatments. *Composite Structures* 2019, *227*, 111321.

[54] Uday, M.; Ahmad Fauzi, M.; Zuhailawati, H.; Ismail, A. Advances in friction welding process: a review. *Science and technology of Welding and Joining* 2010, *15*, 534-558.

[55] Kanawade, D.; Jandali, G.; Mallick, P. Development of thermoplastic matrix composite tubes for automotive applications. In Proceedings of Proc. 17th Technical Conference of the American Society for Composites, West Lafayette, IN.

[56] Morgan, P. Polymer matrices for carbon fiber composites. *Carbon fiber and their composites. New York: Taylor & Francis Group* 2005, 534-535.

[57] Dong, S.; Gauvin, R. Application of dynamic mechanical analysis for the study of the interfacial region in carbon fiber/epoxy composite materials. *Polymer composites* 1993, *14*, 414-420.

[58] Vorderbrüggen, J.; Meschut, G. Investigations on a material-specific joining technology for CFRP hybrid joints along the automotive process chain. *Composite Structures* 2019, *230*, 111533.

[59] Sullivan, R.A. Automotive carbon fiber: Opportunities and challenges. *Jom* 2006, *58*, 77-79.

[60] Kumar, R.; Singh, R.; Ahuja, I.; Penna, R.; Feo, L. Weldability of thermoplastic materials for friction stir welding-A state of art review and future applications. *Composites Part B: Engineering* 2018, *137*, 1-15.

[61] Takahashi, J.; Ishikawa, T. Current Japanese activity in CFRTP for mass production automotive application. In Proceedings of Proceedings of the 13th Japan international SAMPE symposium & exhibition.

[62] Kwon, D.-J.; Kim, J.-H.; Kim, Y.-J.; Kim, J.-J.; Park, S.-M.; Kwon, I.-J.; Shin, P.-S.; DeVries, L.K.; Park, J.-M. Comparison of interfacial adhesion of hybrid materials of aluminum/carbon fiber reinforced epoxy composites with different surface roughness. *Composites Part B: Engineering* 2019, *170*, 11-18.

[63] Quilter, A. Composites in aerospace applications. *IHS White Paper* 2001, *444*.

[64] Liu, Y.; Zhuang, W.; Wu, S. Damage to carbon fibre reinforced polymers (CFRP) in hole-clinched joints with aluminium alloy and CFRP. *Composite Structures* 2020, *234*, 111710.

[65] Ferreira, L.M.M. Study of the Behaviour of Non-Crimp Fabric Laminates by 3D Finite Element Model. Universidad de Sevilla, Escuela Técnica Superior de Arquitectura, 2012.

[66] Jeon, C.-S.; Jeong, Y.-H.; Hong, S.-T.; Hasan, M.T.; Tien, H.N.; Hur, S.-H.; Kwon, Y.-J. Mechanical properties of graphite/aluminum metal matrix

composite joints by friction stir spot welding. *Journal of Mechanical Science and Technology* 2014, *28*, 499-504.

[67] Beylergil, B.; Tanoğlu, M.; Aktaş, E. Effect of polyamide-6, 6 (PA 66) nonwoven veils on the mechanical performance of carbon fiber/epoxy composites. *Composite Structures* 2018, *194*, 21-35.

[68] Huang, Y.; Meng, X.; Wang, Y.; Xie, Y.; Zhou, L. Joining of aluminum alloy and polymer via friction stir lap welding. *Journal of materials Processing technology* 2018, *257*, 148-154.

[69] Huang, Y.; Meng, X.; Xie, Y.; Li, J.; Wan, L. New technique of friction-based filling stacking joining for metal and polymer. *Composites Part B: Engineering* 2019, *163*, 217-223.

[70] Meng, X.; Huang, Y.; Xie, Y.; Li, J.; Guan, M.; Wan, L.; Dong, Z.; Cao, J. Friction self-riveting welding between polymer matrix composites and metals. *Composites Part A: Applied Science and Manufacturing* 2019, *127*, 105624.

[71] Bilici, M.K.; Yükler, A.İ.; Kurtulmuş, M. The optimization of welding parameters for friction stir spot welding of high density polyethylene sheets. *Materials & Design* 2011, *32*, 4074-4079.

[72] Yusof, F.; Muhamad, M.R.b.; Moshwan, R.; Jamaludin, M.F.b.; Miyashita, Y. Effect of surface states on joining mechanisms and mechanical properties of

aluminum alloy (A5052) and polyethylene terephthalate (PET) by dissimilar friction spot welding. *Metals* 2016, *6*, 101.

[73] Oliveira, P.; Amancio-Filho, S.; Dos Santos, J.; Hage Jr, E. Preliminary study on the feasibility of friction spot welding in PMMA. *Materials Letters* 2010, *64*, 2098-2101.

[74] Epstein, S.G.; Kaufman, J.; Pollak, P. *Aluminum and Its Alloys*; Aluminum Association Washington, DC: 1994.

[75] Lumley, R. *Fundamentals of aluminium metallurgy: production, processing and applications*; Elsevier: 2010.

[76] Grushko, O.; Ovsyannikov, B.; Ovchinnokov, V. *Aluminum-lithium Alloys: Process Metallurgy, Physical Metallurgy, and Welding*; CRC press: 2016.

[77] Belov, N.A.; Aksenov, A.A.; Eskin, D.G. *Iron in aluminium alloys: impurity and alloying element*; CRC Press: 2002.

[78] Davis, J.R. *Aluminum and aluminum alloys*; ASM international: 1993.

[79] Pearson, W.B. *A handbook of lattice spacings and structures of metals and alloys: International series of monographs on metal physics and physical metallurgy*; Elsevier: 2013; Vol. 4.

[80] Wrobel, R.; Salt, D.; Simpson, N.; Mellor, P. Comparative study of copper and aluminium conductors-future cost effective PM machines. 2014.

[81] Farid, M.M.; Khudhair, A.M.; Razack, S.A.K.; Al-Hallaj, S. A review on phase change energy storage: materials and applications. *Energy conversion and management* 2004, *45*, 1597-1615.

[82] Su, P.; Gerlich, A.; North, T.; Bendzsak, G. Intermixing in dissimilar friction stir spot welds. *Metallurgical and materials transactions A* 2007, *38*, 584-595.

[83] Gerlich, A.; Su, P.; North, T. Peak temperatures and microstructures in aluminium and magnesium alloy friction stir spot welds. *Science and technology of welding and joining* 2005, *10*, 647-652.

[84] André, N.M. Friction spot joining of aluminum alloy 2024-t3 and carbon-fiber-reinforced polyphenylene sulfide composite laminate with additional pps film interlayer. 2015.

[85] Kumar, R.D.; Muthukumaran, S.; Venkateswaran, T.; Xavier, V.; Sivakumar, D. Failure Analysis And Process Parameter Influence On Mechanical And Metallurgical Behavior Of Friction Stir Welded Aa2219-T87 Joints. *Surface Review and Letters* 2020, *27*, 1950107.

[86] Paoletti, A.; Lambiase, F.; Di Ilio, A. Optimization of friction stir welding of thermoplastics. *Procedia CIRP* 2015, *33*, 562-567.

[87] Asmael, M.; Glaissa, M. Effects of rotation speed and dwell time on the mechanical properties and microstructure of dissimilar aluminum-titanium alloys by friction stir spot welding (FSSW). *Materialwissenschaft und Werkstofftechnik* 2020, *51*, 1002-1008.

[88] Schmidt, H.B.; Hattel, J.H. Thermal modelling of friction stir welding. *Scripta Materialia* 2008, *58*, 332-337.

[89] Su, P.; Gerlich, A.; North, T. *Friction stir spot welding of aluminum and magnesium alloy sheets*; 0148-7191; SAE Technical Paper: 2005.

[90] Gerlich, A.; Avramovic-Cingara, G.; North, T. Stir zone microstructure and strain rate during Al 7075-T6 friction stir spot welding. *Metallurgical and Materials Transactions A* 2006, *37*, 2773-2786.

[91] Gerlich, A.; Yamamoto, M.; North, T. Strain rates and grain growth in Al 5754 and Al 6061 friction stir spot welds. *Metallurgical and materials transactions A* 2007, *38*, 1291-1302.

[92] Paidar, M.; Khodabandeh, A.; Najafi, H.; Rouh-aghdam, A.S. Retracted article: an investigation on mechanical and metallurgical properties of 2024-T3 aluminum alloy spot friction welds. *The International Journal of Advanced Manufacturing Technology* 2015, *80*, 183-197.

[93] Bozzi, S.; Helbert-Etter, A.; Baudin, T.; Klosek, V.; Kerbiguet, J.; Criqui, B. Influence of FSSW parameters on fracture mechanisms of 5182 aluminium welds. *Journal of Materials Processing Technology* 2010, *210*, 1429-1435.

[94] Mitlin, D.; Radmilovic, V.; Pan, T.; Chen, J.; Feng, Z.; Santella, M. Structure–properties relations in spot friction welded (also known as friction stir spot welded) 6111 aluminum. *Materials Science and Engineering: A* 2006, *441*, 79-96.

[95] Xu, L.; Wang, L.; Chen, Y.-C.; Robson, J.D.; Prangnell, P.B. Effect of interfacial reaction on the mechanical performance of steel to aluminum dissimilar ultrasonic spot welds. *Metallurgical and Materials Transactions A* 2016, *47*, 334-346.

[96] Bakavos, D.; Prangnell, P. Effect of reduced or zero pin length and anvil insulation on friction stir spot welding thin gauge 6111 automotive sheet. *Science and Technology of Welding and Joining* 2009, *14*, 443-456.

[97] Shen, Z.; Yang, X.; Zhang, Z.; Cui, L.; Yin, Y. Mechanical properties and failure mechanisms of friction stir spot welds of AA 6061-T4 sheets. *Materials & Design* 2013, *49*, 181-191.

[98] Su, P.; Gerlich, A.; North, T.; Bendzsak, G. Energy generation and stir zone dimensions in friction stir spot welds. *SAE Transactions* 2006, 717-725.

[99] Prangnell, P.B.; Bakavos, D. Novel approaches to friction spot welding thin aluminium automotive sheet. In Proceedings of Materials Science Forum; pp. 1237-1242.

[100] Chen, Y.; Liu, S.; Bakavos, D.; Prangnell, P. The effect of a paint bake treatment on joint performance in friction stir spot welding AA6111-T4 sheet using a pinless tool. *Materials Chemistry and Physics* 2013, *141*, 768-775.

[101] Bakavos, D.; Chen, Y.; Babout, L.; Prangnell, P. Material interactions in a novel pinless tool approach to friction stir spot welding thin aluminum sheet. *Metallurgical and Materials Transactions A* 2011, *42*, 1266-1282.

[102] Aota, K.; Ikeuchi, K. Development of friction stir spot welding using rotating tool without probe and its application to low-carbon steel plates. *Welding International* 2009, *23*, 572-580.

[103] Gerlich, A.; Su, P.; North, T. Tool penetration during friction stir spot welding of Al and Mg alloys. *Journal of Materials Science* 2005, *40*, 6473-6481.

[104] Tozaki, Y.; Uematsu, Y.; Tokaji, K. A newly developed tool without probe for friction stir spot welding and its performance. *Journal of Materials Processing Technology* 2010, *210*, 844-851.

[105] Reilly, A.; Shercliff, H.; Chen, Y.; Prangnell, P. Modelling and visualisation of material flow in friction stir spot welding. *Journal of Materials Processing Technology* 2015, *225*, 473-484.

[106] Xu, R.; Ni, D.; Yang, Q.; Liu, C.; Ma, Z. Pinless friction stir spot welding of Mg–3Al–1Zn alloy with Zn interlayer. *Journal of Materials Science & Technology* 2016, *32*, 76-88.

[107] Shen, Z.; Yang, X.; Zhang, Z.; Cui, L.; Li, T. Microstructure and failure mechanisms of refill friction stir spot welded 7075-T6 aluminum alloy joints. *Materials & design* 2013, *44*, 476-486.

[108] Kubit, A.; Bucior, M.; Wydrzyński, D.; Trzepieciński, T.; Pytel, M. Failure mechanisms of refill friction stir spot welded 7075-T6 aluminium alloy single-lap joints. *The International Journal of Advanced Manufacturing Technology* 2018, *94*, 4479-4491.

[109] Shen, Z.; Yang, X.; Yang, S.; Zhang, Z.; Yin, Y. Microstructure and mechanical properties of friction spot welded 6061-T4 aluminum alloy. *Materials & Design (1980-2015)* 2014, *54*, 766-778.

[110] Kolba, T.; Faes, K.; De Waele, W. Experimental investigation of the weldability of high strength aluminium using friction spot welding. *SUSTAINABLE CONSTRUCTION & DESIGN* 2016, *7*.

[111] Plaine, A.; Suhuddin, U.; Alcântara, N.; Dos Santos, J. Fatigue behavior of friction spot welds in lap shear specimens of AA5754 and Ti6Al4V alloys. *International Journal of Fatigue* 2016, *91*, 149-157.

[112] Junior, W.S.; Handge, U.A.; dos Santos, J.F.; Abetz, V.; Amancio-Filho, S.T. Feasibility study of friction spot welding of dissimilar single-lap joint between poly (methyl methacrylate) and poly (methyl methacrylate)-SiO2 nanocomposite. *Materials & Design* 2014, *64*, 246-250.

[113] Yu, G.; Chen, X.; Zhang, B.; Pan, K.; Yang, L. Tensile-Shear Mechanical Behaviors of Friction Stir Spot Weld and Adhesive Hybrid Joint: Experimental and Numerical Study. *Metals* 2020, *10*, 1028.

[114] Reis, P.N.; Amaro, A.; Loureiro, A. Comparison of mechanical performance between friction-stir spot welded and adhesive bonded joints. *Frattura ed Integrità Strutturale* 2020, *14*, 124-133.

[115] Goushegir, S.; Dos Santos, J.; Amancio-Filho, S. Influence of process parameters on mechanical performance and bonding area of AA2024/carbon-fiber-reinforced poly (phenylene sulfide) friction spot single lap joints. *Materials & Design* 2015, *83*, 431-442.

[116] André, N.M.; Goushegir, S.M.; Dos Santos, J.F.; Canto, L.B.; Amancio-Filho, S.T. Friction Spot Joining of aluminum alloy 2024-T3 and carbon-fiber-reinforced poly (phenylene sulfide) laminate with additional PPS film interlayer: Microstructure, mechanical strength and failure mechanisms. *Composites Part B: Engineering* 2016, *94*, 197-208.

[117] Goushegir, S.; Dos Santos, J.; Amancio-Filho, S. Friction spot joining of aluminum AA2024/carbon-fiber reinforced poly (phenylene sulfide)

composite single lap joints: microstructure and mechanical performance. *Materials & Design (1980-2015)* 2014, *54*, 196-206.

[118] Esteves, J.V.; Goushegir, S.; dos Santos, J.F.; Canto, L.B.; Hage Jr, E.; Amancio-Filho, S. Friction spot joining of aluminum AA6181-T4 and carbon fiber-reinforced poly (phenylene sulfide): Effects of process parameters on the microstructure and mechanical strength. *Materials & Design* 2015, *66*, 437-445.

[119] Manente André, N.; F dos Santos, J.; T Amancio-Filho, S. Evaluation of Joint Formation and Mechanical Performance of the AA7075-T6/CFRP Spot Joints Produced by Frictional Heat. *Materials* 2019, *12*, 891.

[120] André, N.M.; Goushegir, S.M.; Santos, J.; Canto, L.B.; Amancio-Filho, S.T. On the microstructure and mechanical performance of Friction Spot Joining with additional film interlayer. In Proceedings of Proceedings of the Annual Technical Conference of Society of Plastics Engineers (ANTEC 2014); pp. 1791-1797.

[121] Manente André, N.; Goushegir, S.M.; Scharnagl, N.; dos Santos, J.F.; Canto, L.B.; Amancio-Filho, S.T. Composite surface pre-treatments: Improvement on adhesion mechanisms and mechanical performance of metal–composite friction spot joints with additional film interlayer. *The Journal of Adhesion* 2018, *94*, 723-742.

[122] André, N.M.; Goushegir, S.M.; dos Santos, J.F.; Canto, L.B.; Amancio-Filho, S.T. Influence of the interlayer film thickness on the mechanical performance of AA2024-T3/CF-PPS hybrid joints produced by friction spot joining. *Welding international* 2018, *32*, 1-10.

[123] Ogawa, Y.; Akebono, H.; Tanaka, K.; Sugeta, A. Effect of welding time on fatigue properties of friction stir spot welds of Al to carbon fibre-reinforced plastic. *Science and Technology of Welding and Joining* 2019, *24*, 235-242.

[124] Goushegir, S. Friction spot joining (FSpJ) of aluminum-CFRP hybrid structures. *Welding in the World* 2016, *60*, 1073-1093.

[125] Ogawa, Y.; Xiong, Y.; Akebono, H.; Kato, M.; Tanaka, K.; Sugeta, A. Fatigue properties of friction stir welds of treated Al to carbon fibre-reinforced plastic. *Science and Technology of Welding and joining* 2018, *23*, 79-86.

[126] Amancio-Filho, S.; Bueno, C.; Dos Santos, J.; Huber, N.; Hage Jr, E. On the feasibility of friction spot joining in magnesium/fiber-reinforced polymer composite hybrid structures. *Materials Science and Engineering: A* 2011, *528*, 3841-3848.

[127] Gonçalves, J.; Dos Santos, J.; Canto, L.; Amancio-Filho, S. Friction spot welding of carbon fiber-reinforced polyamide 66 laminate. *Materials Letters* 2015, *159*, 506-509.

[128] Huang, Y.; Meng, X.; Xie, Y.; Lv, Z.; Wan, L.; Cao, J.; Feng, J. Friction spot welding of carbon fiber-reinforced polyetherimide laminate. *Composite structures* 2018, *189*, 627-634.

[129] Gonçalves, J.; dos Santos, J.F.; Canto, L.B.; Filho, S.T.A. Improvement of friction spot welding (FSpW) to join polyamide 6 and polyamide 66/carbon fibre laminate. *Welding international* 2016, *30*, 247-254.

[130] Bolouri, A.; Fotouhi, M.; Moseley, W. A New Design for Friction Stir Spot Joining of Al Alloys and Carbon Fiber-Reinforced Composites. *Journal of Materials Engineering and Performance* 2020, 1-9.

[131] Rafiei, R.; Shamanian, M.; Fathi, M.; Khodabakhshi, F. Dissimilar friction-stir lap-welding of aluminum-magnesium (AA5052) and aluminum-copper (AA2024) alloys: microstructural evolution and mechanical properties. *The International Journal of Advanced Manufacturing Technology* 2018, *94*, 3713-3730.

[132] Khosa, S.U.; Weinberger, T.; Enzinger, N. Thermo-mechanical investigations during friction stir spot welding (FSSW) of AA6082-T6. *Welding in the World* 2010, *54*, R134-R146.

[133] Kubit, A.; Wydrzynski, D.; Trzepiecinski, T. Refill friction stir spot welding of 7075-T6 aluminium alloy single-lap joints with polymer sealant interlayer. *Composite Structures* 2018, *201*, 389-397.

[134] Sadoun, A.; Meselhy, A.; Deabs, A. Improved strength and ductility of friction stir tailor-welded blanks of base metal AA2024 reinforced with interlayer strip of AA7075. *Results in Physics* 2020, *16*, 102911.

[135] Abed, B.H.; Salih, O.S.; Sowoud, K.M. Pinless friction stir spot welding of aluminium alloy with copper interlayer. *Open Engineering* 2020, *10*, 804-813.

[136] Dedeoğlu, O.; Güler Özgül, H. The Joint Properties of 5754 Aluminium Alloy by Friction Stir Spot Welding. *Journal of Manufacturing and Materials Processing* 2019, *3*, 8.

[137] Suresh, S.; Venkatesan, K.; Natarajan, E.; Rajesh, S. Influence of tool rotational speed on the properties of friction stir spot welded AA7075-T6/Al2O3 composite joint. *Materials Today: Proceedings* 2020, *27*, 62-67.

[138] NASIR, T.; KALAF, O.; ASMAEL, M. Effect of rotational speed, and dwell time on the mechanical properties and microstructure of dissimilar AA5754 and AA7075-T651 aluminum sheet alloys by friction stir spot welding. *Materials Science* 2021.

[139] Suryanarayanan, R.; Sridhar, V. Effect of Process Parameters in Pinless Friction Stir Spot Welding of Al 5754-Al 6061 Alloys. *Metallography, Microstructure, and Analysis* 2020, 1-12.

[140] Li, W.; Chu, Q.; Yang, X.; Shen, J.; Vairis, A.; Wang, W. Microstructure and morphology evolution of probeless friction stir spot welded joints of aluminum alloy. *Journal of Materials Processing Technology* 2018, *252*, 69-80.

[141] Pathak, N.; Bandyopadhyay, K.; Sarangi, M.; Panda, S.K. Microstructure and mechanical performance of friction stir spot-welded aluminum-5754 sheets. *Journal of Materials Engineering and Performance* 2013, *22*, 131-144.

[142] Schilling, C.; dos Santos, J. Method and device for joining at least two adjoining work pieces by friction welding. Google Patents: 2004.

[143] Tier, M.; Rosendo, T.; Olea, C.; Mazzaferro, C.; Ramos, F.; Bayer, M.; Dos Santos, J.; da Silva, A.; Mazzaferro, J.; Strohaecker, T. The influence of weld microstructure on mechanical properties of refill friction spot welding of 5042 aluminium alloy. In Proceedings of 7th International Friction Stir Welding Symposium; p. 2287.

[144] Shen, Z.; Ding, Y.; Chen, J.; Fu, L.; Liu, X.; Chen, H.; Guo, W.; Gerlich, A. Microstructure, static and fatigue properties of refill friction stir spot welded 7075-T6 aluminium alloy using a modified tool. *Science and Technology of Welding and Joining* 2019, *24*, 587-600.

[145] Larsen, B.A. Increasing the Manufacturing Readiness of Refill Friction Stir Spot Welding. 2020.

[146] Suhuddin, U.; Fischer, V.; Dos Santos, J. The thermal cycle during the dissimilar friction spot welding of aluminum and magnesium alloy. *Scripta Materialia* 2013, *68*, 87-90.

[147] Rosendo, T.; Parra, B.; Tier, M.; Da Silva, A.; Dos Santos, J.; Strohaecker, T.; Alcântara, N. Mechanical and microstructural investigation of friction spot welded AA6181-T4 aluminium alloy. *Materials & design* 2011, *32*, 1094-1100.

[148] Shen, Z.; Ding, Y.; Gopkalo, O.; Diak, B.; Gerlich, A. Effects of tool design on the microstructure and mechanical properties of refill friction stir spot welding of dissimilar Al alloys. *Journal of Materials Processing Technology* 2018, *252*, 751-759.

[149] Shen, Z.; Chen, J.; Ding, Y.; Hou, J.; Shalchi Amirkhiz, B.; Chan, K.; Gerlich, A. Role of interfacial reaction on the mechanical performance of Al/steel dissimilar refill friction stir spot welds. *Science and Technology of Welding and Joining* 2018, *23*, 462-477.

[150] Reimann, M.; Goebel, J.; dos Santos, J.F. Microstructure and mechanical properties of keyhole repair welds in AA 7075-T651 using refill friction stir spot welding. *Materials & Design* 2017, *132*, 283-294.

[151] Allen, C.D.; Arbegast, W.J. Evaluation of friction spot welds in aluminum alloys. *SAE transactions* 2005, 612-618.

[152] Nasiri, A.M.; Shen, Z.; Hou, J.S.C.; Gerlich, A.P. Failure analysis of tool used in refill friction stir spot welding of Al 2099 alloy. *Engineering Failure Analysis* 2018, *84*, 25-33.

[153] Dong, H.; Chen, S.; Song, Y.; Guo, X.; Zhang, X.; Sun, Z. Refilled friction stir spot welding of aluminum alloy to galvanized steel sheets. *Materials & Design* 2016, *94*, 457-466.

[154] Shen, Z.; Ding, Y.; Chen, J.; Amirkhiz, B.S.; Wen, J.; Fu, L.; Gerlich, A. Interfacial bonding mechanism in Al/coated steel dissimilar refill friction stir spot welds. *Journal of Materials Science & Technology* 2019, *35*, 1027-1038.

[155] Chen, Y.; Chen, J.; Shalchi Amirkhiz, B.; Worswick, M.; Gerlich, A. Microstructures and properties of Mg alloy/DP600 steel dissimilar refill friction stir spot welds. *Science and Technology of Welding and Joining* 2015, *20*, 494-501.

[156] Plaine, A.; Suhuddin, U.; Afonso, C.; Alcântara, N.; Dos Santos, J. Interface formation and properties of friction spot welded joints of AA5754 and Ti6Al4V alloys. *Materials & Design* 2016, *93*, 224-231.

[157] Shen, J.; Suhuddin, U.F.; Cardillo, M.E.; dos Santos, J.F. Eutectic structures in friction spot welding joint of aluminum alloy to copper. *Applied Physics Letters* 2014, *104*, 191901.

[158] Patnaik, A.; Koch, K.; Arbegast, W.; Allen, C. *Static properties of "refill" friction spot welded skin stiffened compression panels*; 0148-7191; SAE Technical Paper: 2006.

[159] Lacki, P.; Derlatka, A. Strength evaluation of beam made of the aluminum 6061-T6 and titanium grade 5 alloys sheets joined by RFSSW and RSW. *Composite Structures* 2017, *159*, 491-497.

[160] Cox, C.D.; Gibson, B.T.; Strauss, A.M.; Cook, G.E. Effect of pin length and rotation rate on the tensile strength of a friction stir spot-welded al alloy: a contribution to automated production. *Materials and Manufacturing Processes* 2012, *27*, 472-478.

[161] Tozaki, Y.; Uematsu, Y.; Tokaji, K. Effect of tool geometry on microstructure and static strength in friction stir spot welded aluminium alloys. *International Journal of Machine Tools and Manufacture* 2007, *47*, 2230-2236.

[162] Shen, Z.; Li, W.; Ding, Y.; Hou, W.; Liu, X.; Guo, W.; Chen, H.; Liu, X.; Yang, J.; Gerlich, A. Material flow during refill friction stir spot welded dissimilar Al alloys using a grooved tool. *Journal of Manufacturing Processes* 2020, *49*, 260-270.

[163] Cao, J.; Zhang, C.; Xing, Y.; Wang, M. Pin plunging reinforced refill friction stir spot welding of Alclad 2219 to 7075 alloy. *Journal of Materials Processing Technology* 2020, *284*, 116760.

[164] Montag, T.; Wulfsberg, J.-P.; Hameister, H.; Marschner, R. Influence of tool wear on quality criteria for refill friction stir spot welding (RFSSW) process. *Procedia CIRP* 2014, *24*, 108-113.

[165] Ji, S.; Wang, Y.; Li, Z.; Yue, Y.; Chai, P. Effect of tool geometry on material flow behavior of refill friction stir spot welding. *Transactions of the Indian Institute of Metals* 2017, *70*, 1417-1430.

[166] Pabandi, H.K.; Movahedi, M.; Kokabi, A.H. A new refill friction spot welding process for aluminum/polymer composite hybrid structures. *Composite Structures* 2017, *174*, 59-69.

[167] Ashong, A.N.; Lee, M.; Hong, S.-T.; Lee, Y.S.; Kim, J.H. Refill Friction Stir Spot Welding of Dissimilar AA6014 Al Alloy and Carbon-Fiber-Reinforced Polymer Composite. *Metals and Materials International* 2020, 1-11.

[168] Özel, T.; Karpat, Y.; Srivastava, A. Hard turning with variable micro-geometry PcBN tools. *CIRP annals* 2008, *57*, 73-76.

[169] Ramachandran, K.; Murugan, N.; Kumar, S.S. Effect of tool axis offset and geometry of tool pin profile on the characteristics of friction stir welded dissimilar joints of aluminum alloy AA5052 and HSLA steel. *Materials Science and Engineering: A* 2015, *639*, 219-233.

[170] Suri, A. An improved FSW tool for joining commercial aluminum plates. *Procedia materials science* 2014, *6*, 1857-1864.

[171] Shah, L.H.A.; Sonbolestan, S.; Midawi, A.R.; Walbridge, S.; Gerlich, A. Dissimilar friction stir welding of thick plate AA5052-AA6061 aluminum alloys: effects of material positioning and tool eccentricity. *The International Journal of Advanced Manufacturing Technology* 2019, *105*, 889-904.

[172] Mehta, K.P.; Badheka, V.J. Influence of tool design and process parameters on dissimilar friction stir welding of copper to AA6061-T651 joints. *The International Journal of Advanced Manufacturing Technology* 2015, *80*, 2073-2082.

[173] Sharifitabar, M.; Nami, H. Microstructures of dissimilar friction stir welded joints between 2024-T4 aluminum alloy and Al/Mg2Si metal matrix cast composite. *Composites Part B: Engineering* 2011, *42*, 2004-2012.

[174] Amancio-Filho, S.; Dos Santos, J. Joining of polymers and polymer–metal hybrid structures: recent developments and trends. *Polymer Engineering & Science* 2009, *49*, 1461-1476.

[175] Meng, X.; Huang, Y.; Cao, J.; Shen, J.; dos Santos, J.F. Recent progress on control strategies for inherent issues in friction stir welding. *Progress in Materials Science* 2020, 100706.

[176] Uzun, H.; Dalle Donne, C.; Argagnotto, A.; Ghidini, T.; Gambaro, C. Friction stir welding of dissimilar Al 6013-T4 to X5CrNi18-10 stainless steel. *Materials & design* 2005, *26*, 41-46.

[177] Gibson, B.T.; Lammlein, D.; Prater, T.; Longhurst, W.; Cox, C.; Ballun, M.; Dharmaraj, K.; Cook, G.; Strauss, A. Friction stir welding: Process, automation, and control. *Journal of Manufacturing Processes* 2014, *16*, 56-73.

[178] Thomas, W.; Nicholas, E. Friction stir welding for the transportation industries. *Materials & design* 1997, *18*, 269-273.

[179] Williams, S.W. Welding of airframes using friction stir. *Air & Space Europe* 2001, *3*, 64-66.

[180] Kumar, R.; Singh, R.; Ahuja, I.; Amendola, A.; Penna, R. Friction welding for the manufacturing of PA6 and ABS structures reinforced with Fe particles. *Composites Part B: Engineering* 2018, *132*, 244-257.

[181] Mishra, R.S.; Ma, Z. Friction stir welding and processing. *Materials science and engineering: R: reports* 2005, *50*, 1-78.

[182] Wu, L.; Xiao, B.; Nagatsuka, K.; Nakata, K.; Ma, Z. Achieving strong friction lap joints of carbon-fiber reinforced plastic and metals by modifying metal surface structure via laser-processing pretreatment. *Composite Structures* 2020, 112167.

[183] Krishnan, K. On the formation of onion rings in friction stir welds. *Materials science and engineering: A* 2002, *327*, 246-251.

[184] Kimapong, K.; Watanabe, T. Friction stir welding of aluminum alloy to steel. *Welding journal* 2004, *83*, 277.

[185] Anand, R.; Sridhar, V. Studies on process parameters and tool geometry selecting aspects of friction stir welding–A review. *Materials Today: Proceedings* 2020, *27*, 576-583.

[186] Kumar, S.; Roy, B.S. Novel study of joining of acrylonitrile butadiene styrene and polycarbonate plate by using friction stir welding with double-step shoulder. *Journal of Manufacturing Processes* 2019, *45*, 322-330.

[187] Yasui, T.; Tsubaki, M.; Fukumoto, M.; Shimoda, Y.; Ishii, T. High-speed weldability between 6063 and S45C by friction stir welding. Study of welding of dissimilar metals by friction stir welding (1st report). *Welding international* 2006, *20*, 284-289.

[188] Messler, R.W. Joining comes of age: from pragmatic process to enabling technology. *Assembly Automation* 2003.

[189] Arora, A.; Dien, B.S.; Belyea, R.L.; Singh, V.; Tumbleson, M.E.; Rausch, K.D. Nutrient recovery from the dry grind process using sequential micro and ultrafiltration of thin stillage. *Bioresource technology* 2010, *101*, 3859-3863.

[190] Peel, M.; Steuwer, A.; Preuss, M.; Withers, P. Microstructure, mechanical properties and residual stresses as a function of welding speed in aluminium AA5083 friction stir welds. *Acta materialia* 2003, *51*, 4791-4801.

[191] Glaissa, M.A.A.; Asmael, M.; Zeeshan, Q. Recent Applications of Residual Stress Measurement Techniques for FSW Joints: A. *Jurnal Kejuruteraan* 2020, *32*, 1-15.

[192] McKnight, S.H.; Holmes, S.T.; Gillespie Jr, J.W.; Lambing, C.L.; Marinelli, J.M. Scaling issues in resistance-welded thermoplastic composite joints. *Advances in Polymer Technology: Journal of the Polymer Processing Institute* 1997, *16*, 279-295.

[193] Tauqir, N.; Mohammed, A.; Qassim, Z.; Davut, S. Applications of Machine Learning to Friction stir Welding Process Optimization. *Jurnal Kejuruteraan* 2020, *32*, 171-186.

[194] Yalavarthy, H. Friction stir welding process and material microstructure evolution modeling in 2000 and 5000 series of aluminum alloys. 2009.

[195] Cao, X.; Shi, Q.; Liu, D.; Feng, Z.; Liu, Q.; Chen, G. Fabrication of in situ carbon fiber/aluminum composites via friction stir processing: Evaluation of microstructural, mechanical and tribological behaviors. *Composites Part B: Engineering* 2018, *139*, 97-105.

[196] Krasnowski, K.; Hamilton, C.; Dymek, S. Influence of the tool shape and weld configuration on microstructure and mechanical properties of the Al 6082 alloy FSW joints. *Archives of civil and mechanical engineering* 2015, *15*, 133-141.

[197] Kusuda, Y. Honda develops robotized FSW technology to weld steel and aluminum and applied it to a mass-production vehicle. *Industrial Robot: An International Journal* 2013, *40*, 208-212.

[198] Haghshenas, M.; Gerlich, A. Joining of automotive sheet materials by friction-based welding methods: a review. *Engineering science and technology, an international journal* 2018, *21*, 130-148.

[199] Chen, Y.; Nakata, K. Effect of tool geometry on microstructure and mechanical properties of friction stir lap welded magnesium alloy and steel. *Materials & Design* 2009, *30*, 3913-3919.

[200] Haghshenas, M.; Abdel-Gwad, A.; Omran, A.; Gökçe, B.; Sahraeinejad, S.; Gerlich, A. Friction stir weld assisted diffusion bonding of 5754 aluminum alloy to coated high strength steels. *Materials & Design* 2014, *55*, 442-449.

[201] Qiu, R.; Iwamoto, C.; Satonaka, S. The influence of reaction layer on the strength of aluminum/steel joint welded by resistance spot welding. *Materials Characterization* 2009, *60*, 156-159.

[202] Singh, R.; Kumar, V.; Feo, L.; Fraternali, F. Experimental investigations for mechanical and metallurgical properties of friction stir welded recycled dissimilar polymer materials with metal powder reinforcement. *Composites Part B: Engineering* 2016, *103*, 90-97.

[203] Gerlich, A.; Yamamoto, M.; Shibayanagi, T.; North, T. Selection of welding parameter during friction stir spot welding. *SAE International Journal of Materials and Manufacturing* 2009, *1*, 1-8.

[204] Rao, H.; Jordon, J.; Barkey, M.; Guo, Y.; Su, X.; Badarinarayan, H. Influence of structural integrity on fatigue behavior of friction stir spot welded AZ31 Mg alloy. *Materials Science and Engineering: A* 2013, *564*, 369-380.

[205] Khosa, S.U.; Weinberger, T.; Enzinger, N. Thermo-mechanical investigations during friction stir spot welding (FSSW) of AA6082-T6. *Welding in the World* 2010, *54*, R134-R146.

[206] Saunders, N.; Miles, M.; Hartman, T.; Hovanski, Y.; Hong, S.-T.; Steel, R. Joint strength in high speed friction stir spot welded DP 980 steel. *International journal of precision engineering and manufacturing* 2014, *15*, 841-848.

[207] Lathabai, S.; Painter, M.; Cantin, G.; Tyagi, V. Friction spot joining of an extruded Al–Mg–Si alloy. *Scripta materialia* 2006, *55*, 899-902.

[208] Fujimoto, M.; Koga, S.; Abe, N.; Sato, S.Y.; Kokawa, H. Analysis of plastic flow of the Al alloy joint produced by friction stir spot welding. *Welding International* 2009, *23*, 589-596.

[209] Fujimoto, M.; Inuzuka, M.; Koga, S.; Seta, Y. Development of friction spot joining. *Welding in the World* 2005, *49*, 18-21.

[210] Paidar, M.; Tahani, K.; Vignesh, R.V.; Ojo, O.; Ezatpour, H.; Moharrami, A. Modified friction stir clinching of 2024-T3 to 6061-T6 aluminium alloy: Effect of dwell time and precipitation-hardening heat treatment. *Materials Science and Engineering: A* 2020, *791*, 139734.

[211] Gemme, F.; Verreman, Y.; Dubourg, L.; Jahazi, M. Numerical analysis of the dwell phase in friction stir welding and comparison with experimental data. *Materials Science and Engineering: A* 2010, *527*, 4152-4160.

[212] Gerlich, A.; Yamamoto, M.; North, T.H. Local melting and tool slippage during friction stir spot welding of Al-alloys. *Journal of Materials Science* 2008, *43*, 2-11.

[213] De Leon, M.; Shin, H.-S. Material flow behaviours during friction stir spot welding of lightweight alloys using pin and pinless tools. *Science and Technology of Welding and Joining* 2016, *21*, 140-146.

[214] Derazkola, H.A.; Eyvazian, A.; Simchi, A. Modeling and experimental validation of material flow during FSW of polycarbonate. *Materials Today Communications* 2020, *22*, 100796.

[215] Sun, Z.; Wu, C. Influence of tool thread pitch on material flow and thermal process in friction stir welding. *Journal of Materials Processing Technology* 2020, *275*, 116281.

[216] Hirasawa, S.; Badarinarayan, H.; Okamoto, K.; Tomimura, T.; Kawanami, T. Analysis of effect of tool geometry on plastic flow during friction stir spot welding using particle method. *Journal of materials processing technology* 2010, *210*, 1455-1463.

[217] Gadakh, V.S.; Adepu, K. Heat generation model for taper cylindrical pin profile in FSW. *Journal of Materials Research and Technology* 2013, *2*, 370-375.

[218] Dialami, N.; Cervera, M.; Chiumenti, M. Effect of the tool tilt angle on the heat generation and the material flow in friction stir welding. *Metals* 2019, *9*, 28.

[219] Huang, Y.; Meng, X.; Xie, Y.; Li, J.; Wan, L. Joining of carbon fiber reinforced thermoplastic and metal via friction stir welding with co-controlling shape and performance. *Composites Part A: Applied Science and Manufacturing* 2018, *112*, 328-336.

[220] Das, A.; Bang, H. Numerical modelling in friction lap joining of aluminium alloy and carbon-fiber-reinforced-plastic sheets. In Proceedings of IOP Conference Series: Materials Science and Engineering; p. 012032.

[221] Bang, H.; Das, A.; Lee, S. Friction stir lap joining of automotive aluminium alloy and carbon-fiber-reinforced plastic. In Proceedings of IOP Conference Series: Materials Science and Engineering; p. 012033.

[222] Nagatsuka, K.; Yoshida, S.; Tsuchiya, A.; Nakata, K. Direct joining of carbon-fiber–reinforced plastic to an aluminum alloy using friction lap joining. *Composites Part B: Engineering* 2015, *73*, 82-88.

[223] Huang, Y.; Meng, X.; Xie, Y.; Li, J.; Si, X.; Fan, Q. Improving mechanical properties of composite/metal friction stir lap welding joints via a taper-screwed pin with triple facets. *Journal of Materials Processing Technology* 2019, *268*, 80-86.

[224] Franke, D.J.; Morrow, J.D.; Zinn, M.R.; Pfefferkorn, F.E. Solid-state infiltration of 6061-T6 aluminum alloy into carbon fibers via friction stir welding. *Journal of Manufacturing Science and Engineering* 2017, *139*.

[225] Wu, L.; Nagatsuka, K.; Nakata, K. Achieving superior mechanical properties in friction lap joints of copper to carbon-fiber-reinforced plastic by tool offsetting. *Journal of materials science & technology* 2018, *34*, 1628-1637.

[226] Wu, L.; Nagatsuka, K.; Nakata, K. Direct joining of oxygen-free copper and carbon-fiber-reinforced plastic by friction lap joining. *Journal of Materials Science & Technology* 2018, *34*, 192-197.

[227] Wang, T.; Upadhyay, P.; Reza-E-Rabby, M.; Li, X.; Li, L.; Soulami, A.; Kappagantula, K.S.; Whalen, S. Joining of thermoset carbon fiber reinforced polymer and AZ31 magnesium alloy sheet via friction stir interlocking. *The International Journal of Advanced Manufacturing Technology* 2020, 1-10.

[228] Choi, J.-W.; Morisada, Y.; Liu, H.; Ushioda, K.; Fujii, H.; Nagatsuka, K.; Nakata, K. Dissimilar friction stir welding of pure Ti and carbon fibre reinforced plastic. *Science and Technology of Welding and Joining* 2020, 1-9.

[229] Lambiase, F.; Grossi, V.; Di Ilio, A.; Paoletti, A. Feasibility of friction stir joining of polycarbonate to CFRP with thermosetting matrix. *The International Journal of Advanced Manufacturing Technology* 2020, *106*, 2451-2462.

[230] Lambiase, F.; Grossi, V.; Paoletti, A. Friction Stir Joining of CFRP laminates with amorphous polymers: Influence of processing speeds. *Journal of Manufacturing Processes* 2020, *55*, 186-197.

[231] Kimura, M.; Choji, M.; Kusaka, M.; Seo, K.; Fuji, A. Effect of friction welding conditions on mechanical properties of A5052 aluminium alloy friction welded joint. *Science and Technology of Welding and Joining* 2006, *11*, 209-215.

[232] Kimura, M.; Choji, M.; Kusaka, M.; Seo, K.; Fuji, A. Effect of friction welding conditions and aging treatment on mechanical properties of A7075-T6 aluminium alloy friction joints. *Science and Technology of Welding and Joining* 2005, *10*, 406-412.

[233] Khidhir, G.I.; Baban, S.A. Efficiency of dissimilar friction welded 1045 medium carbon steel and 316L austenitic stainless steel joints. *Journal of Materials Research and Technology* 2019, *8*, 1926-1932.

[234] Campilho, R.; Pinto, A.; Banea, M.D.; da Silva, L.F. Optimization study of hybrid spot-welded/bonded single-lap joints. *International Journal of Adhesion and Adhesives* 2012, *37*, 86-95.

[235] Devaraju, A.; Kumar, A.; Kotiveerachari, B. Influence of addition of Grp/Al2O3p with SiCp on wear properties of aluminum alloy 6061-T6 hybrid composites via friction stir processing. *Transactions of Nonferrous Metals Society of China* 2013, *23*, 1275-1280.

[236] Gao, H.; Huang, Y. Geometrically necessary dislocation and size-dependent plasticity. *Scripta Materialia* 2003, *48*, 113-118.

[237] Esteves, J.; Goushegir, S.; Dos Santos, J.; Canto, L.; Hage Jr, E.; Amancio-Filho, S. Friction spot joining of aluminum AA6181-T4 and carbon fiber-reinforced poly (phenylene sulfide): Effects of process parameters on the microstructure and mechanical strength. *Materials & Design* 2015, *66*, 437-445.

[238] Khodabakhshi, F.; Haghshenas, M.; Sahraeinejad, S.; Chen, J.; Shalchi, B.; Li, J.; Gerlich, A. Microstructure-property characterization of a friction-stir welded joint between AA5059 aluminum alloy and high density polyethylene. *Materials Characterization* 2014, *98*, 73-82.

[239] Shorowordi, K.M.; Haseeb, A.; Celis, J.P. Tribo-surface characteristics of Al–B4C and Al–SiC composites worn under different contact pressures. *Wear* 2006, *261*, 634-641.

[240] Arrabal, R.; Pardo, A.; Merino, M.; Mohedano, M.; Casajús, P.; Merino, S. Al/SiC thermal spray coatings for corrosion protection of Mg–Al alloys in humid and saline environments. *Surface and Coatings Technology* 2010, *204*, 2767-2774.

[241] Chandran, P.; Sirimuvva, T.; Nayan, N.; Shukla, A.; Murty, S.N.; Pramod, S.; Sharma, S.; Bakshi, S.R. Effect of carbon nanotube dispersion on mechanical properties of aluminum-silicon alloy matrix composites. *Journal of materials engineering and performance* 2014, *23*, 1028-1037.

[242] Junaedi, H.; Abdo, H.S.; Khalil, K.A.; Almajid, A.A. Aluminum-Carbon Metal Matrix Composites: Effect of Carbon Fiber and Aspect Ratio on the Mechanical Properties. In Proceedings of Advanced Materials Research; pp. 119-122.

[243] Kubit, A.; Kluz, R.; Trzepieciński, T.; Wydrzyński, D.; Bochnowski, W. Analysis of the mechanical properties and of micrographs of refill friction stir spot welded 7075-T6 aluminium sheets. *Archives of Civil and Mechanical Engineering* 2018, *18*, 235-244.

[244] Zhao, Y.; Dong, C.; Wang, C.; Miao, S.; Tan, J.; Yi, Y. Microstructures evolution in refill friction stir spot welding of Al-Zn-Mg-Cu alloy. *Metals* 2020, *10*, 145.

[245] Farmanbar, N.; Mousavizade, S.; Ezatpour, H. Achieving special mechanical properties with considering dwell time of AA5052 sheets welded by a simple novel friction stir spot welding. *Marine Structures* 2019, *65*, 197-214.

[246] Gu, S.H.; Nicolas, V.; Lalis, A.; Sathirapongsasuti, N.; Yanagihara, R. Complete genome sequence and molecular phylogeny of a newfound hantavirus harbored by the Doucet's musk shrew (Crocidura douceti) in Guinea. *Infection, Genetics and Evolution* 2013, *20*, 118-123.

[247] Sun, Y.; Fujii, H.; Takaki, N.; Okitsu, Y. Novel spot friction stir welding of 6061 and 5052 Al alloys. *Science and Technology of Welding and Joining* 2011, *16*, 605-612.

[248] Bodaghi, M.; Dehghani, K. Friction stir welding of AA5052: the effects of SiC nano-particles addition. *The International Journal of Advanced Manufacturing Technology* 2017, *88*, 2651-2660.

[249] Farmanbar, N.; Mousavizade, S.; Elsa, M.; Ezatpour, H. AA5052 sheets welded by protrusion friction stir spot welding: High mechanical performance with considering sheets thickness at low dwelling time and tool rotation speed. *Proceedings of the Institution of Mechanical Engineers, Part C: Journal of Mechanical Engineering Science* 2019, *233*, 5836-5847.

[250] Al-Jarrah, J.A.; Swalha, S.; Mansour, T.A.; Ibrahim, M.; Al-Rashdan, M.; Al-Qahsi, D.A. Welding equality and mechanical properties of aluminum alloys

joints prepared by friction stir welding. *Materials & Design (1980-2015)* 2014, *56*, 929-936.

[251] Cai, W.; Wang, J.; Zhou, Q.; Yang, Y.; Jiang, P. Equipment and Machine Learning in Welding Monitoring: A Short Review. In Proceedings of Proceedings of the 5th International Conference on Mechatronics and Robotics Engineering; pp. 9-15.

[252] Zhou, B.; Svetashova, Y.; Byeon, S.; Pychynski, T.; Mikut, R.; Kharlamov, E. Predicting quality of automated welding with machine learning and semantics: a Bosch case study. In Proceedings of Proceedings of the 29th ACM International Conference on Information & Knowledge Management; pp. 2933-2940.

[253] Yaman, M.A.; Abd Elaty, M.; Taman, M. Predicting the ingredients of self compacting concrete using artificial neural network. *Alexandria Engineering Journal* 2017, *56*, 523-532.

[254] Keshavarz, Z.; Torkian, H. Application of ANN and ANFIS models in determining compressive strength of concrete. *Journal of Soft Computing in Civil Engineering* 2018, *2*, 62-70.

[255] Sitton, J.D.; Zeinali, Y.; Story, B.A. Rapid soil classification using artificial neural networks for use in constructing compressed earth blocks. *Construction and Building Materials* 2017, *138*, 214-221.

[256] Khademi, F.; Akbari, M.; Jamal, S. Prediction of compressive strength of concrete by data-driven models. *I-Manager's J Civ Eng* 2015, *5*, 16.

[257] Satpathy, M.P.; Mishra, S.B.; Sahoo, S.K. Ultrasonic spot welding of aluminum-copper dissimilar metals: a study on joint strength by experimentation and machine learning techniques. *Journal of Manufacturing Processes* 2018, *33*, 96-110.

[258] Maleki, E. Artificial neural networks application for modeling of friction stir welding effects on mechanical properties of 7075-T6 aluminum alloy. In Proceedings of IOP Conference Series: Materials Science and Engineering; p. 012034.

[259] Khourshid, A.; El-Kassas, A.M.; Sabry, I. Integration between artificial neural network and responses surfaces methodology for modeling of friction stir welding. *International Journal of Advanced Engineering Research and Science (IJAERS)* 2015, *2*.

[260] Wong, C. A Novel Operational Partition between Neural Network Classifiers on Vulnerability to Data Mining Bias. *Journal of Software Engineering and Applications* 2014, *2014*.

[261] Agrawal, R.K.; Muchahary, F.; Tripathi, M.M. Ensemble of relevance vector machines and boosted trees for electricity price forecasting. *Applied Energy* 2019, *250*, 540-548.

[262] Kong, D.; Chen, Y.; Li, N.; Duan, C.; Lu, L.; Chen, D. Relevance vector machine for tool wear prediction. *Mechanical Systems and Signal Processing* 2019, *127*, 573-594.

[263] Tagimalek, H.; Maraki, M.R.; Mahmoodi, M.; Azargoman, M. A Hybrid SVM-RVM Algorithm to Mechanical Properties in the Friction Stir Welding Process. *Journal of Applied and Computational Mechanics* 2019.

[264] Gurgenc, T.; Altay, O.; Ulas, M.; Ozel, C. Extreme learning machine and support vector regression wear loss predictions for magnesium alloys coated using various spray coating methods. *Journal of Applied Physics* 2020, *127*, 185103.

[265] Bilhan, O.; Emiroglu, M.E.; Miller, C.J.; Ulas, M. The evaluation of the effect of nappe breakers on the discharge capacity of trapezoidal labyrinth weirs by ELM and SVR approaches. *Flow Measurement and Instrumentation* 2018, *64*, 71-82.

[266] Tang, X.; Zhuang, L.; Jiang, C. Prediction of silicon content in hot metal using support vector regression based on chaos particle swarm optimization. *Expert Systems with Applications* 2009, *36*, 11853-11857.

[267] Gill, S.S.; Singh, R.; Singh, J.; Singh, H. Adaptive neuro-fuzzy inference system modeling of cryogenically treated AISI M2 HSS turning tool for estimation of flank wear. *Expert Systems with Applications* 2012, *39*, 4171-4180.

[268] Takagi, T.; Sugeno, M. Fuzzy identification of systems and its applications to modeling and control. *IEEE transactions on systems, man, and cybernetics* 1985, 116-132.

[269] Larsen, P.M. Industrial applications of fuzzy logic control. *International Journal of Man-Machine Studies* 1980, *12*, 3-10.

[270] Dewan, M.W.; Huggett, D.J.; Liao, T.W.; Wahab, M.A.; Okeil, A.M. Prediction of tensile strength of friction stir weld joints with adaptive neuro-fuzzy inference system (ANFIS) and neural network. *Materials & Design* 2016, *92*, 288-299.

[271] Praga-Alejo, R.; Torres-Treviño, L.; Piña-Monarrez, M. Prediction in Welding Process Using Multiple Linear Regression and Neural Network. *International Journal of Industrial Engineering* 2008, 481-488.

[272] Verma, S.; Misra, J.P.; Singh, J.; Batra, U.; Kumar, Y. Prediction of tensile behavior of FS welded AA7039 using machine learning. *Materials Today Communications* 2021, *26*, 101933.

[273] Elatharasan, G.; Kumar, V.S. Modelling and optimization of friction stir welding parameters for dissimilar aluminium alloys using RSM. *Procedia engineering* 2012, *38*, 3477-3481.

[274] Rao, M.S.; Ramanaiah, N. Optimization of Process Parameters For Fsw Of Al-Mg-Mn-Sc-Zr Alloy Using Ccd And RSM. *Strojnícky časopis-Journal of Mechanical Engineering* 2018, *68*, 195-224.